


11-7-2014

Mechanisms of Arsenic Detoxification and Resistance

Jitesh Kannan Pillai

Florida International University, jpill001@fiu.edu

Follow this and additional works at: <http://digitalcommons.fiu.edu/etd>

 Part of the [Biochemistry, Biophysics, and Structural Biology Commons](#), and the [Toxicology Commons](#)

Recommended Citation

Pillai, Jitesh Kannan, "Mechanisms of Arsenic Detoxification and Resistance" (2014). *FIU Electronic Theses and Dissertations*. Paper 1699.

<http://digitalcommons.fiu.edu/etd/1699>

This work is brought to you for free and open access by the University Graduate School at FIU Digital Commons. It has been accepted for inclusion in FIU Electronic Theses and Dissertations by an authorized administrator of FIU Digital Commons. For more information, please contact dcc@fiu.edu.

FLORIDA INTERNATIONAL UNIVERSITY
Miami, Florida

MECHANISMS OF ARSENIC DETOXIFICATION AND RESISTANCE

A dissertation submitted in partial fulfillment of the
requirements for the degree of
DOCTOR OF PHILOSOPHY
in
BIOLOGY
by
Jitesh Kannan Pillai
2014

To: Interim Dean Michael R. Heithaus
College of Arts and Sciences

This dissertation, written by Jitesh Kannan Pillai, and entitled Mechanisms of Arsenic Detoxification and Resistance, having been approved in respect to style and intellectual content, is referred to you for judgment.

We have read this dissertation and recommend that it be approved.

Hiranmoy Bhattacharjee

Alejandro Barbieri

John Makemson

Yong Cai

Barry P. Rosen, Major Professor

Date of Defense: November 7, 2014

The dissertation of Jitesh Kannan Pillai is approved.

Interim Dean Michael R. Heithaus
College of Arts and Sciences

Dean Lakshmi N. Reddi
University Graduate School

Florida International University, 2014

© Copyright 2014 by Jitesh Kannan Pillai

All rights reserved.

DEDICATION

To my family and teachers.

ACKNOWLEDGMENTS

This dissertation is the result of many people and I am indebted to all of them. I owe my deepest gratitude to my supervisor, Dr. Barry Rosen, whose encouragement, guidance and support from the beginning to the end has enabled me to develop my project. It has been a great learning experiencing under his mentorship. I am also heartily thankful to my committee members, Dr. Hiranmoy Bhattacharjee, Dr. John Makemson, Dr. Alejandro Barbieri and Dr. Yong Cai who assisted me in the right direction of my graduate research. I wish to thank Dr. Jianbo Yang for his help during the initial stage of my PhD with many techniques particularly yeast two hybrid system. I wish to recognize Dr. Abdul Ajees for help with protein purification. The docking studies on ArsA and ArsD are a collaboration with Dr. Venkadesh Sarkarai Nadar and Dr. Abdul Ajees. The synthetic CrArsM structure study is a collaboration with Dr. Charles Packianathan who performed crystal screening, data collection and refinement. Dr. Dharmendra S. Dheeman, Dr. Jian Chen and Dr. Masafumi Yoshinaga for help with analytical techniques and their sound advice.

I would also like to thank all of my present and past laboratory colleagues: Dr. Hui Dong, Dr. Kavitha Marapakala, Dr. Wenzhong Xu, Dr. Jie Qin, Mr. Shashank Pawitwar and Ms. Jiaojiao Li. I want to express my thanks to all the faculties and staffs in our department who continuously supported me with advice and friendship. My special regards to Mr. Gorakh D. Tatke for being a fabulous friend close to a decade and seeing me through thick and thin. My regards to Mr. Pratik Nyati and Ms. Parul Maheshwari for being great friends. My thanks to Dr.

Vidya Sagar, Dr. Deepak Balasubramanian, Dr. Kishore Dhavala, Ms. Mansi Sharma, Mr. Adwait Kabra, Mr. Sharief Rehman and Mr. Mayur Doke for their friendship and peer support.

Lastly, I am grateful to my parents Mr. K.N. Pillai , Mrs. Jaya K. Pillai, my father and mother-in-law Mr. Thamban Karatha and Mrs. Thankamani Karatha for their unwavering support and inspiration , my dear wife Ranitha Karatha for her faith and confidence in me, my brother Mr. Sreejith K. Pillai for his support and my grandmother Meenakshiamma for her love.

ABSTRACT OF THE DISSERTATION
MECHANISMS OF ARSENIC DETOXIFICATION AND RESISTANCE

by

Jitesh Kannan Pillai

Florida International University, 2014

Miami, Florida

Professor Barry P. Rosen, Major Professor

Arsenic is a ubiquitous environmental toxic substance. As a consequence of continual exposure to arsenic, nearly every organism, from *Escherichia coli* to humans have evolved arsenic detoxification pathways. One of the pathways is extrusion of arsenic from inside the cells, thereby conferring resistance. The R773 *arsRDABC* operon in *E. coli* encodes an ArsAB efflux pump that confers resistance to arsenite. ArsA is the catalytic subunit of the pump, while ArsB forms the oxyanion conducting pathway. ArsD is an arsenite metallochaperone that binds arsenite and transfers it to ArsA. The interaction of ArsA and ArsD allows for resistance to As(III) at environmental concentrations.

The interaction between ArsA ATPase and ArsD metallochaperone was examined. A quadruple mutant in the *arsD* gene encoding a K2A/K37A/K62A/K104A ArsD is unable to interact with ArsA. An error-prone mutagenesis approach was used to generate random mutations in the *arsA* gene that restored interaction with the quadruple *arsD* mutant in yeast two-hybrid assays. Three such mutants encoding Q56R, F120I and D137V ArsA were able to restore interaction with the quadruple ArsD mutant. Structural models

generated by *in silico* docking suggest that an electrostatic interface favors reversible interaction between ArsA and ArsD. Mutations in ArsA that propagate changes in hydrogen bonding and salt bridges to the ArsA-ArsD interface also affect their interactions.

The second objective was to examine the mechanism of arsenite resistance through methylation and subsequent volatilization. Microbial ArsM (As(III) S-adenosylmethyltransferase) catalyzes the formation of trimethylarsine as the volatile end product. The net result is loss of arsenic from cells. The gene for CrArsM from the eukaryotic green alga *Chlamydomonas reinhardtii* was chemically synthesized and expressed in *E. coli*. The purified protein catalyzed the methylation of arsenite into methyl-, dimethyl- and trimethyl products. Synthetic purified CrArsM was crystallized in an unliganded form. Biochemical and biophysical studies conducted on CrArsM sheds new light on the pathways of biomethylation. While in microbes ArsM detoxifies arsenic, the human homolog, hAS3MT, converts inorganic arsenic into more toxic and carcinogenic forms. An understanding of the enzymatic mechanism of ArsM will be critical in deciphering its parallel roles in arsenic detoxification and carcinogenesis.

TABLE OF CONTENTS

CHAPTER	PAGE
I. Review of the Literature	1
Ubiquity of arsenic in the environment and its toxicity	1
Arsenic uptake systems	3
Arsenic extrusion systems	5
Arsenate Reductases	8
R773 <i>ars</i> operon	9
Co-existence of <i>arsA</i> and <i>arsD</i> in <i>ars</i> operons	10
ArsA ATPase	11
ArsD	17
Evidence of physical interaction between ArsD and ArsA	17
Proposed mechanism of metalloid transfer from ArsD to ArsA	18
Biomethylation and its importance	23
Evolution of methyltransferases	25
Arsenic biomethylation	26
II. Genetic mapping of the interface between the ArsA ATPase and ArsD metallochaperone	31
Introduction	31
Materials and methods	33
Reagents	33
Strains, plasmids and media	33
DNA manipulation and mutagenesis	35
Generation of a random mutated library of PCR fragments	36
Yeast two-hybrid analysis	36
Sequencing of <i>arsA</i> mutant genes in yeast colonies	37
Protein expression and purification	37
ATPase activity assays	38
Measurement of metalloid binding	39
Model building and docking analysis	40
Results	41
ArsA ATPase mutants exhibiting stronger interaction with ArsD	41
Analysis of altered ArsAs	45
ATPase activity of ArsA mutants	46
Binding of Sb(III) to altered ArsAs	48
Docking analysis of the interaction between Q56R ArsA and ArsD	49
Discussion	55
III. Biochemical and biophysical characterization of CrArsM, an As(III) S-adenosylmethionine methyltransferase, from	

<i>Chlamydomonas reinhardtii</i>	59
Introduction	59
Materials and methods	65
Reagents	65
Cloning, expression and purification of CrArsM	65
Arsenic methylation	66
Fluorescence assays	67
Crystallization	68
Data collection and processing	69
Results	70
Chemical synthesis of CrArsM	70
Catalytic properties of synthetic CrArsM	73
Tryptophan fluorescence spectroscopy	75
Crystallization studies	78
Structure of CrArsM	81
Discussion	82
IV. Conclusion	87
V. References	94
VI. VITA	108

LIST OF FIGURES

FIGURE	PAGE
Figure 1. Pathways of arsenical uptake and detoxification in prokaryotes and eukaryotes	7
Figure 2. Organization of <i>E. coli</i> R773 <i>ars</i> operon	9
Figure 3. A cross section of <i>ars</i> operons representing the coexistence of <i>arsA</i> and <i>arsD</i> genes	10
Figure 4. Overall structure of R773 ArsA ATPase	13
Figure 5. Crystal structure of ArsD dimer	20
Figure 6. Proposed mechanism of metalloid transfer between ArsD and ArsA	22
Figure 7. Topology of the core fold of SAM methyltransferases with SAM and substrate binding fold	25
Figure 8. The Challenger's pathway for reductive methylation of inorganic As(V) into volatile, organic TMA(III)	28
Figure 9. Yeast two-hybrid analysis of ArsA mutants exhibiting increased interaction with ArsD	42
Figure 10. Expression of altered ArsAs	45
Figure 11. Activation of ArsA ATPase activity by ArsD.	46
Figure 12. ArsA mutants bind antimonite	49
Figure 13. <i>In silico</i> docking analysis of ArsA-ArsD complex	52
Figure 14. Multiple alignment of ArsM orthologs.	63
Figure 15. Comparison of sequence of native and synthetic CrArsM	71
Figure 16. Translation of optimized sequence of synthetic CrArsM	72
Figure 17. Methylation of As(III) by wild-type and synthetic CrArsM	74
Figure 18. Homology modeling of CrArsM based on CmArsM native structure	75

LIST OF FIGURES

FIGURE	PAGE
Figure 19. Emission spectra of synthetic CrArsM	76
Figure 20. Effect of As(OH) ₃ and As(GS) ₃ on the fluorescence of synthetic CrArsM	77
Figure 21. Crystals of CrArsM were grown by hanging drop vapor Diffusion	78
Figure 22. The diffraction images (1° oscillation) were collected from CmArsM crystals at APL, Argonne National Laboratory, using a MAR 300 detector at 100 °K.	79
Figure 23. Overall structure of CrArsM	81
Figure 24. Proposed CrArsM reaction scheme	85

LIST OF TABLES

TABLE	PAGE
Table 1. Conserved motifs of SAM methyltransferases	26
Table 2. Strains and plasmids	34
Table 3. ArsA mutants exhibiting interaction with 4KA ArsD	43
Table 4. ArsA ATPase kinetics in the presence or absence of either wild type or 4KA ArsD	47
Table 5. Q56R ArsA and wild-type ArsD residues predicted from <i>in silico</i> docking to be within 4 Å of each other	53
Table 6. Data collection and processing	80

ABBREVIATIONS AND ACRONYMS

ACRONYM/ ABBREVIATION	TERM
ABC	Adenosine triphosphate binding cassette
AQP	Aquaporin
ArsA	Arsenical ATPase
ArsB	Arsenical pump membrane protein
ArsD	Arsenical metallochaperone
ArsM	As(III) S-adenosylmethionine methyltransferase
ArsP	Arsenical membrane permease
ArsR	Arsenical repressor
As(III)	Trivalent arsenite
As(V)	Pentavalent arsenate
ATP	Adenosine triphosphate
ATSDR	Agency for Toxic Substances and Disease Registry
Cdc25	Cell-cycle protein tyrosine phosphatase
CmArsM	<i>Cyanidioschyzon merolae</i> ArsM
CrArsM	<i>Chlamydomonas reinhardtii</i> ArsM

DMAs(GS)	Glutathionylated trivalent dimethyl arsenite
DMAs(III)	Trivalent dimethyl arsenite
DMAs(V)	Dimethylarsenate
DMSA	Meso-2,3-dimercaptosuccinic acid
DTT	Dithiotrietol
EDTA	Ethylenediaminetetraacetic acid
EPA	Environmental Protection Agency
EXAFS	Extended X-ray Absorption Fine Structure
GlpF	Aquaglyceroporin
GLUT	Glucose permease
Grx	Glutaredoxin
GSH	Glutathione
hAS3MT	As(III) S-adenosylmethionine methyltransferase from humans
HXT	Hexose transporter
MA(GS) ₂	Glutathionylated trivalent monomethyl arsenite
MA(III)	Trivalent methyl arsenite
MA(V)	Pentavalent methylarsenate

MBP	Maltose binding protein
MODELLER	MODELLER is a computer program used in producing homology models of protein tertiary structures as well as quaternary structures.
MOPS	3-(N-morpholino)propanesulfonic acid
MRP	Multidrug resistance-associated protein
NBD	Nucleotide binding domain
15N TROSY HSQC 15N	Transverse Relaxation Optimized Spectroscopy with Heteronuclear Single Quantum Coherence Spectroscopy
Nitarsonsone	4-nitrophenyl) arsonic acid
NMR	Nuclear Magnetic Resonance
OATPB	Organic anion transporting polypeptide 2B1
OATPC	Organic anion transporting polypeptide C
PEG	Polyethylene glycol
Roxarsone	(4-hydroxy-3-nitrobenzenearsonic acid)
Sb(III)	Trivalent antimony
STD	Signal transduction domain
TMA(III)	Trivalent methyl arsenic
Trx	Thioredoxin

TMA_s(V)O

Trimethylarsine oxide

CHAPTER I

Review of the Literature

Ubiquity of arsenic in the environment and its toxicity

Arsenic is widely distributed in the Earth's crust and occurs primarily in three oxidation states +5, +3, and -3. Humans are exposed to arsenic from mining, copper smelting, coal burning, other combustion processes as well as volcanic eruptions that bring arsenic into the environment. Anthropogenic sources of arsenic includes its use in various commonly used herbicides, insecticides, rodenticides, wood-preservatives, animal feeds, paints, dyes, and semiconductors. In addition, arsenic enters the food chain from drinking water that has flowed through arsenic rich soil. As a result, arsenic is the most ubiquitous environmental toxin and carcinogen according to the U.S. Environmental Protection Agency (EPA) and Agency for Toxic Substances and Disease Registry (ATSDR), and has consistently ranked first on the ATSDR priority list of hazardous substances (<http://www.atsdr.cdc.gov/SPL/index.html>).

Chronic exposure to arsenic has been implicated to increased risk of lung, bladder, kidney and liver cancers, cardiovascular diseases, peripheral neuropathies and diabetes mellitus (Chappell et al., 1997). Ingestion of arsenic predominantly from drinking water can result in skin hyperpigmentation and keratosis of the hands and feet that subsequently progress to skin cancers. In countries like Taiwan, Bangladesh and Chile, approximately 10% of such

hyperpigmentation and keratosis are associated with a high incidence of lung, bladder, and other cancers (Chappell et al., 1997). Long-term occupational exposure to arsenic has been associated with increased prevalence of cancer of the buccal cavity, pharynx, lung, kidney, bone, large intestine, and rectum. Chronic exposure to arsenic severely compromises the immune response to respiratory influenza A (H1N1) virus (Kozul et al., 2009). In response to new and compelling research linking high arsenic levels in drinking water with certain forms of cancer, the USEPA lowered the arsenic maximum contaminant level (MCL) in drinking water from 50 ppb to 10 ppb (Smith et al., 2002).

The two biologically relevant oxidation states of arsenic are the pentavalent arsenate (As(V)) and trivalent arsenite (As(III)) forms. In solution the pentavalent form, H_3AsO_4 , exists as the oxyanion arsenate, which is a substrate analog of phosphate. Arsenate disrupts phosphorylation reactions by substituting for phosphate and eventual formation of unstable arsenyl compounds. The term "arsenolysis" was introduced to describe an over-all hydrolytic process in which the first step is the replacement of arsenate for phosphate (Doudoroff et al., 1947). Isotope O^{18} -labeling techniques showed the formation of a transient acyl arsenate or arsenate ester intermediate in arsenolysis reactions (Slocum and Varner, 1960). At the substrate level, arsenolysis may occur during glycolysis. In one of the steps of the glycolytic pathway, phosphate is linked enzymatically to D-glyceraldehyde-3-phosphate to form 1,3-biphospho-D-glycerate. Arsenate can replace phosphate in this reaction to form the anhydride, 1-arsenato-3-phospho-D-glycerate, which then

spontaneously hydrolyses to 3-phosphoglycerate and arsenate thereby reducing ATP production of glycolysis from two to zero. At the mitochondrial level, arsenolysis also occurs during oxidative phosphorylation (Moore et al., 1983). Depletion of ATP by arsenate has been observed in rabbit (Delnomdedieu et al., 1994) and human erythrocytes (Winski and Carter, 1998) after in vitro exposure to arsenate.

Trivalent As(III) are much more toxic than As(V) and is primarily responsible for the biological effects of this metalloid. As(III) has the propensity to form strong, nearly covalent bonds with the thiolates of closely spaced cysteine residues, thereby inhibiting the function of many proteins. For example, As(III) inhibits the pyruvate dehydrogenase complex by binding to its lipoic acid moiety. As(III) also reacts with other cellular thiols such as reduced glutathione (GSH), raising the intracellular redox potential, and leading to oxidative damage.

Arsenic uptake systems

Both the pentavalent and trivalent forms of arsenic use uptake systems that bring these compounds adventitiously into cells. As arsenate is a substrate analogue of phosphate, most organisms takes up arsenate via the phosphate transporters (Figure 1 below). The prokaryotic microbe, *Escherichia coli*, has two phosphate transporters, Pit and Pst (Rosenberg et al., 1977), both of which catalyze arsenate uptake. Of the two transporters, Pit is the major arsenate uptake system (Willsky and Malamy, 1980a, b). In the eukaryotic microbe, *Saccharomyces cerevisiae*, As(V) enters the cell via the phosphate transporters

Pho84 and Pho87 (Bun-Ya et al., 1991; Bun-ya et al., 1996). In mammalian cells, As(V) uptake is mediated by the high-affinity phosphate transporter NaPiIIb (Villa-Bellosta and Sorribas, 2010).

Arsenite in water has a pK_a of 9.2 and exists as the undissociated oxyacid, $As(OH)_3$, at physiological pH (Ramirez-Solis et al., 2004). $As(OH)_3$ shows very strong similarity with the conformation of glycerol (Porquet and Filella, 2007) and is adventitiously taken up by the aquaglyceroporin, GlpF, in *E. coli* (Figure 1 below) (Meng et al., 2004; Sanders et al., 1997). GlpF is a member of the major intrinsic protein (MIP) superfamily that allow the transport of water and small solutes such as glycerol and urea by an energy independent mechanism. Members of the MIP superfamily fall into a number of branches, but the two main evolutionary groups are the aquaporins or water specific channels, and the aquaglyceroporins, which allow the transport of water, glycerol, and other small, uncharged solutes (Mukhopadhyay et al., 2014). Similarly, Fps1p, the yeast homologue of GlpF, conducts arsenite uptake in *S. cerevisiae* (Wysocki et al., 2001). In humans, four aquaglyceroporins conduct As(III) in the order of effectiveness AQP9 > AQP7 >> AQP3 >> AQP10 (Liu et al., 2004b).

A second family of membrane transporters catalyzing arsenite uptake are the glucose permeases (Liu et al., 2004a). In *S. cerevisiae*, the hexose transporters, HXT1, HXT3, HXT4, HXT5, HXT7 and HXT9, allow the adventitious uptake of $As(OH)_3$ (Liu et al., 2004a). The mammalian glucose transporter, GLUT1, which is a homologue of the yeast HXT hexose permeases, facilitates the uptake of trivalent arsenicals (Liu et al., 2006). Two other mammalian

glucose permeases, GLUT2 in hepatocytes (Drobna et al., 2010) and GLUT5 in small intestine (Calatayud et al., 2012), also mediate As(III) accumulation. Additionally, OATPB (Calatayud et al., 2012) and OATPC (Lu et al., 2006), two human members of the organic anion transporting polypeptide family that mediate the transmembrane transport of a wide range of amphipathic endogenous and exogenous organic compounds (Hagenbuch and Meier, 2004), are also involved in As(III) influx.

Arsenic extrusion systems

All living organisms have systems for arsenic detoxification (Figure 1 below). The most common detoxification mechanism is either efflux of As(III) from cytosol into the external environment or sequestration in an organelle. Interestingly, all identified arsenic efflux systems are for trivalent As(III); none have been reported for the pentavalent As(V) form. Extrusion systems for As(V) do not exist or have not been found. It is postulated that life originated in an anoxic world in the presence of high concentrations of heavy metals and metalloids (Zhu et al., 2014). On account of a reducing environment, arsenic would have existed as As(III) rather than As(V), thereby favoring the evolution of transporters that extrude arsenite out of cells. As the atmosphere became oxidizing, most As(III) were oxidized to As(V), and so proteins evolved that reduce arsenate to arsenite, the substrate of the existing transport systems. In prokaryotes, arsenic resistance genes are usually organized in *ars* operons that are controlled by the As(III)-responsive transcriptional repressor, ArsR. Nearly every *ars* operon has a

gene encoding one of the two unrelated families of permeases, ArsB and Acr3. ArsB is widespread in bacteria and archaea. ArsB from plasmid R773 is a 429-residue membrane protein with twelve membrane spanning segments, which is similar to many carrier proteins (Wu et al., 1992). It is an antiporter catalyzing the extrusion of As(III) or Sb(III) from *E.coli* cells by H⁺/As(OH)₃ exchange that is coupled to the electrochemical proton gradient (Meng et al., 2004). Although ArsB transports As(III), it has a higher affinity for Sb(III) in comparison to the former (Meng et al., 2004).

The Acr3 family of arsenic efflux proteins is probably more widespread than ArsB and includes members found in bacteria, archaea and fungi. The first identified member of this family is encoded by the *ars* operon of the skin (*sigK* intervening) element in the chromosome of *B. subtilis* (Sato and Kobayashi, 1998). Fungal members of this family include the *S. cerevisiae* Acr3p metalloid efflux protein (Bobrowicz et al., 1997; Ghosh et al., 1999). The membrane topology of *Alkaliphilus metalliredigens* AmAcr3-1 shows that, it has ten transmembrane spanning segments, with the N- and C-termini localized in the cytosol (Fu et al., 2009). Acr3 has been demonstrated to be an antiporter that catalyzes arsenite-proton exchange (Villadangos et al., 2012). Bacterial Acr3 proteins appear to be specific for As(III) and do not transport Sb(III) (Fu et al., 2009; Villadangos et al., 2012). On the other hand, yeast Acr3p has been suggested to transport both As(III) and Sb(III) (Maciaszczyk-Dziubinska et al., 2010).

A third class of arsenic permease has recently been reported (Shen et al., 2014). The *arsP* gene is a part of the *ars* operon in *Campylobacter jejuni* and confers resistance specifically to organoarsenicals, such as roxarsone (4-hydroxy-3-nitrobenzenearsonic acid) and nitarsonic acid ((4-nitrophenyl) arsonic acid), but not inorganic arsenicals, including arsenite and arsenate. ArsP is predicted

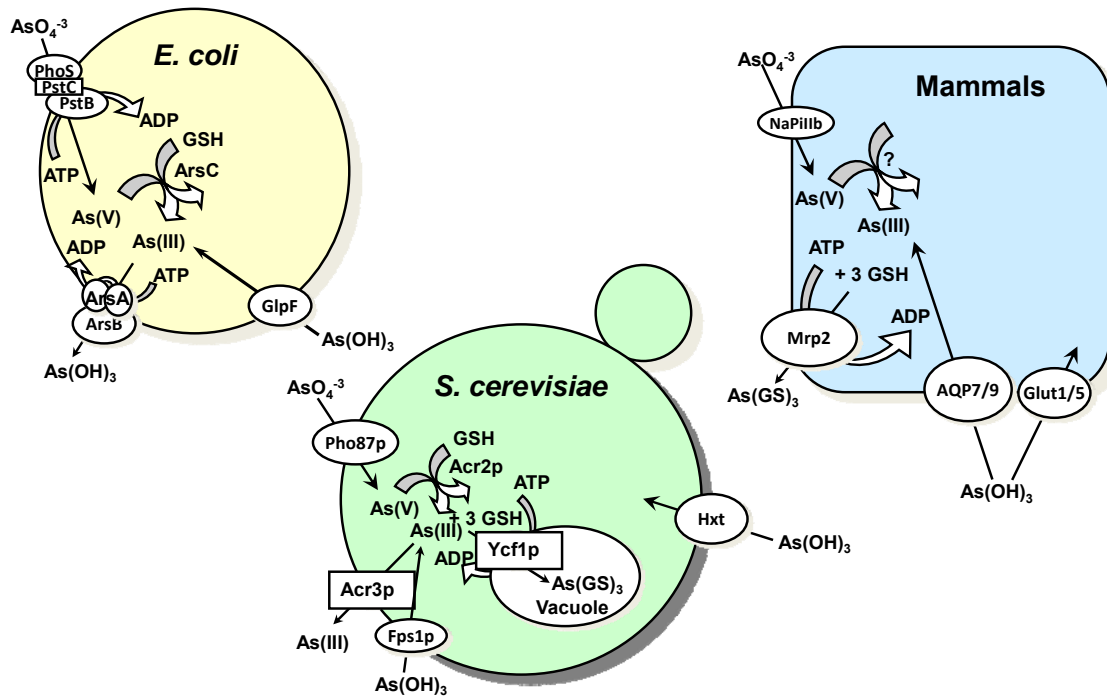


Figure 1. Pathways of arsenical uptake and detoxification in prokaryotes and eukaryotes. $As(V)$ is taken up by phosphate transporters, while $As(III)$ is taken up by aquaglyceroporins (GlpF in *E. coli*, Fps1p in yeast, and AQP7 and AQP9 in mammals), and hexose permeases (HXT1, HXT3, HXT4, HXT5, HXT7, or HXT9 in yeast, and GLUT1 and GLUT5 in mammals). In both *E. coli* and *S. cerevisiae*, arsenate is reduced to arsenite by the bacterial ArsC or yeast Acr2p enzymes. In both organisms, glutathione and glutaredoxin serve as the source of reducing potential. The proteins responsible for arsenate reduction in mammals have not yet been identified. In *E. coli*, arsenite is extruded from the cells by ArsB alone or by the ArsAB ATPase. In yeast Acr3p is a plasma membrane arsenite efflux protein, and Ycf1p, which is a member of the MRP family of the ABC superfamily of drug-resistance pumps, transports $As(GS)_3$ into the vacuole. In mammals, Mrp isoforms such as Mrp2, pump $As(GS)_3$ out of cells. (Rosen et al. 1995).

to be a membrane permease containing eight transmembrane helices, distinct from other known arsenic transporters.

In many eukaryotic microbes, multidrug resistance-associated protein (MRP) homologues have been shown to confer arsenic resistance. MRP1 is an adenosine triphosphate binding cassette (ABC) transporter that confers multidrug resistance in human small cell lung carcinoma (Cole et al., 1994). The yeast protein Ycf1 (yeast cadmium factor), a close homologue of human MRP1, catalyzes the vacuolar sequestration of As(III) (Ghosh et al., 1999). Both MRP1 and Ycf1 pump glutathione S-conjugated drugs out of the cytosol. MRP1 transports arsenic as a tri-glutathione conjugate out of the cell (Leslie et al., 2004), while Ycf1 catalyzes the ATP-driven uptake of As(III)-glutathione conjugate into the yeast vacuole (Ghosh et al., 1999). In liver, MRP2 extrudes arsenic-glutathione complexes into bile and may be a major route of arsenic detoxification in humans (Cui et al., 2004).

Arsenate Reductases

Cytosolic arsenate reductases catalyze the two electron reduction of inorganic As(V) to As(III), which is transported out of the cell by the various arsenic transporters, thereby extending the range of resistance to include As(V). Arsenate reductases arose independently at least three times by convergent evolution and one family of arsenate reductase that includes the *E. coli* plasmid R773 ArsC uses glutaredoxin (Grx) and glutathione (GSH) as reductants (Mukhopadhyay and Rosen, 2002). A second family, represented by the *S.*

aureus plasmid pl258 ArsC (Ji and Silver, 1992) and the *B. subtilis* chromosomal ArsC, uses thioredoxin (Trx) as a reductant. This bacterial family of arsenate reductases is distantly related to mammalian low molecular weight protein tyrosine phosphatases (Bennett et al., 2001; Messens et al., 1999). A third family of eukaryotic arsenate reductases includes Acr2p (Bobrowicz et al., 1997; Mukhopadhyay and Rosen, 1998) from the Baker's yeast, *S. cerevisiae*, and LmAcr2p (Zhou et al., 2004) from the parasitic protozoa *Leishmania major*. The eukaryotic reductases are related to the catalytic domain of the Cdc25 cell-cycle protein tyrosine phosphatase (Fauman et al., 1998). Human Cdc25B and Cdc25C also moonlight as arsenate reductase, reducing inorganic arsenate to arsenite activity, while using glutaredoxin and glutathione as reductants (Bhattacharjee et al., 2010).

R773 *ars* operon

Nearly every sequenced bacterial genome contains an *ars* operon and the minimal gene set in an operon is a three gene arrangement, *arsRBC*, where ArsR is an As(III)-responsive repressor (San Francisco et al., 1990), ArsB is an As(OH)₃/H⁺ antiporter (Meng et al., 2004) that extrudes trivalent As(III) from cells, and ArsC is an arsenate reductase that converts As(V) to As(III)

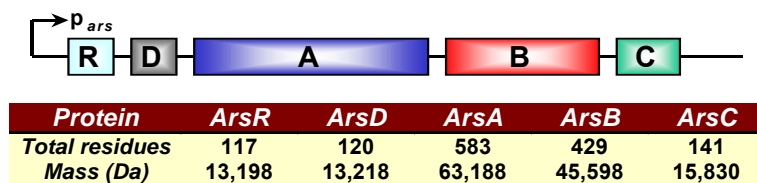


Figure 2. Organization of *E. coli* R773 *ars* operon

(Gladysheva et al., 1994). Some *ars* operons contain two additional genes, *arsD* and *arsA*, such as

the *arsRDABC* operon in *E. coli* plasmid R773 (Figure 2) (Mobley et al., 1983). ArsA is an ATPase that provides energy to ArsB for the extrusion of arsenite and antimonite. ArsD is an arsenic chaperone, which transfers trivalent metalloids As(III) and antimonite (Sb(III)) to ArsA. Interaction with ArsD increases the affinity of ArsA for arsenite, thus increasing its ATPase activity at lower concentrations of arsenite and enhancing the rate of arsenite extrusion. These cells are consequently resistant to environmental concentrations of arsenic (Lin et al., 2006).

Co-existence of *arsA* and *arsD* in *ars* operons

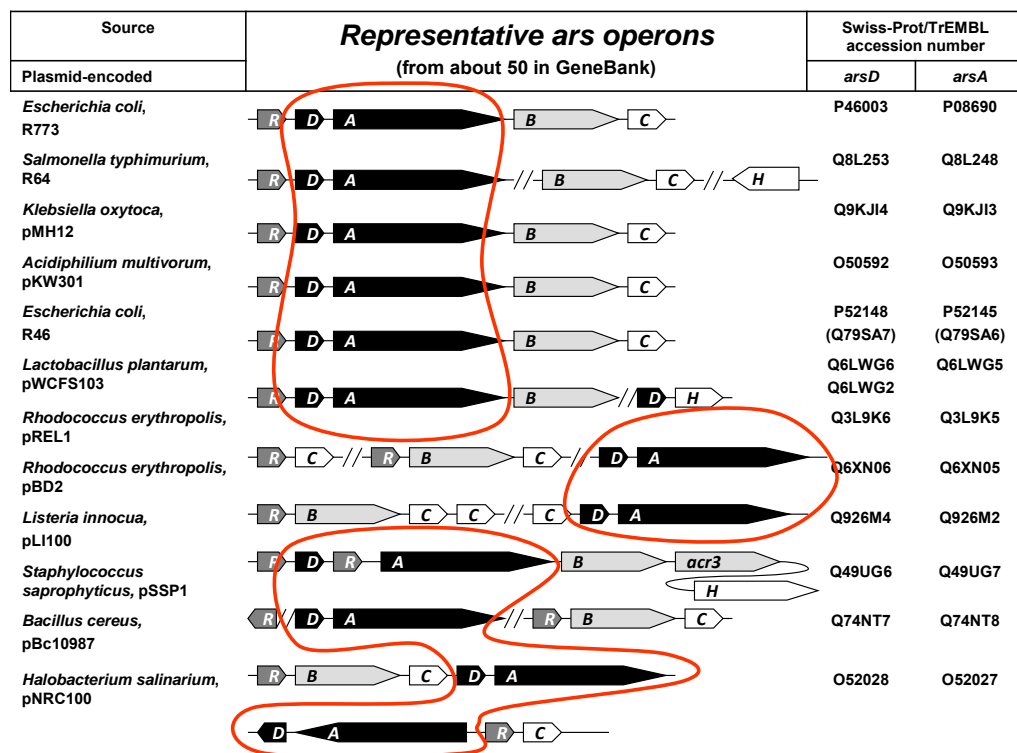


Figure 3. A cross section of *ars* operons representing the coexistence of *arsA* and *arsD* genes (Lin et al. 2006)

There are more than fifty bacterial and archaeal arsenic resistance operons and gene clusters that contain *arsA* and *arsD* genes (Figure 3). It is striking that *arsA* and *arsD* genes are always found together in *ars* operons. The order of the genes in those operons may differ from each other, but the *arsD* gene nearly always precedes an *arsA* gene. The linkage of these two genes suggests first, that ArsD and ArsA co-evolved before their association with ArsB, second that the *arsDA* genes moved laterally into an *ars* operon as a unit, and third, that ArsD has a biochemical function related to ArsA in arsenic detoxification (Lin et al., 2007b).

ArsA ATPase

The *ars* operon of R-factor R773 encodes a metalloid extrusion pump that confers resistance to As(III) and Sb(III) in *E. coli*. This efflux pump has two subunits, ArsA and ArsB. ArsA ATPase is the 63-kDa catalytic subunit of the pump. ArsB is a 45-kDa integral membrane protein that serves as the membrane anchor for ArsA and also the oxyanion-translocating sector of the pump (Dey et al., 1994). Arsenic efflux in bacteria can be catalyzed by either ArsB alone, functioning as a secondary transporter, or by the ArsAB complex, functioning as a transport ATPase (Dey and Rosen, 1995). *E. coli* can utilize either mode physiologically; however, the ATP-coupled pump is more efficient, capable of producing concentration gradients as high as 10^6 , equivalent to a concentration of 1 nM intracellular arsenite at 1 mM external arsenite.

ArsA is normally bound to ArsB *in vivo*, but it can be overexpressed and purified as a soluble protein from the cytosol (Rosen et al., 1988a). The soluble ArsA exhibits ATPase activity that is stimulated by either As(III) or Sb(III). The 583-residue ArsA ATPase has two homologous halves, A1 and A2, connected by a short linker. Each half has a consensus nucleotide binding domain (NBD) and both NBDs are required for ATPase activity and oxyanion transport (Karkaria et al., 1990; Kaur and Rosen, 1992). The crystal structure of the MgADP bound form of ArsA was determined (Figure 4) at 2.3 Å resolution (Zhou et al., 2000). The A1 and A2 halves of the enzyme are related by a pseudo-2-fold axis of symmetry. The two NBDs are in close proximity to each other and are located at the A1-A2 interface. In each NBD, Mg²⁺ is octahedrally coordinated with the β-phosphate of ADP, a threonine hydroxyl group, and several water molecules. In the solved structure, the two NBDs appear to be in different conformations despite extensive topological similarities, with NBD1 almost completely closed and the NBD2 fully open (Zhou et al., 2000, 2001). To determine the role of each NBD in substrate binding and catalysis, a thrombin site was introduced into the linker region that connects the A1 and A2 halves. Following covalent radiolabeling with 8-azidoATP and thrombin cleavage, the A1 and A2 halves migrated with different mobilities on sodium dodecyl sulfate – polyacrylamide gel electrophoresis. In the absence of metalloids, both NBDs bind and hydrolyze ATP. However, in the presence of metalloids, although both NBDs hydrolyze ATP, hydrolysis in NBD1 is stimulated to a much greater extent than NBD2.

These experiments suggested that the two homologous halves of ArsA are functionally nonequivalent (Jiang et al., 2005).

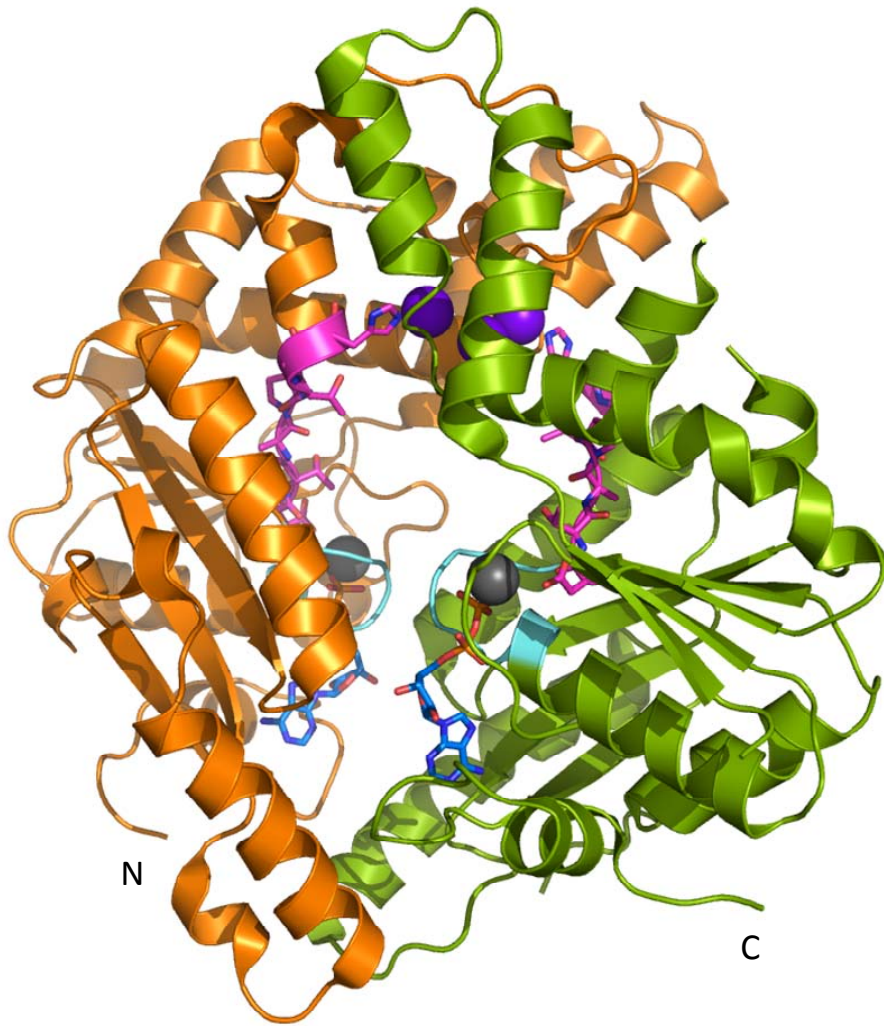


Figure 4. Overall structure of R773 ArsA ATPase (Zhou et al., 2000). The secondary structure elements are drawn as cartoon diagram. The A1 domain is colored in orange and the A2 domain in split pea. The phosphate binding loops (P-loops) are colored cyan. ADP bound in the two NBDs is shown as stick models and colored according to atom type (carbon, sky blue; nitrogen, blue; oxygen, red; phosphorus, yellow). Two stretches of seven residues with the identical sequence D_{142/447}TAPTGH_{148/453} connect the A1 and A2 NBDs with the MBD. The DTAPTGH sequences are shown as stick models and colored as carbon, magenta; nitrogen, blue; and oxygen, red. Bound Sb(III) (purple) and Mg²⁺ (gray) are shown as space-filling models. (Zhou et al, 2000)

A novel metalloid binding domain (MBD) is also located at the A1-A2 interface and is over 20 Å distant from the NBDs. The MBD contains three metalloid atoms: one As(III) or Sb(III) is coordinated to His148 (A1) and Ser420 (A2), a second to Cys113 (A1) and Cys422 (A2), and the third to Cys172 (A1) and His453 (A2) (Zhou et al., 2000). Kinetic studies indicated that the three metalloid atoms bind with different affinities (Walmsley et al., 2001b), suggesting that the three metalloid binding sites may allow the pump to operate in different ranges of ion concentration. Each of the amino acid lining the MBD has been altered by site directed mutagenesis. Alteration of Cys113, Cys172, and Cys422 resulted in substantial loss of metalloid stimulated ATPase activity (Bhattacharjee et al., 1995; Bhattacharjee and Rosen, 1996; Ruan et al., 2006, 2008), while mutation of His148 and His453 showed a modest decrease in allosteric activation of the enzyme (Bhattacharjee and Rosen, 2000). Cys113 and Cys422 form the high affinity metalloid binding site (Ruan et al., 2006). Although, metalloid stimulation of ArsA ATPase activity enhances the ability of the pump to reduce the intracellular concentration of oxyanions, high affinity binding of metalloid by ArsA is not obligatory for transport or resistance.

It appears that binding of metalloid to MBD provides an evolutionary advantage to survive in low levels of arsenite ubiquitously present in the environment (Ruan et al., 2006). As indicated above, the crystal structure of ArsA shows two other bound metalloid atoms, one bound to Cys172 and His453, and the other liganded to His148 and Ser420. The contribution of those putative

metalloid sites was examined. There was little effect of mutagenesis of residues His148 and Ser420 on metalloid binding. However, a C172A ArsA mutant and C172A/H453A double mutant exhibited significantly decreased affinity for Sb(III). These results suggested that, first, there is only a single high-affinity metalloid binding site in ArsA, and second, Cys172 controls the affinity of this site for metalloid and hence the efficiency of metalloactivation of the ArsAB efflux pump (Ruan et al., 2008).

The transfer of information of metal occupancy at MBD to the two NBDs is performed by two signal transduction domains (STDs). Two stretches of residues, D₁₄₂TAPTGH₁₄₈ in A1 STD and D₄₄₇TAPTGH₄₅₃ in A2 STD, physically connect the MBD to NBD1 and NBD2, respectively. By introducing tryptophan residues in proximity to the D_{142/447}TAPTGH_{148/453} sequence, conformational changes have been observed in response to binding of nucleotide and metalloid at the NBDs and MBD, respectively (Zhou et al., 1995; Zhou and Rosen, 1997; Zhou et al., 2002). The roles of Asp142 in A1 D₁₄₂TAPTGH sequence, and Asp447 in A2 D₄₄₇TAPTGH sequence was investigated after altering the aspartates individually to alanine, asparagine, and glutamate by site-directed mutagenesis. The Asp142 mutants were sensitive to As(III) to varying degrees, whereas the Asp447 mutants showed the same resistance phenotype as the wild type. Each altered protein exhibited varying levels of both basal and metalloid-stimulated activity, indicating that neither Asp142 nor Asp447 is essential for catalysis. Biochemical characterization of the altered proteins imply that Asp142 is involved in Mg²⁺ binding and also plays a role in signal transduction between

the catalytic and activation domains. In contrast, Asp447 is not nearly as critical for Mg^{2+} binding as Asp142 but appears to be in communication between the MBD and NBD. These results indicate that Asp142 and Asp447, located on the A1 and A2 halves of the protein, have different roles in ArsA catalysis (Bhattacharjee et al., 2008), consistent with the hypothesis that these two halves are functionally nonequivalent.

The mechanism of allosteric activation of ArsA ATPase has been elucidated at the molecular level from a combination of biochemical (Bhattacharjee et al., 2000), structural (Zhou et al., 2000, 2001) and kinetic experiments (Walmsley et al., 1999, 2001a, b). In summary, these studies indicate that ArsA exists in at least two different conformational forms, where bound ATP favors one form and bound metalloids the other. In the absence of activator, the enzyme undergoes a slow conformational change between these forms, leading to a lag in attaining maximal steady-state activity. Binding of oxyanions at MBD acts as molecular glue to bring the A1 and A2 halves of ArsA together and enhances the steady-state ATPase activity by inducing rapid product release and allowing the protein to adopt a conformation that can bind MgATP for the next catalytic cycle. In the presence of activator, ArsA avoids the rate-limiting isomerization at the end of the ATPase reaction and now ATP hydrolysis becomes rate-limiting for the reaction. When ArsA is bound to ArsB, the complex probably functions as a reciprocating engine, where cytosolic As(III)/Sb(III) accesses the high affinity metalloid binding site of ArsA. ATP

hydrolysis is linked with step wise transfer of the metalloid to the low affinity sites, followed by vectorial transport of metalloid into ArsB (Zhou et al., 2001).

ArsD

The R773 ArsD, a 120-residue polypeptide, was originally identified as a weak As(III)-responsive transcriptional repressor (Chen and Rosen, 1997). Since its regulatory properties are so poor, it is questionable whether that is the primary function of ArsD. More recently, ArsD has been shown to be a metalloid chaperone that delivers As(III) to ArsA, increasing ArsA's affinity for As(III), thus conferring resistance to environmental concentrations of arsenic (Lin et al., 2006). Without ArsD, ArsAB pump can only work in very high concentrations of As(III) found in extreme environments (Lin et al., 2006).

Evidence of physical interaction between ArsD and ArsA

ArsA and arsD genes are located in tandem in many ars operons, it suggests co-evolution for a common function, most likely arsenic detoxification. Cells coexpressing arsDAB are more resistant to As(III) ($IC_{50} = 13$ mM) compared to cells expressing only arsAB ($IC_{50} = 9$ mM) (Lin et al., 2007a). In a molecular competition experiment designed to resemble environmental conditions, a culture of cells of *E. coli* expressing either arsDAB or arsAB were mixed and grown at 10 μ M arsenite, a sub-toxic concentration that is found in many of the arsenic-contaminated regions of the world. After a week, the only cells remaining had all three genes, arsDAB. Thus, having an arsD gene gives bacteria a competitive advantage over cells having only arsAB while growing in sub-toxic concentrations

of arsenic. Additionally, cells expressing *arsDAB* accumulate less As(III) than those expressing only *arsAB* (Lin et al., 2006). The above observations suggest that ArsD acts to increase the efficiency of arsenic extrusion by the ArsAB pump and also implies that the two proteins must physically interact.

The interaction of ArsA and ArsD was demonstrated by yeast two-hybrid analysis (Lin et al., 2006). Among the four soluble proteins encoded by the R773 *arsRDABC* operon, ArsD was shown to interact with itself (as ArsD is a homodimer) and with ArsA. ArsD did not interact with either the ArsR repressor or the ArsC arsenate reductase. Conversely, ArsA interacted with ArsD only. Notably no As(III) or Sb(III) was added to the yeast culture media, indicating that ArsD and ArsA interact to some extent in the absence of added metalloid.

Chemical cross-linking with dibromobimane has shown that the metalloid binding sites of ArsA and ArsD come together within 6 Å of each other during interaction. This crosslinking was increased upon addition of MgATP which means there is increased interaction between the ArsD and the nucleotide bound form of ArsA (Lin et al., 2006).

Proposed mechanism of metalloid transfer from ArsD to ArsA

Native ArsD has 3 vicinal cysteine pairs, Cys12-Cys13, Cys112-Cys113 and Cys119-Cys120. Each of the vicinal cysteine pairs form a metalloid binding site (Li et al., 2001) and binds Sb(III) with a K_d of approximately 1 μ M (Lin et al., 2007a). When homologues of ArsD are aligned with R773 ArsD, only the Cys12, Cys13 and Cys18 are absolutely conserved and these three cysteines were

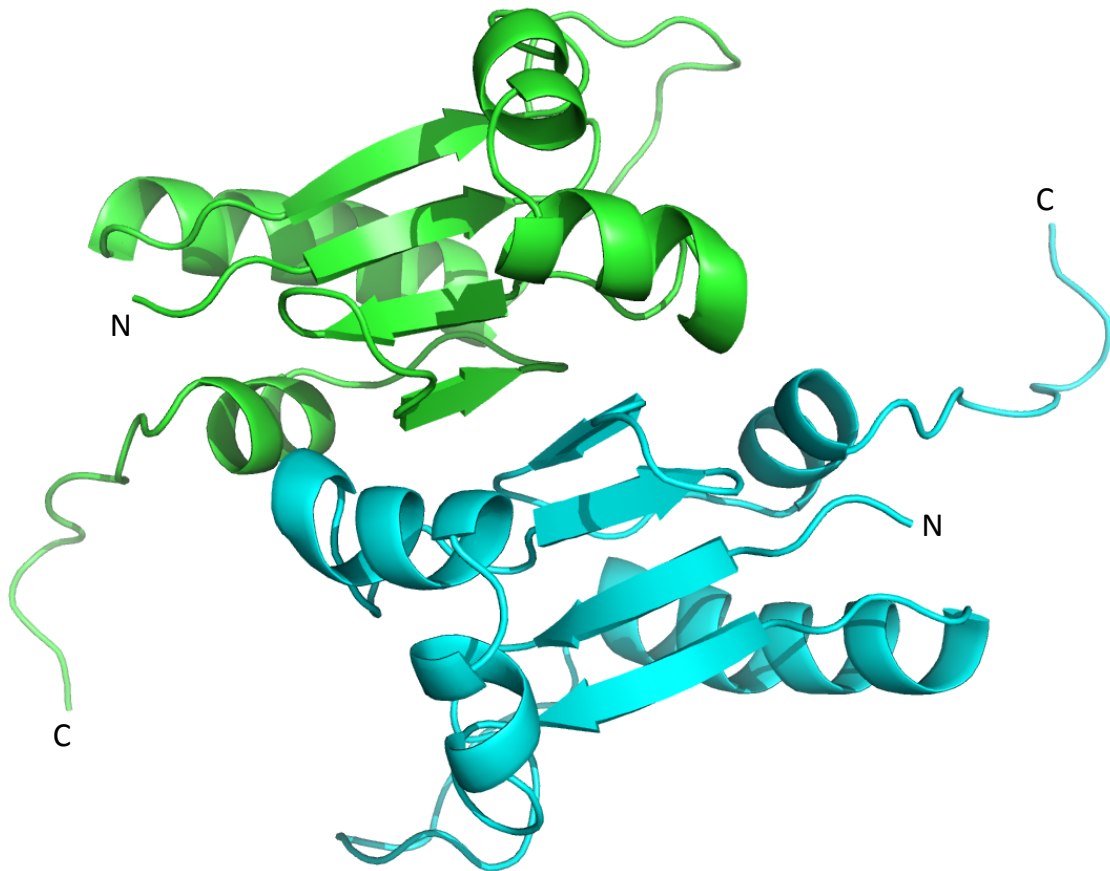
found to be critical for metalloid binding (Lin et al., 2007a). A construct of R773 ArsD with truncation at 109th residue (ArsD₁₀₉) was used to perform Extended X-ray Absorption Fine Structure (EXAFS) studies, which showed that Cys12, Cys13 and Cys18 form a three-coordinate thiol system for As(III) binding. A tryptophan-free construct based on the ArsD₁₀₉ construct was made and tryptophan inserted near the metalloid binding site was used to study binding with As(III) and Sb(III). The K_d of As(III) binding to ArsD was measured to be $\sim 2 \mu\text{M}$ with either the T15W or V17W ArsD (Yang et al., 2010).

An assay to measure transfer of As(III) from ArsD was designed in which ArsD with a maltose binding protein tag (MBP-tag) was pre-incubated with As(III) and bound to an amylose column and excess As(III) was washed from the column. Next, ArsA was passed through the column in various conditions to see if ArsD is able to transfer the As(III) to ArsA. The protein concentration and As(III) concentration of ArsA eluents were determined. The results showed that ArsD transfers As(III) to ArsA in presence of MgATP at room temperature but not at 4°C. Metalloid transfer does not occur in the presence of MgADP or the non-hydrolysable nucleotides, MgATPyS or MgAMP-PNP which means that ATP hydrolysis is required for As(III) transfer from ArsD to ArsA (Yang et al., 2010). It is inferred that As(III) transfer takes place in a conformation of ArsA attained during ATP hydrolysis.

The metalloid transfer could have taken place, either by dissociation of As(III) from ArsD and then binding to ArsA or by direct transfer from ArsD to ArsA. The ATPase assay was carried out in presence of meso-2,3-

dimercaptosuccinic acid (DMSA) which is a strong chelator of free As(III). ArsD was able to stimulate ArsA showing that transfer is direct (Yang et al., 2010). ArsD increases the affinity of ArsA for As(III) from millimolar to micromolar range (Lin et al., 2006). The affinity of ArsD for As(III) is greater than that for ArsA. Hence, it does not seem likely that As(III) transfer from ArsD to ArsA can be explained by free dissociation of As(III) from ArsD. However, it is likely that the energy of ATP hydrolysis at NBD of ArsA coupled with mass action of As(III) efflux from cell should explain the transfer of As(III) from ArsD to ArsA.

ApoArsD has been crystallized as wild type and cysteine free derivatives



(Figure

Figure 5. Crystal structure of ArsD dimer (Ye et al., 2010)

5) (Ye et al.,

2010). Wild type ArsD crystals were determined to 2.1 Å resolution in X-ray data collection whereas the cysteine free mutant was solved to 1.4 Å. The ArsD monomer has a core of four β-strands flanked by four α-helices with a thioredoxin fold (PDB ID 3MWH). ArsD aligns with *E.coli* thioredoxin TrxA (PDB ID 2TRX) with a RMSD (root mean square deviation) of 2.5 Å between the Cα atoms of the 72 aligned residues. The active site cysteine residues of TrxA are not congruent with Cys12, Cys13 or Cys18 in ArsD indicating that the As(III) binding site evolved independently. Nuclear Magnetic Resonance Spectroscopy (NMR) solution structure determination of ArsD was carried out to identify amino-acid specific chemical environmental changes in ArsD coupled with binding of As(III) or Sb(III). High resolution ¹⁵N TROSY HSQC (¹⁵N Transverse Relaxation Optimized Spectroscopy with Heteronuclear Single Quantum Coherence Spectroscopy) spectrum indicates that the protein is well-folded with the number of peaks consistent with the protein existing as a symmetric homodimer (Ye et al., 2011). Partial assignments were made for the protein residues. The predicted secondary structure in solution is in reasonable agreement with the crystal structure with only a few differences. The structure of oxidized orthologue of ArsD (PDB ID 3KTB) has allowed modeling of the arsenic binding loop. PDB ID 3KTB's 2.1 Å structure can be superimposed with a RMSD of 1 Å. The 11-residue metalloid binding loop of ArsD is present as a 14-residue loop in 3KTB with intermolecular and intramolecular disulfide bonds. The distances of 2.24 Å between As(III) and cysteines was determined from EXAFS (Extended X-ray Absorption Fine Structure) studies (Yang et al., 2010).

Metal bound ArsD interacts with ArsA as it alternates between open and closed conformations during its catalytic cycle (Figure 6) (Li and Rosen, 2000). The crystal structure of the closed form of ArsA has been obtained (Zhou et al., 2000). The open form of ArsA has been modeled based on the Get3 homolog of ArsA in yeast which is involved in targeting tail-anchored proteins in the endoplasmic reticulum (Auld et al., 2006). Get3 has been crystallized in open (nucleotide free) and closed conformations (ADP.AIF₄⁻ bound) (Bozkurt et al., 2009; Mateja et al., 2009). The NBD1 and NBD2 of ArsA was superimposed with the two monomers in Get3 open structure with RMSD of 2.3 Å and 3.0 Å, respectively. Thus, an open model of ArsA based on the open Get3 structure was generated which was used to examine if ArsA and ArsD have

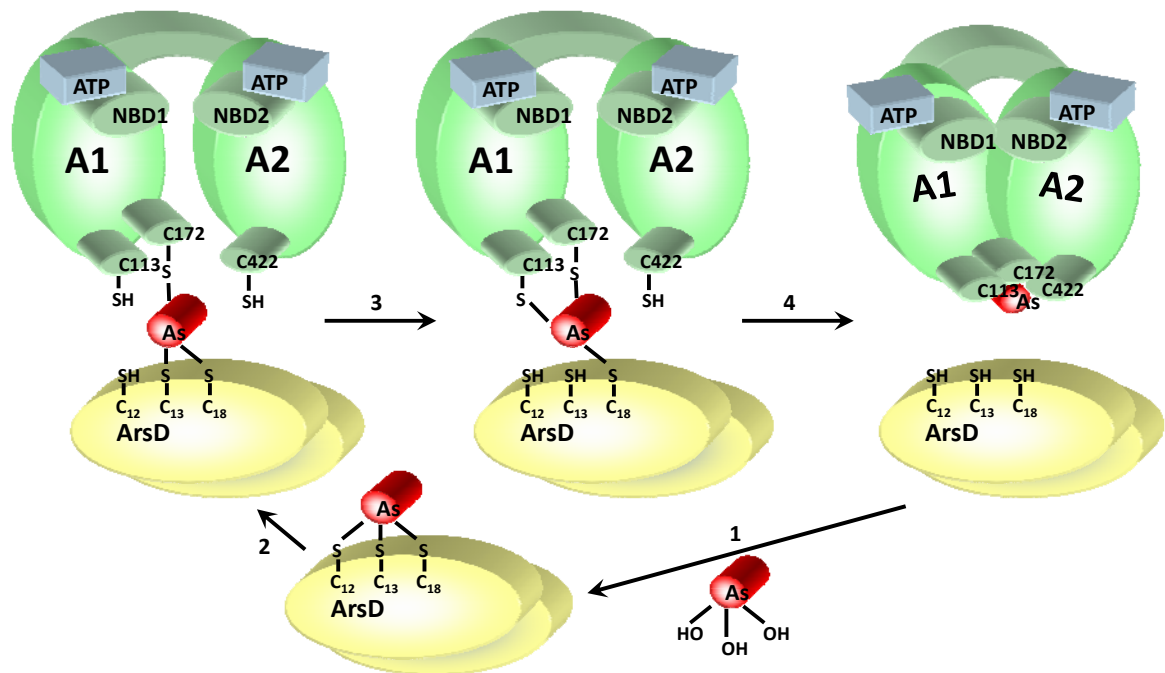


Figure 6. Proposed mechanism of metalloid transfer between ArsD and ArsA. ArsA alternates between open and closed conformations accepting As(III) from ArsD and translocating it out of the cell with the help of ArsB (not shown in figure) while expending ATP (Lin et al., 2007a).

complementary surfaces using web based ClusPro version 2.0. Out of the 108 top-scoring results from ClusPro docking server, one model had ArsD fitting into ArsA and showing close proximity between cysteine residues of ArsD and ArsA corroborating with the biochemical data of ArsA and ArsD metalloid binding sites (Ye et al., 2010). A separate yeast two hybrid study of ArsA and ArsD mutants corroborated with the residues found in the docking study (Yang et al., 2010) .

The arsenic chaperone, ArsD, is the first and, to date, only example of a metallochaperone that protects the cell from metal toxicity. Traditionally, metallochaperones ensure the safe delivery of the metal ion to its proper intracellular destination, guiding and protecting the metal ion, while facilitating appropriate partnerships (O'Halloran and Culotta, 2000). These include prokaryotic and eukaryotic metallochaperones for copper (Palumaa, 2013) and iron (Philpott, 2012), and prokaryotic nickel (Ge et al., 2013) chaperones.

Although extensive research have been carried out on both the structural details of ArsA and ArsD and their biochemical roles, limited work has been performed to understand and identify the surface residues of ArsA interacting with ArsD. Chapter II of this dissertation discusses the experiments conducted to examine the interaction between ArsA and ArsD.

Biomethylation and its importance

Biomethylation is one of the common transformations observed in nature. It is the addition of a methyl moiety to an atom. Methylation modulates the bioavailability, bioactivity and reactivity of acceptor atoms and the most common

methyl accepting atoms are C, O, N and S (Liscombe et al., 2012). Addition of methyl group is done enzymatically and requires an activated methyl group. One of the most common activated methyl group used by organisms is the one found in S-adenosylmethionine (SAM). SAM is a conjugate of methionine and adenosine moiety of ATP formed in an enzyme catalyzed reaction by methionine adenosyl transferase. SAM is one of the most used metabolic substrates after ATP (Loenen, 2006). The chemical reactivity of SAM is a consequence of the electrophilic nature of its methyl group beside the sulfonium center (Fontecave et al., 2004). SAM may have predated life itself on earth as a result of experiments showing that the basic reactions required for SAM synthesis could have been possible in the early earth environment (Waddell et al., 2000). The favorable thermodynamics associated with SAM is responsible for it becoming the second most used substrate after ATP. The SAM reaction proceeds mostly by a S_N2 type mechanism with the methionine sulfur as the nucleophile and the substrate atom as the electrophile (Scavetta et al., 2000). SAM is the methyl donor for a wide variety of biological molecules like DNA, RNA, histones and proteins. The reactions with these biological molecules are important for replication, transcription, DNA repair and epigenetic modifications.

Imbalance of methionine cycle for SAM recycling can cause human disease. One of the primary sources of the methyl group for humans is folate from foodstuffs. Low levels of serum folate, high levels of plasma homocysteine and polymorphisms in the MTHF receptor are implicated in SAM depletion and a

wide range of diseases (Coppen and Bolander-Gouaille, 2005; Ulrey et al., 2005). The natural product methyltransferases are SAM methyltransferases found in plants which are responsible for methylation of phenolics, catechols, hexoses, non-ribosomal peptides, hexosamines, primary, secondary and tertiary amines, and are also involved in caffeine biosynthesis (Liscombe et al., 2012).

Evolution of methyltransferases

Early sequence alignments of SAM dependent methyltransferases showed the presence of three motifs that were found to be common to this class of protein (Figure 7) (Martin and McMillan, 2002). The conserved sequences were predicted to contribute in binding of the substrate SAM and/or the product S-adenosylhomocysteine (SAH). Some of the motifs were also identified in certain nonmethyltransferases like SAM synthetase and SAH hydrolase (Kagan and Clarke, 1994). SAM methyltransferases show both functional divergence

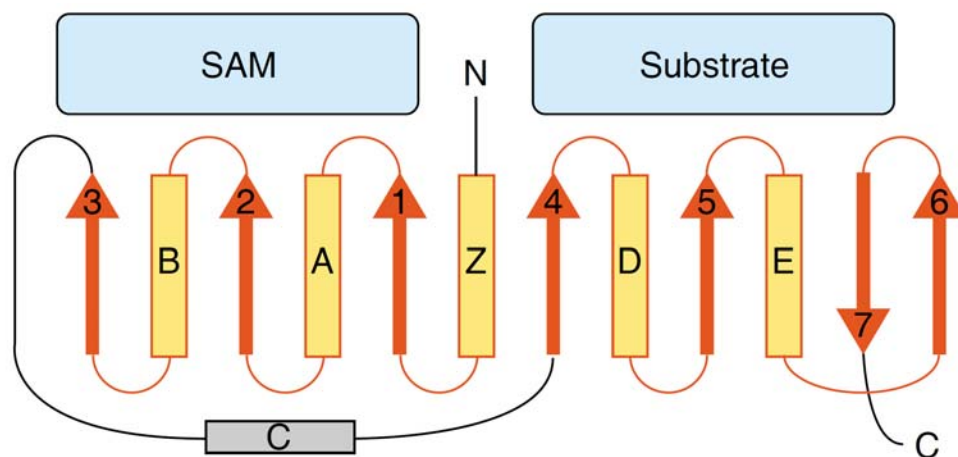


Figure 7. Topology of the core fold of SAM methyltransferases with SAM and substrate binding fold. Yellow cylinders are helices and red arrows are β -strands (Martin and McMillan, 2002).

and convergence in its evolution. The Rossmann fold and triosephosphate isomerase (TIM) barrel have been repeatedly used for different types of SAM conversion during evolution. The Rossmann fold is a protein spatial structure consisting of alternating β pleated sheets and α helices, the β pleated sheets forming a central planar sheet and the helices filling two layers, one on each side of the plane (Kozbial and Mushegian, 2005). The functionally important conserved residues are often located in the C terminus of the β -strands or in the loops adjoining the β -strands (Lesk, 1995). There are six highly conserved regions of SAM binding region which have been categorized as motif I through VI. The important features of which have been summarized in Table 1.

Table 1. Conserved motifs of SAM methyltransferases (Kozbial and Mushegian, 2005)

Motifs	Characteristics
I	GXGXXG conserved in the C-terminal and is hallmark SAM-binding site of Rossmann-fold SAM-dependent methyltransferases. Well-conserved aspartate or glutamine residue in middle of β -strand 1 and positively charged residue/residues close to the N-terminus of this β -strand.
II	Includes β -strand 2 and adjoining turn. Partially conserved acidic residue at the C-terminus of the strand.
III	Corresponds to Motif III and located at edge of Rossmann fold's β -sheet
IV	β -strand 4 and flanking loops with a conserved aspartate/ glutamate/ asparagine residue located at the extreme N-terminus of the strand
V	Helix after motif IV
VI	β -strand 5

Arsenic biomethylation

Biomethylation of arsenic is widespread and occurs in all three domains of life, bacteria, archaea and eukaryota (Sumi and Himeno, 2012; Ye et al., 2012).

The first example of biomethylation of a metalloid was given by the Italian physician Bartolomeo Gosio in the 1890s, who described the production of a toxic, arsenic gas with a garlic-like odor (hence the name “Gosio gas”) from various fungi, when they were grown on organic matter or soil samples containing arsenic compounds. Frederick Challenger demonstrated that Gosio gas is trimethylarsine, $(\text{CH}_3)_3\text{As}$ or $\text{TMA}(\text{III})$ (Challenger and Higginbottom, 1935). In 2002, Thomas and colleagues identified an $\text{As}(\text{III})$ -methyltransferase ($\text{As}3\text{MT}$) from rat liver cytosol as an enzyme responsible for arsenic methylation (Lin et al., 2002).

While the molecular mechanisms of arsenic biomethylation have been studied intensively over the past few years, many of the mechanistic details of the pathway are still elusive. Challenger proposed a scheme in which arsenate can be converted to $\text{TMA}(\text{III})$ (Figure 8) via a series of alternating reduction and oxidative methylation (Challenger, 1947, 1951). At the time the Challenger mechanism was proposed, neither the methyl donor nor the reducing equivalents were known. Later, it was generally accepted that SAM is the methyl donor. The starting species in the Challenger pathway (also known as the classical pathway) is $\text{As}(\text{V})$ and then in each successive step, there is the reduction of pentavalent arsenic species to trivalent species followed by an oxidative methylation by SAM to obtain the methylated pentavalent form. In all, $\text{As}(\text{III})$ undergoes four reductions and three methylations to form $\text{TMA}(\text{III})$. The pentavalent arsenical species in the Challenger pathway are $\text{As}(\text{V})$, $\text{MA}(\text{V})$, $\text{DMA}(\text{V})$, $\text{TMA}(\text{V})\text{O}$ and the trivalent species are $\text{As}(\text{III})$, $\text{MA}(\text{III})$, $\text{DMA}(\text{III})$ and $\text{TMA}(\text{III})$.

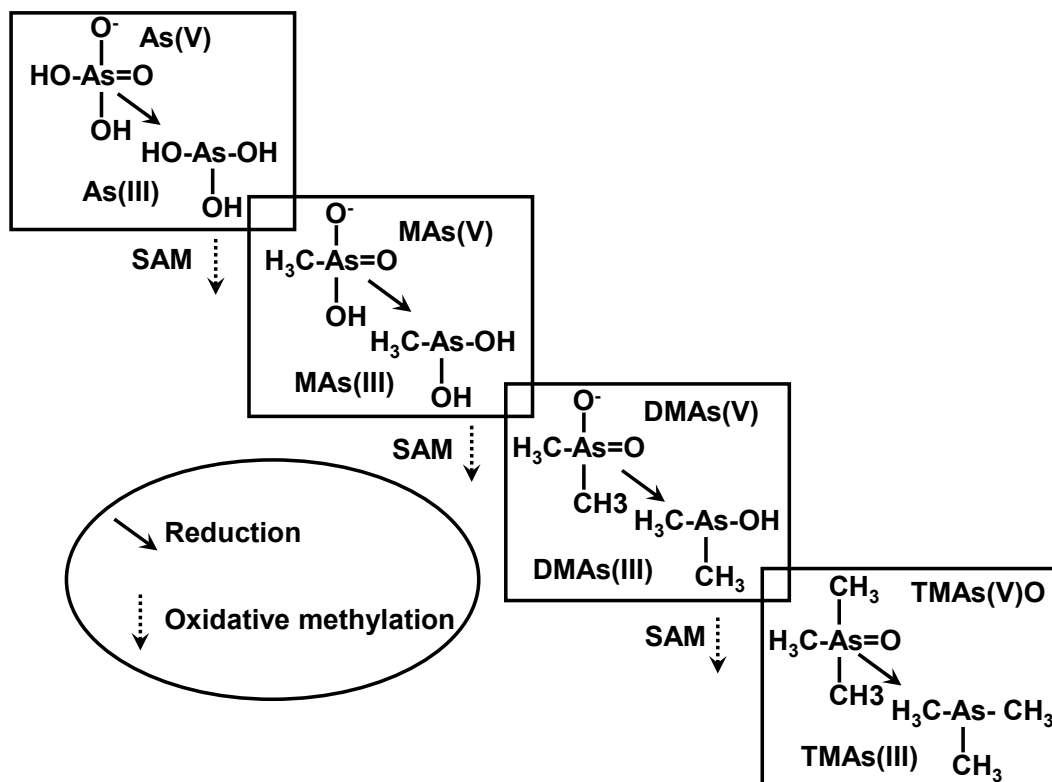


Figure 8. The Challenger's pathway for reductive methylation of inorganic As(V) into volatile, organic TMA(III).

While many of the arsenic species proposed by the Challenger pathway were identified, it was also observed that metabolism of As(III) in rat liver leads to the excretion of arsenic-glutathione (As-GSH) complexes, such as arsenic triglutathione, As(GS)₃, and monomethylarsenic diglutathione, MAs(GS)₂, in bile (Kala et al., 2000). These arsenicals were not described in the Challenger pathway. To address this anomaly, Hirano and his group (Hayakawa et al., 2005) proposed an alternate metabolic pathway in which glutathione conjugation of As(III) occurs first to form As(GS)₃, followed by methylation of As(GS)₃ in the presence of SAM to yield MAs(GS)₂. MAs(GS)₂ is subsequently methylated to dimethylarsinic glutathione, DMAsSG. Depending on GSH concentration,

MAs(GS)₂ and DMAsSG are in equilibrium with MAs(III) and DMAs(III), respectively, which may oxidize non-enzymatically or after exposure to air to MAs(V) and DMAs(V), the observed urinary species (Hayakawa et al., 2005).

The bacterial homologue of As₃MT, designated as ArsM, has been observed in a number of *ars* operons and under the control of ArsR repressor, suggesting that ArsM might have a role in arsenic resistance. ArsM from *Rhodopseudomonas palustris* has been shown to confer As(III) resistance when expressed in Δ *ars E. coli* (Qin et al., 2006). Further chemical speciation analysis showed that the purified enzyme in the presence of SAM and GSH can convert As(III) to DMAs(V) and TMs(V)O and finally TMs(III) gas. Methylation of As(III) by ArsM resulted in the loss of arsenic from both the medium and the cells through volatilization. Therefore, methylation may also be considered a detoxifying process.

Whether arsenic biomethylation is a pathway of detoxification is still being debated. Some of the intermediate products, MAs(III) and DMAs(III), are more toxic than As(III) (Hirano and Kobayashi, 2006; Sakurai et al., 2006; Styblo et al., 2000). However, the pentavalent intermediate products, MAs(V) and DMAs(V), are much less toxic than As(III) (Styblo et al., 2000), and the end product, TMA(III), is almost nontoxic (Cullen, 2005). Research on the biomethylation of arsenic by bacteria and mammals have provided an understanding of some of the molecular processes. However, less is known about these processes in cyanobacteria and algae, and almost nothing is known in higher plants. No enzyme responsible for arsenic methylation has been found in plants. Therefore,

understanding the mechanism is the first step to harnessing the biomethylation process for bioremediation and the production of safe food.

Knowledge of enzymatic mechanism can only be acquired from studies with purified enzyme. One of the objectives of my research was to perform structure-function analysis of an AS3MT orthologue, *Chlamydomonas reinhardtii* ArsM (CrArsM) and is described in Chapter III.

CHAPTER II

Genetic mapping of the interface between the ArsA ATPase and ArsD metallochaperone

Introduction

Arsenic is a ubiquitous environmental toxic substance and enters the environment from both geochemical and anthropogenic sources. The Agency for Toxic Substances and Disease Registry puts arsenic at the top of its Substance Priority List (<http://www.atsdr.cdc.gov/spl/>) because this metalloid poses the most significant potential threat to human health due to its toxicity and potential for human exposure. In humans, exposure to arsenic is associated with a number of diseases, including several forms of cancer, cardiovascular disease, peripheral neuropathies and diabetes mellitus (Abernathy et al., 1999; Beane Freeman et al., 2004). As a consequence of continual exposure to arsenic, nearly every organism, from *Escherichia coli* to humans, has evolved pathways for arsenic detoxification (Zhu et al., 2014). The *arsRDABC* operon of *E. coli* plasmid R773 encodes five genes for arsenic detoxification (Chen et al., 1986; San Francisco et al., 1990). The ArsAB complex is an efflux pump that confers resistance to arsenicals and antimonials. ArsA is the catalytic subunit of the pump that hydrolyzes ATP in the presence of As(III) or Sb(III) (Hsu and Rosen, 1989). The ATP hydrolysis is coupled to extrusion of As(III) or Sb(III) through ArsB, which serves both as a membrane anchor for ArsA and as the substrate-conducting pathway (Tisa and Rosen, 1990). ArsD is an As(III) metallochaperone that

interacts with ArsA to increase arsenic resistance (Lin et al., 2006). Purified ArsD binds As(III) and transfers it to ArsA, stimulating its ATPase activity (Lin et al., 2006; Yang et al., 2010). The apo structure of ArsA (Zhou et al., 2000) and ArsD (Ye et al., 2010) have each been determined by x-ray crystallography, and structural models of the As(III)-bound forms of both protein and the ArsD-ArsA complex have been constructed (Ye et al., 2010).

A yeast two-hybrid genetic mapping approach identified seventeen residues of ArsD that either enhance or reduce interaction with ArsA (Yang et al., 2011). These residues included Cys12, Cys13 and Cys18, which form the As(III) binding site, and a series of N-terminal residues that form a spine along the surface of the protein. Independently, an *in silico* docking model (Ye et al., 2010) identified many of the same residues obtained from the genetic mapping studies, suggesting that ArsD and ArsA interact at an interface between the two proteins (Yang et al., 2011).

ArsD has six lysine residues at positions 2, 37, 60, 62, 90, and 104. The quadruple lysine mutant K2A/K37A/K62A/K104A of ArsD (4KA ArsD) did not interact with wild type ArsA in yeast two hybrid studies and also was not able to stimulate ATPase activity in wild type ArsA (Yang et al., 2011). The metalloid binding ability of 4KA ArsD was determined to be similar as the wild type (Yang et al., 2011). In contrast, the quadruple K2A/K37R/K62R/K104A ArsD derivative stimulated ArsA activity nearly as well as wild type ArsD. In the 100 closest ArsD homologues in the NCBI database, residue 37 is either lysine or arginine, and residue 62 is always lysine (Yang et al., 2011). These observations suggested

that alanine substitutions in ArsD abolish its interaction with ArsA, but arginine substitutions are permitted in Lys37 and Lys62.

As mentioned above, ArsD has a dual role: first, transfer of metalloids from ArsD to ArsA and second, to enhance the catalytic activity of ArsA. Although extensive research have been carried out on both the structural details of ArsA and ArsD and their biochemical roles, limited studies have been performed to understand and identify residues of ArsA that either directly interact with ArsD or indirectly facilitate interaction. In the present study, the interaction between ArsA and ArsD was further examined by screening for suppressor mutants of ArsA that interact with 4KA ArsD.

Materials and methods

Reagents

3-Amino-1, 2, 4-triazole (3-AT) was purchased from MP Biomedicals (Solon, OH). 5-Fluoroorotic Acid (5-FOA) was purchased from Thermo Scientific (Pittsburgh, PA). Yeast Minimal Media-SD Base and Amino Acid Dropout Mixes (-Leu/-Trp and -His/-Leu/-Trp) were purchased from Clontech (Mountain View, CA). Unless otherwise mentioned, all other chemicals were obtained from Sigma-Aldrich (St. Louis, MO).

Strains, plasmids and media

E. coli strain JM109 was used for molecular cloning (Table 2). *E. coli* strain BL21(DE3) was used for protein expression and purification. The *arsA* gene with

Table 2. Strains and plasmids

Strains/Plasmids	Genotype/description	Reference
<u><i>E. coli</i> strains</u>		
JM109	e14 ⁻ (McrA ⁻) <i>recA1 endA1 gyrA96 thi-1 hsdR17</i> (<i>rK⁻ mK⁺</i>) <i>supE44 relA1 Δ(lac-proAB)</i> [F' <i>traD36 proAB lac^R ZΔM15</i>]	(Green et al., 2012)
BL21(DE3)	<i>fhuA2 [lon] ompT gal (λ DE3) [dcm] ΔhsdS λ DE3 = λ sBamHlo ΔEcoRI-B int:::(lac::PlacUV5::T7 gene1) i21 Δnin5</i>	(Green et al., 2012)
<u><i>S. cerevisiae</i> strains</u>		
AH109	<i>MATa, trp1-901, leu2-3, 112, ura3-52, his3-200, gal4Δ, gal80Δ, LYS2 :: GAL1_{UAS}-GAL1_{TATA}-HIS3, GAL2_{UAS}-GAL2_{TATA}-ADE2, URA3 :: MEL1_{UAS}-MEL1_{TATA}-lacZ</i>	Clontech
<u>Plasmids</u>		
pACT2	GAL4 ₍₇₆₈₋₈₈₁₎ activation domain, <i>LEU2</i> (Ap ^r)	Clontech
pGBT9	GAL4 ₍₁₋₁₄₇₎ DNA-binding domain, <i>TRP1</i> (Ap ^r)	Clontech
pAD-A	<i>arsA</i> gene cloned in pACT2 (Ap ^r)	(Lin et al., 2006)
pBD-k	Kanamycin resistance gene PCR amplified from pET28a and inserted into pGBT9 at AatII site (Kn ^r)	(Yang et al., 2011)
pBD-k-D	Kanamycin resistance gene PCR amplified from pET28a and inserted into pBD-D at AatII site (Kn ^r)	(Yang et al., 2011)
pBD-k-4KA	DNA fragment encoding ArsD mutation K2A/K37A/K62A/K104A inserted into pBD-k (Kn ^r) at the EcoRI and BamHI sites.	(Yang et al., 2011)
pAD-AX	Single mutations (X) Q56R, V90F, T115K, F120I, V190I, K404R, and E506G separately introduced by site-directed mutagenesis into pAD-A	This study
pETy-dAhB	<i>arsA</i> cloned into pET28a with six histidine tags at the C-terminus	(Lin et al., 2006)
pETy-dAxB	Single mutations (X) Q56R, F120I, D137V separately introduced by site directed mutagenesis into pETy-dAhB	This study
pET28a	Expression vector for his-tagged proteins controlled by T7 promoter (Kn ^r)	Novagen
pET28a-ArsD109	<i>arsD</i> ₁₋₁₀₉ truncation inserted into pET28a at EcoRI and Sall sites (Kn ^r)	(Yang et al., 2011)
pET28a-ArsD109 _{K2A/K37A/K62A/K104A}	Mutations K2A/K37A/K62A/K104A constructed by site directed mutagenesis into pET28a-ArsD109 (Kn ^r)	(Yang et al., 2011)

a C-terminal six-histidine tag was cloned into the expression vector pET-28a as pETy-dAhB (Lin et al., 2006). Two forms of ArsD were used in this study. The gene for full-length wild type *arsD* was used in yeast two-hybrid analyses. All biochemical assays were performed with a fully active ArsD that is C-terminally truncated at residue 109 with a six-histidine tag (termed simply ArsD in this study). The gene for this ArsD was cloned in the expression vector pET28a as pET28a-ArsD109. *E. coli* cells were grown at 37 °C in Luria-Bertani (LB) medium (Green et al., 2012). Ampicillin (100 µg/ml), kanamycin (40 µg/ml) and 0.3 mM isopropyl-β-D-thiogalactopyranoside (IPTG) were added as required. Yeast cells were grown in complete yeast extract-peptone-dextrose (YPD) or minimal synthetic dextrose (SD) media with the appropriate supplements at 30 °C (Adams et al., 1998). Growth in liquid culture was estimated from the optical density at 600 nm.

DNA manipulation and mutagenesis

Plasmid extraction, DNA restriction endonuclease analysis, ligation and other general molecular biological procedures were performed as described (Green et al., 2012). Transformation of *E. coli* cells was carried out using a MicroPulser Electroporator (Bio-Rad, Hercules, CA). Transformation of yeast cells was performed using Fast Yeast Transformation kit from G-Biosciences (St. Louis, MO). DNA purification kits were purchased from Qiagen (Valencia, CA). Either a Qiaprep Spin Miniprep kit or a Qiaquick Gel Extraction kit was used to prepare plasmid DNA for restriction enzyme digestion, sequencing, and recovering DNA

fragments from agarose gels. Single mutants of *arsA* were made in pACT2-ArsA construct by site-directed mutagenesis using QuikChange Site-Directed Mutagenesis Kit from Agilent Technologies (Santa Clara, CA). The sequence of new plasmid constructs was confirmed by DNA sequencing using Sequetech DNA Sequencing Services (Mountain View, CA).

Generation of a random mutated library of PCR fragments

Random mutagenesis of *arsA* was performed using error-prone (ep)-PCR employing biased nucleotide composition of the PCR buffer, increasing the concentration of Mg^{2+} , and addition of Mn^{2+} to the reaction mixture (Cadwell and Joyce, 1992). The ep-PCR reaction mixture (50 μ l) contained 20 mM Tris-HCl (pH 8.4), 50 mM KCl, 7 mM $MgCl_2$, 0.5 mM $MnCl_2$, 0.2 mM each of dATP and dGTP, 1 mM each of dCTP and dTTP, 25 pmol each of the oligonucleotide primers (forward, CTA TTC GAT GAT GAA GAT ACC CCA CCA AAC CC; reverse, AGG TTA CAT GGC CAA GAT TGA AAC TTA GAG GAG), 80 ng of template DNA, 2.5 U of *Taq* DNA polymerase (Life Technologies). The PCR condition was 1 cycle of 96 °C for 3 min, 30 cycles of 94 °C for 30 s, 55 °C for 30 s, and 72 °C for 100 s, and, finally, 1 cycle of 72 °C for 10 min. The ep-PCR product was purified by agarose gel and quantified by absorption at 260 nm.

Yeast two-hybrid analysis

Plasmids pGBT9 and pACT2 were used as *S. cerevisiae* / *E. coli* shuttle vectors for yeast two-hybrid assay (Lin et al., 2006). The yeast strain, AH109 (Fields and Song, 1989) was used for yeast two-hybrid assays which is a GAL4-based yeast

two-hybrid system. AH109 was used to analyze protein-protein interaction or for selection of mutants retaining capability of interaction or showing stronger interaction in the presence of 3-AT. The plasmid pGBT9 was modified to pBD-k by inserting kanamycin resistance gene through *Aat*II site (Yang et al., 2011). To determine protein-protein interaction by growth of serial dilutions, the transformed cells were cultured overnight in SD medium at 30 °C, centrifuged at 10,000 *g*, and the pellets were washed with 20 mM Tris-HCl (pH 7.5) and adjusted to an OD₆₀₀ of 1. Portions of the cell suspension (1 µl) were inoculated in serial 10-fold dilutions on SD agar plates lacking histidine or with 3-AT at the indicated concentration. The plates were incubated at 30 °C for 3 days.

Sequencing of arsA mutant genes in yeast colonies

Each yeast colony was grown in SD medium. The plasmids were isolated from yeast by Zymoprep™ Yeast Plasmid Miniprep II kit (Zymo Research Corporation, Irvine, CA), transformed to *E. coli* JM109 and grown on LB plates with ampicillin. The plasmids were extracted from *E. coli* JM109, and *arsA* mutations in the pAD vector were sequenced with the pACT2 sequencing primers GAL4A3 (ACT TGC GGG GTT TTT CAG) and GAL4Act (TAC CAC TAC AAT GGA TG).

Protein expression and purification

Cells bearing the indicated plasmids were grown in LB medium overnight at 37°C and then diluted 50-fold into 1 L of the same medium. Proteins were expressed by induction with 0.3 mM isopropyl-β-D-thiogalactopyranoside at A₆₀₀ of 0.6-0.8 for 3 hrs. Cells were harvested by centrifugation and washed once with a buffer

containing 50 mM MOPS, pH 7.5, 0.5 M NaCl, 5 mM DTT and 10 mM 2-mercaptoethanol (Buffer A). The cells were suspended in 5 ml of Buffer A per gram of wet cells and lysed by a single passage through a French press at 20,000 psi. Diisopropyl fluorophosphate (DIFP) was added at 2.5 μ l/g wet cells immediately following French press. Unbroken cells and membranes were removed by centrifugation at 150,000 x g for 1 h at 4 °C. The supernatant was loaded at a flow rate of 0.5 ml/min onto a 10-ml Ni²⁺-nitrilotriacetic acid column (Qiagen) preequilibrated with Buffer A. The column was then washed with 200 ml of Buffer A followed by elution with 100 ml of Buffer A in which the concentration of imidazole was increased to 200 mM. ArsA-containing fractions were identified by sodium dodecyl sulfate-polyacrylamide gel electrophoresis (SDS-PAGE), pooled, concentrated by centrifugation using a 10-kDa-cutoff Amicon ultracentrifugal filter (Millipore), mixed with 10% glycerol, aliquoted and stored at -80 °C until used. The protein concentrations were determined from their absorption at 280 nm (Gill and von Hippel, 1989).

ATPase activity assays

ATPase activity was estimated using a coupled assay (Vogel and Steinhart, 1976), as described previously (Hsu and Rosen, 1989). The assay mixture contained in 200 μ l: 50 mM MOPS-KOH, pH 7.5, 0.25 mM Na₂EDTA, 5 mM ATP, 1.25 mM phosphoenolpyruvate, 0.25 mM NADH, 2 units of pyruvate kinase (Sigma) and lactate dehydrogenase (Sigma), 0.3 μ M ArsA, 3 μ M ArsD, and increasing concentrations of sodium arsenite, all pre-warmed to 37 °C. The

reaction was initiated by the addition of 2.5 mM MgCl₂ and followed by monitoring the decrease in absorbance at 340 nm using a Synergy H4 Hybrid Multi-Mode Microplate Reader (BioTek, Winooski, VT). The pathlength correction feature of the microplate reader was used to automatically normalize absorbance values to a 1 cm pathlength. The linear steady state rates were used to calculate the specific activity. Each assay was repeated at least three times with two separate batches of purified protein. The data were analyzed using SigmaPlot 12.0.

Measurement of metalloid binding

The buffer used for purification of ArsA was exchanged with a buffer containing 50 mM MOPS-KOH, pH 7.5, 0.25 mM EDTA using a Micro Bio-Spin P-6 gel column (Bio-Rad, Hercules, CA). Purified ArsA (10 μM) was incubated at 4 °C with 2.5 mM MgCl₂, 2 mM ATPγS, and 100 μM antimonite. After 1 h, each sample was passed through a Micro Bio-Spin P-6 gel column equilibrated with the same buffer. The concentration of protein in the flow-through was quantified from the absorption at 280 nm (Gill and von Hippel, 1989). An aliquot of the flow-through (50 μl) was diluted with 2% HNO₃, and the quantity of metalloid was measured by inductively coupled plasma-mass spectrometry (ICP-MS) with a PerkinElmer ELAN DRC-e. Antimony standard solutions in the range of 0-50 ppb in 2% HNO₃ were obtained from Ultra Scientific (North Kingstown, RI). From these data the molar ratio of Sb(III) to protein was calculated.

Model building and docking analysis

The model for the open form of ArsA was generated as described earlier (Ye et al., 2010). ArsD was modeled based on its crystal structure (PDB ID: 3MWH), and its missing active site loop (residues 10 to 19) was built using the MODELLER program (Sali and Blundell, 1993). The ArsA and ArsD models were energy minimized individually before being docked by the NAMD/VMD program (Humphrey et al., 1996; Phillips et al., 2005). Docking was done by the online server HexServer (<http://hexserver.loria.fr>) (Macindoe et al., 2010). Hydrogen bonds and interactions (ΔG^{diss} values) were calculated by the PDBePISA server (http://www.ebi.ac.uk/pdbe/prot_int/pistart.html) (Krissinel and Henrick, 2007). Domain rotation was performed using Chimera (<http://www.cgl.ucsf.edu/chimera>) (Pettersen et al., 2004). Structural models were rendered using PyMOL (<http://www.pymol.org>) (DeLano, 2001).

Results

ArsA ATPase mutants exhibiting stronger interaction with ArsD

The interaction of ArsA ATPase and ArsD metallochaperone has been demonstrated earlier (Lin et al., 2006) using the yeast two-hybrid analysis (Fields and Song, 1989). The *arsD* gene was cloned into the C-terminal DNA-binding domain (BD) as *bait*, and the *arsA* gene was cloned into the C-terminal activation domain (AD) as *prey* of the split *GAL4* transcriptional activator. Interaction of the two proteins resulted in expression of the *HIS3* reporter gene, allowing growth of yeast cells on media lacking histidine (Lin et al., 2006) (Figure 9). The yeast two-hybrid showed that the quadruple ArsD mutant K2A/K37A/K62A/K104A (4KA ArsD) does not interact with wild type ArsA (Yang et al., 2011) (Figure 9). In the present study, random mutagenesis of *arsA* was performed by ep-PCR induced with Mn^{2+} (Cadwell and Joyce, 1992) using a pair of primers homologous to the flanking regions of the *arsA* gene in plasmid pAD-WT ArsA, in which *arsA* was fused to the sequence for the GAL4 DNA-activation domain. The purified ep-PCR product was mixed with plasmid pAD-ArsA linearized with *Bam*HI and *Eco*RI, co-transformed with pBD-4KA ArsD into *Saccharomyces cerevisiae* strain AH109 and selected on SD (-His/-Leu/-Trp) plates. By this method the ep-PCR fragments integrate into pAD-ArsA *in vivo* through homologous recombination (Hua et al., 1997). Twenty-two colonies were isolated on SD (-His/-Leu/-Trp) plates that showed interaction with 4KA ArsD. The *arsA* gene from each colony

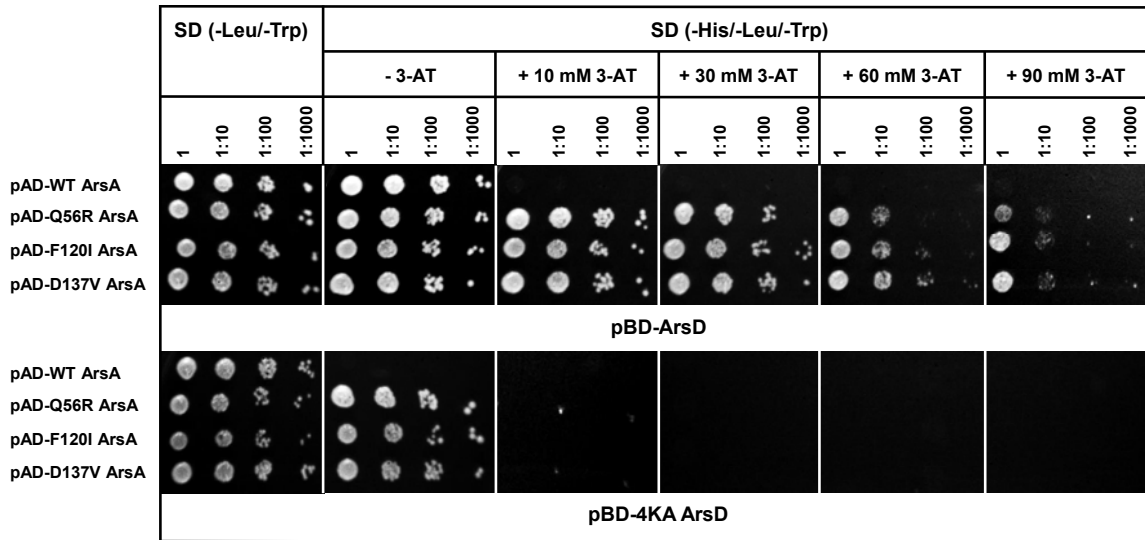


Figure 9. Yeast two-hybrid analysis of ArsA mutants exhibiting increased interaction with ArsD. *S. cerevisiae* strain AH109 bearing pAD-A (wild-type ArsA) or pAD-AX (single ArsA mutants Q56R, F120I or D137V) and either pBD-ArsD or pBD-4KA ArsD plasmids was grown in SD medium overnight and inoculated with 10-fold serial dilutions on SD agar plates lacking leucine, tryptophan or histidine and supplemented with the indicated concentrations of 3-AT. The plates were incubated at 30 °C for 3 days and scored for growth.

was sequenced. Of the 22 colonies, some were duplicates, and 15 were unique (Table 3). Of those 15, only one clone contained a single mutation (D137V), while the other clones contained multiple mutations in the *arsA* gene. Some substitutions such as Q56R, T115K, F120L and K404R were found in more than one mutant. Conservative substitutions were found at residue 120; Phe120 altered to either Ile or Leu. Using a combination of X-ray crystallography and *in silico* modeling and docking studies, 20 residues of ArsA were predicted to be within 4 Å of 30 ArsD residues, and they may form the contact regions between the two proteins (Ye et al., 2010). On the basis of the *in silico* predictions (Ye et al., 2010) and also because some of the mutations occurred more than once,

seven mutations (Q56R, V90F, T115K, F120I, V190I, K404R, and E506G) were reintroduced individually by site-directed mutagenesis into the *arsA* gene to

Table 3. *ArsA* mutants exhibiting interaction with 4KA *ArsD*

ArsA mutations	Times isolated
E34K/ G51C/ S55T/ R88I/ V90F/ V101L	1
E34K/ G51C/ R88I/ F120L/ K404R	1
Q56R/ T115K/ Q182L/ S210T/ N229D/ A345G/ T497M	1
Q56R/ T115K/ Q182L/ S210T/ N229D/ T497M	1
L71S/ V190I	1
V96A/ D121E	3
F120L/ E168G/ M354V/ N374I/ S376I	1
F120L/ L201P/ V435A/ S560R	1
F120I/ K404R	1
D137V	5
F162I/ Q307R	2
E168G/ M354V/ N374I/ K402M	1
Q182R/ E258V/ T451S/ E506G	1
Y188N/ Y305C/ E415G/ D447G	1
Y188N/ E415G/ D447G	1

examine whether the single *ArsA* mutants could interact with 4KA *ArsD*. Other multiple mutations in the *arsA* gene have not yet been analyzed. From the results of yeast two-hybrid analysis, three single *ArsA* mutants (Q56R, F120I and D137V) exhibited interaction with 4KA *ArsD* (Figure 9). These *ArsA* mutants also interacted with wild type *ArsD* (Figure 9).

The repressed transactivator two-hybrid system has been used to select for mutants with increased affinity for a binding partner (Hirst et al., 2001; Joshi et al., 2007; Yang et al., 2011). The *HIS3* gene encodes imidazole glycerol-phosphate dehydratase, catalyzing the sixth step in histidine biosynthesis. Histidine synthesis by this enzyme is competitively inhibited by 3-AT (Klopotowski and Wiater, 1965). If 3-AT is added to the medium, yeast cells must express higher levels of His3p to grow in the absence of histidine. AH109 yeast cells co-transformed with pBD-k-4KA (*ArsD* mutant K2A/K37A/K62A/K104A inserted into GAL4 binding domain in plasmid pGBT9) and pAD-AX (each of the single *ArsA* mutants (Q56R, F120I and D137V) fused to the GAL4 activation domain sequence in plasmid pACT2) could not grow on SD plates containing 10 mM 3-AT but lacking histidine, leucine and tryptophan. In contrast, AH109 yeast cells co-transformed with pBD-k-D (wild type *ArsD*) and pAD-AX (single *ArsA* mutants Q56R, F120I and D137V) were able to grow in the presence of up to 90 mM 3-AT (Figure 9). These results indicate that the single *ArsA* mutants have increased interaction with wild type *ArsD* but not with 4KA *ArsD*.

Analysis of altered ArsAs

Under physiological conditions, ArsA is a part of a complex with the ArsB protein in the inner membrane of *E. coli*. When expressed at high levels, ArsA is found predominantly as a soluble protein in the cytosol (Rosen et al., 1988b). Soluble ArsA has been purified and shown to be an As(III)-stimulated ATPase (Hsu and Rosen, 1989; Rosen et al., 1988b). Each altered ArsA was soluble in the cytosol and purified to >95% homogeneity using nickel affinity chromatography (Green et al., 2012). There was no difference between the wild type and altered proteins in mobility on sodium dodecyl sulfate - polyacrylamide gel electrophoresis, nor was abnormal degradation of the altered proteins observed (Figure 10), indicating that the altered proteins folded relatively normally.

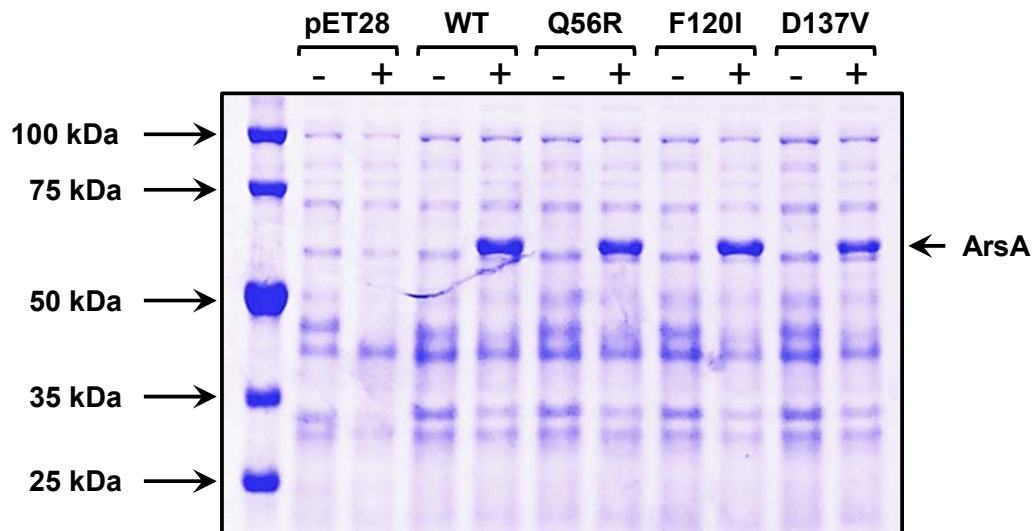


Figure 10. Expression of altered ArsAs. BL21(DE3) cells bearing either vector plasmid, wild type or altered *arsA* genes were grown and induced in the presence or absence of 0.3 mM IPTG. Cell suspensions were boiled in SDS sample buffer and analyzed by SDS-PAGE on 10% acrylamide gel. The position of migration of purified ArsA is indicated by an arrow.

ATPase activity of ArsA mutants

The ATPase activity of ArsA is stimulated by As(III) (Hsu and Rosen, 1989; Rosen et al., 1988b). In the absence of metalloid, the wild type showed a basal ATPase activity of 25 nanomoles of ATP hydrolyzed/min/mg of protein. In the presence of As(III), the wild type ArsA showed a 5.5-fold stimulation of ATPase activity over its basal rate. Addition of ArsD to the assay mix increases the affinity of ArsA for As(III), i.e., decreases the concentration of As(III) required for half-maximal stimulation of ArsA ATPase activity, thereby increasing its ATPase activity at even lower concentrations of As(III) (Lin et al., 2006). When wild type ArsD was added to the ATPase assay, the apparent affinity of ArsA for As(III) increased 8.5-fold (Figure 11 and Table 4). Addition of 4KA ArsD to the

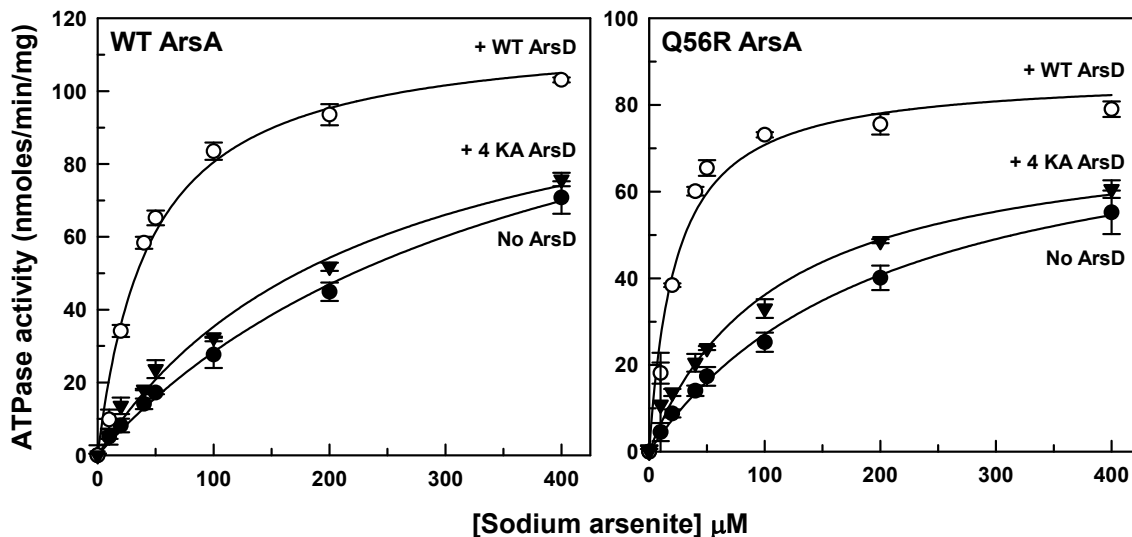


Figure 11. Activation of ArsA ATPase activity by ArsD. ArsA ATPase activity was assayed at the indicated concentrations of sodium arsenite in the presence or absence of either wild type or 4KA ArsD, as described under “Materials and Methods.” The basal ATPase activity was subtracted from the total activity. The curves were fitted using SigmaPlot 12.0, with the error bars representing the standard error. *Left panel*, Wild-type ArsA; *Right panel*, Q56R ArsA. (●), no ArsD; (○), wild type ArsD; (▼), 4KA ArsD.

Table 4. ArsA ATPase kinetics in the presence or absence of either wild type or 4KA ArsD

ArsA	ArsD ¹	V _{max} (nmol of ATP hydrolyzed/min/mg of protein)		As(III) [C] _{50% activation} (μ M)
		-As(III)	+As(III)	
Wild type	none	25 \pm 5	137 \pm 10	382 \pm 48
	Wild type	35 \pm 2	117 \pm 6	45 \pm 7
	4KA ArsD	35 \pm 2	117 \pm 10	231 \pm 40
Q56R	none	32 \pm 2	83 \pm 4	205 \pm 20
	Wild type	40 \pm 2	87 \pm 4	23 \pm 4
	4KA ArsD	40 \pm 2	75 \pm 5	109 \pm 16
F120I	none	75 \pm 2	75 \pm 2	-
	Wild type	80 \pm 2	80 \pm 2	-
	4KA ArsD	82 \pm 3	82 \pm 3	-
D137V	none	55 \pm 2	55 \pm 2	-
	Wild type	57 \pm 2	57 \pm 2	-
	4KA ArsD	59 \pm 2	59 \pm 2	-

¹ArsD was added in a 10-fold molar excess over ArsA

assay decreased the half maximal concentration for As(III) by 1.6-fold. Q56R ArsA showed a similar basal ATPase activity as the wild type, which was stimulated 2.8-fold in the presence of As(III). Addition of either wild type or 4KA ArsD to the assay mix increased the affinity for As(III) by 9-fold and 2-fold, respectively. These results indicate that, although 4KA ArsD does not stimulate ArsA ATPase activity to the same degree as the wild type, it has a small but significant effect on the affinity of ArsA for As(III).

The F120I and D137V ArsA showed a basal ATPase rate of 80 and 60 nanomoles of ATP hydrolyzed/min/mg of protein, respectively. The ATPase activity of either proteins were not stimulated by As(III); nor were any changes observed upon addition of either wild type or 4KA ArsD. Note that both F120I and D137V ArsA show a basal ATPase rate that is similar to the As(III)-stimulated rate of Q56R ArsA.

Binding of Sb(III) to altered ArsAs

To directly examine the binding of metalloid to ArsA, Sb(III) was used because it is bound with higher affinity than As(III) (Ruan et al., 2006). ArsA has a single high affinity metalloid binding domain (Bhattacharjee et al., 1995; Bhattacharjee and Rosen, 1996; Ruan et al., 2006, 2008). Each Sb atom is bound three-coordinately with Cys113, Cys172, and Cys422. Binding of Sb(III) to altered ArsAs was measured by rapid gel filtration. In the presence of saturating Mg^{2+} and the nonhydrolyzable nucleotide ATP γ S, a stoichiometry of one mole of Sb(III) per mole of protein was observed for both wild type and Q56R ArsA, whereas a stoichiometry of 0.8 mole of Sb(III) per mole of protein was observed for F120I and D137V ArsA (Figure 12). We do not consider this difference in Sb(III) binding as significant. Overall, these results indicate that while F120I and D137V ArsA do not show metalloid-stimulated ATPase activity, their affinity for metalloid is unaffected by the mutations.

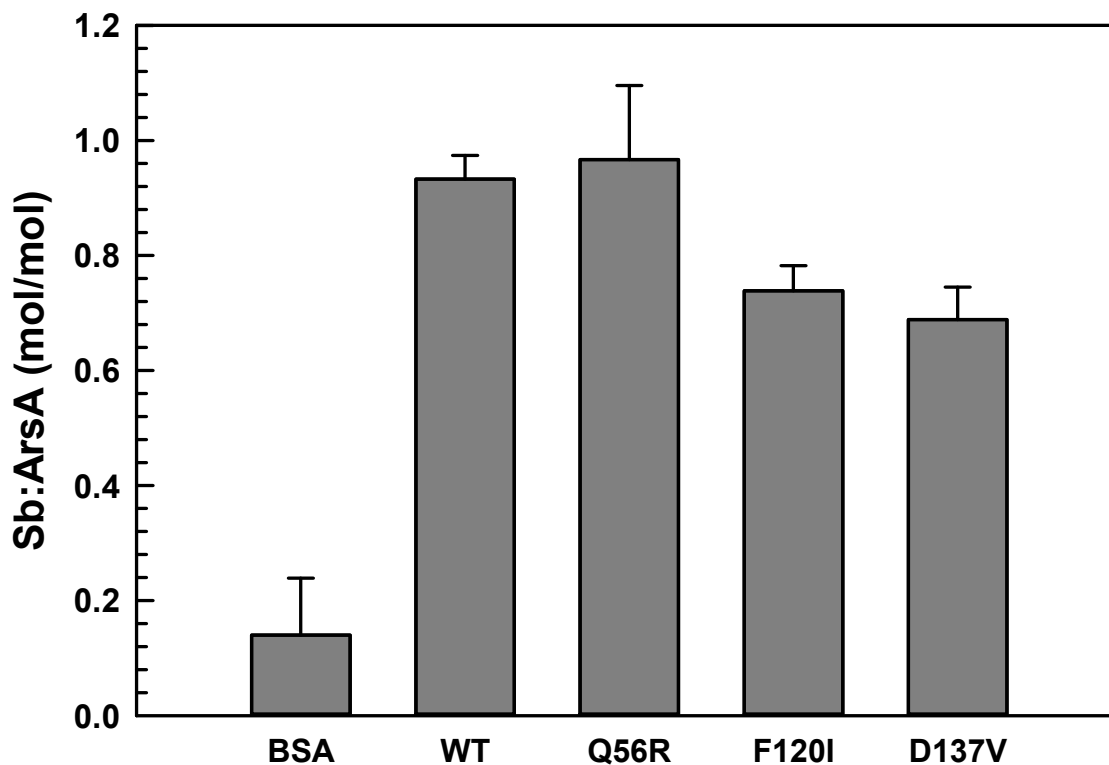


Figure 12. ArsA mutants bind antimonite. The antimony binding ability of wild-type and altered ArsA was assayed as described under “Materials and Methods.” After incubation of 10 μ M ArsA and 100 μ M potassium antimonyl tartrate at 4 °C in the presence of ATP γ S and Mg²⁺, free Sb(III) was removed by gel filtration, and the Sb(III):ArsA molar ratio determined. Bovine serum albumin (BSA) was used as a negative control. The error bars represent the standard deviation from three assays.

Docking analysis of the interaction between Q56R ArsA and ArsD

ArsA undergoes a number of conformational transitions during the catalytic cycle, an open form in the absence of ATP and As(III), and a closed form when both are present (Ruan et al., 2008; Zhou and Rosen, 1997). The X-ray crystal structure of ArsA has been solved in the closed form with different nucleotides and metalloid (Zhou et al., 2000, 2001). However, since metalloid transfer requires ArsA to be undergoing catalysis (Yang et al., 2010), it is likely that ArsD interacts initially with an open form of ArsA. A *S. cerevisiae*

homologue of ArsA, Arr4p or Get3 (Auld et al., 2006; Shen et al., 2003) is involved in targeting tail-anchored proteins in the endoplasmic reticulum (Denic et al., 2013). The crystal structures of Get3 from different yeast strains were solved in the open (nucleotide free) and closed (ADP-AlF₄⁻) conformations (Bozkurt et al., 2009; Mateja et al., 2009). An open model of the Q56R ArsA based on the open Get3 structure was generated, as described earlier (Ye et al., 2010). A model of the metalated form of ArsD was constructed on the basis of its crystal structure (PDB ID: 3MWH) with the missing active site loop (residues 10-19) built using MODELLER (Sali and Blundell, 1993) and subjected to energy minimization using VMD/NAMD program (Humphrey et al., 1996; Phillips et al., 2005). The ArsA and ArsD structures were docked by the online protein docking server, HexServer (<http://hexserver.loria.fr/>), which produced a ranked list of 100 docking predictions. Since biochemical analysis indicates that the three cysteines of ArsD and the three cysteines of ArsA must be in proximity for transfer (Lin et al., 2007a), and also that Q56R ArsA interacts strongly with wild type ArsD, the single model most consistent with these parameters was selected (Figure 13A). The docking analysis predicts 40 Q56R ArsA residues are within 4 Å of 39 residues of wild type ArsD (Table 5). Many of these ArsA residues are positively charged (e.g. Arg56, Arg86 and Arg556) or negatively charged (e.g., Glu75, Asp77, Glu515 and Glu552). These residues are close enough to form charge pairs with residues in ArsD. For example, ArsA residues Glu75 and Arg86 are close enough to ArsD residues Lys37 and Asp21, respectively, to form three salt bridges. Similarly, the *in silico* modeling of Q56R ArsA and 4KA ArsD

complex predicts 13-hydrogen bonds and 2-salt bridges between ArsA and ArsD. Our results are consistent with an arginine substitution at ArsA residue 56 altering the interaction with ArsD by changes in hydrogen bonding and salt bridges that propagate to the interface between the two proteins.

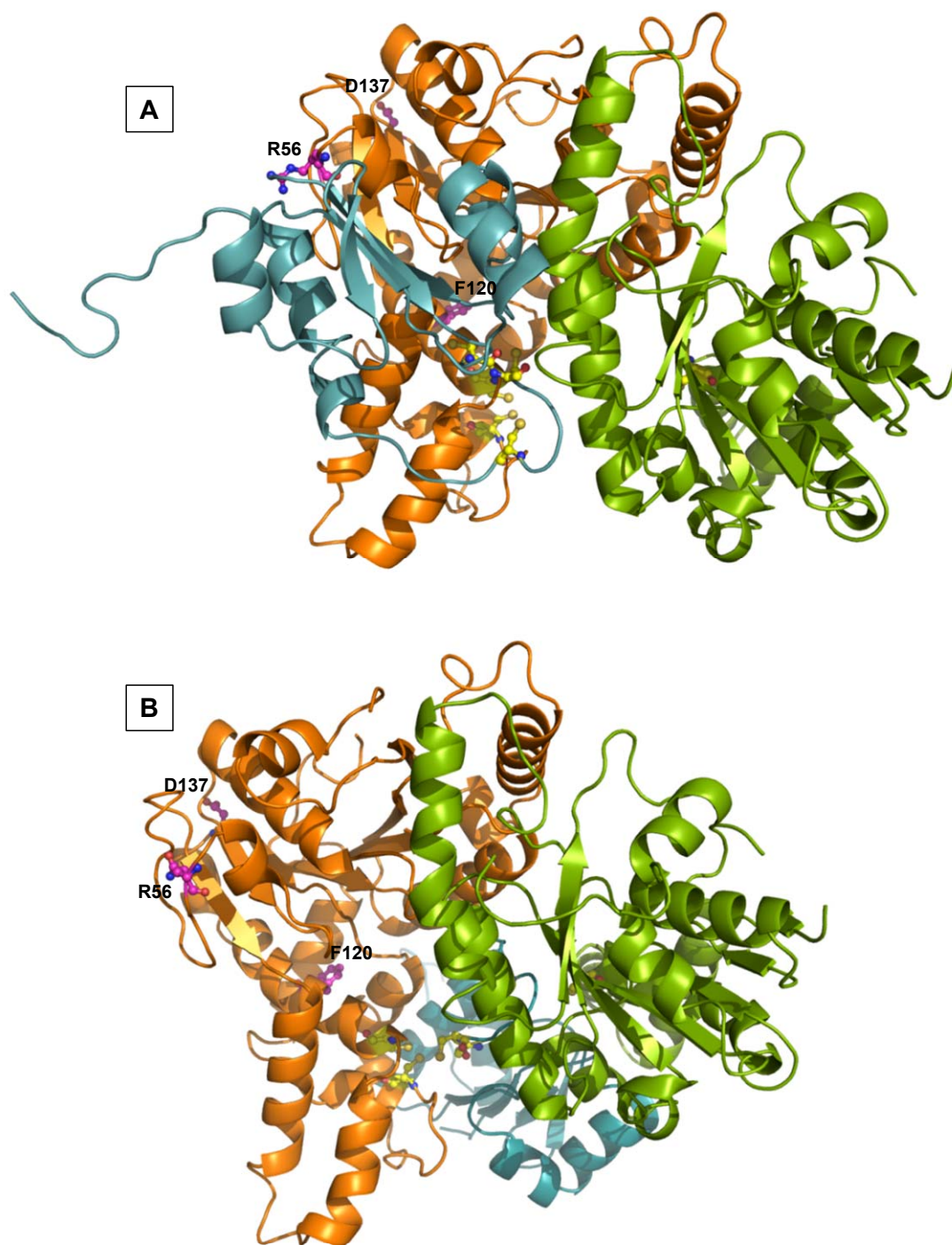


Figure 13. *In silico* docking analysis of ArsA-ArsD complex. (A) Cartoon diagram of the interaction between Q56R ArsA and wild type ArsD. ArsD attaches to the back of ArsA with the cysteine rich loop (Cys12, Cys13, and Cys18) of ArsD (cyan) hanging down the metalloloid binding domain of the open form of ArsA (ArsA1 in orange and ArsA2 in split pea). R56, F120 and D137 in ArsA are represented by magenta ball and sticks. The active site thiolates in both ArsA and ArsD are represented by yellow ball and sticks. (B) Cartoon diagram of the interaction of Q56R ArsA and wild type ArsD based on an earlier model (Ye et al., 2010). ArsD (cyan) is proposed to fit into the cavity of the open form of ArsA (ArsA1 in orange and ArsA2 in split pea).

Table 5. Q56R ArsA and wild-type ArsD residues predicted from *in silico* docking to be within 4 Å of each other

Q56R ArsA residues	Wild-type ArsD residues
Pro46	Arg45, Gln51
Ala47	Phe46
Ser48	Glu44
Gly51	Gln42
Gln52	Met5
Ser55	Gln42
Arg56	Gln38, Cys39, Gly40, Gln42
Thr57	Gly40, Val41, Gln42, Glu44
Ile58	Lys37, Gln38
Gly59	Gln34
Asn60	Gln34, Gln38
Thr61	Gln38
Gln63	Gln38
Glu75	Lys37, Glu44
Asp77	Gln34
Gln79	Arg45, Asn47, Gln51
Ala80	Gln34
Gln83	Ser30, Arg45
Gln84	Ser30, Thr31
Arg86	Asp21, Val22
Ser103	Asp21
Asn106	Asp21

Glu107	Thr20, Asp21, Val22
Asn281	Gln57
Met282	Gln57
Thr501	Pro52, Met53
Leu505	Cys13
Ala508	Ser14, Thr15
Asn509	Cys13, Ser14
Gln511	Thr15
Ala512	Thr15, Gly16
Glu515	Gly16
Gln545	Glu59, Lys62
Gln546	Val56, Gln57
Pro549	Phe55, Val56, Lys62
Gln550	Pro52, Val56
Glu552	Ile65, Glu66
Arg556	Ile65, Glu66, Ala67, Ser68, Gly69, Ala70, Glu71
Gln557	Pro9, Ala10, Ala70, Glu71
His558	Thr15

Discussion

The ArsD metallochaperone delivers As(III) to ArsA ATPase, the catalytic subunit of ArsAB pump. Interaction with ArsD increases the affinity of ArsA for As(III), conferring resistance to environmental concentrations of arsenic (Lin et al., 2006). Genetic, biochemical and crystallographic data indicate that ArsD residues Cys12, Cys13, and Cys18 are involved in the transfer of As(III) to ArsA (Lin et al., 2007a; Yang et al., 2010; Ye et al., 2010). ArsA has two homologous halves, ArsA1 and ArsA2, each with a nucleotide binding domain, NBD1 (residue 1-296) and NBD2 (residue 305-583) connected by a short linker (Zhou et al., 2000). Two cysteine residues from NBD1 (Cys113 and Cys172) and a single cysteine (Cys422) from NBD2, form a high-affinity metalloid binding site (Bhattacharjee and Rosen, 1996; Ruan et al., 2008). ArsA undergoes a number of conformational transitions during the catalytic cycle, an open form in the absence of ATP and As(III), and a closed form when both are present (Ruan et al., 2008; Zhou et al., 2000, 2001; Zhou and Rosen, 1997). Biochemical analysis suggests that the three cysteines of ArsD must be in proximity to the three cysteines of ArsA for metalloid transfer (Lin et al., 2007a). However, since metalloid transfer requires ArsA to be undergoing catalysis (Yang et al., 2010), it is likely that ArsD initially interacts with an open form of ArsA.

ArsD mutant K2A/K37A/K62A/K104A (4KA ArsD) does not interact with wild type ArsA in a two-hybrid assay (Yang et al., 2011). Three suppressor mutations in ArsA (Q56R, F120I, and D137V) were isolated that exhibits

increased interaction with wild type ArsD than 4KA ArsD (Figure 9). Each of these three residues in ArsA (Gln56, Phe120, and Asp137) is located in NBD1. Gln56 is situated in between the H3-S3 loop and exposed to solvent. Phe120 is in the middle of H6 helix and surrounded by hydrophobic residues. Asp137 is in the H7-S5 loop and exposed to solvent.

A combination of *in silico* modeling and docking was used earlier to examine the interaction of ArsD metallochaperone with ArsA ATPase (Ye et al., 2010). The model depicted ArsD to fit into the cavity of the open form of ArsA (Fig. 13B). This model predicted that ArsA residues His148, Arg151, Gly157, Ala158, Ser160, Ser161, Glu168, Ala170, Tyr394, Thr401, Lys402, Lys404, Glu405, Asp417, His453, Leu457, Leu458, Ala460, Thr461, and Arg516 are within 4 Å of the ArsD interface (Ye et al., 2010). However, our two-hybrid screening for suppressor mutants with increased ArsA-ArsD interaction did not pick up any of the ArsA residues indicated above, except Lys404 (Table 3). Interestingly, the single ArsA mutant K404R did not interact with either the wild type or 4KA ArsD (data not shown). This model also cannot explain the increased interaction of Q56R ArsA with ArsD. As shown in Fig. 13B, Gln56 or its replacement is exposed to solvent and distant from the ArsA-ArsD interface.

We now propose an alternate model for ArsA-ArsD interaction (Fig. 13A). While in the previous model, ArsD goes in a 'frontal-attack' mode with the open form of ArsA (Fig. 13B), in the new model, ArsD interacts such that its cysteine (Cys12, Cys13, and Cys 18) bearing loop is lowered into the active site of ArsA from its top (Fig 13A). In this model, wild type ArsA-ArsD complex shows 16-

intermolecular hydrogen bonds and 4-salt bridges, with a ΔG^{diss} of 11.1 kcal/mol. The Q56R ArsA-wild type ArsD complex exhibits 28-intermolecular hydrogen bonds and 3-salt bridges, with a ΔG^{diss} of 16.0 kcal/mol. Thus, the alteration of Gln56 to arginine builds increased interaction with wild type ArsD, which supports the two-hybrid data. The Q56R ArsA-4KA ArsD complex shows 13-intermolecular hydrogen bonds and 2-salt bridges, and a ΔG^{diss} of 7.8 kcal/mol. The alteration of four lysine residues in ArsD attenuates the positive charge, which in turn rearranges the surface charge on the protein surface and affects its interaction with ArsA. However, if we determine the free energy of assembly dissociation using the earlier model (Ye et al., 2010) (Fig. 13B), the ΔG^{diss} values for wild type ArsA and ArsD, Q56R ArsA-wild type ArsD, and Q56R ArsA-4KA ArsD complex are 15.4, 15.4, and 14.9 kcal/mol, respectively, predicting no differences in interaction between the altered ArsA and ArsD. Thus, the new *in-silico* model (Fig. 13A) supports our experimental data of Q56R ArsA strongly interacting with wild-type ArsD and weakly with 4KA ArsD. The new model also accommodates most of the ArsD residues that were shown to interact with ArsA by two-hybrid analysis (Yang et al., 2011). A side-by-side analysis comparing the two hybrid data (Table 2) and *in silico* docking predictions (Table 5) suggests that ArsA residues Gly51, Ser55, Arg88, Val90, Val101 and Ser560 might play a role in protein-protein interaction. However, the effect of any of this single-residue alteration on ArsA-ArsD interaction was not examined.

It should be noted that the new model (Fig. 13A) predicts that the sulfur atoms of ArsA residues Cys113 and Cys172 are approximately 12 Å distant from

Cys12 and Cys13 of ArsD. It is reasonable to assume that the complex undergoes multiple conformational changes that bring those residues in proximity to each other during other steps in the catalytic cycle.

Neither model explains the increased interaction between F120I or D137V ArsA with the wild type or 4KA ArsD. Both proteins show a basal ATPase activity that is not stimulated by As(III). Both proteins bound Sb(III), albeit at a slightly lower stoichiometry than either the wild type or Q56R ArsA. This suggests that neither the nucleotide nor metalloid binding site of F120I and D137V ArsA are affected by the mutation. However, both showed a higher basal rate that is similar as the activated rate for Q56R ArsA. We interpret this observation as the conformation of F120I and D137V are permanently locked in the metalloid bound form of the protein. Why do these mutants interact strongly with ArsD? An Asp137 to Val substitution is a major alteration of charge on the protein surface and probably creates a 'sticky' surface. We predict that a Phe120 to Ile change affects the surface hydrophobicity of the protein that result in increased hydrophobic interactions with either wild type or 4KA ArsD, forming abortive complexes. Identification of suppressor mutants that exhibit stronger interaction with ArsD provides an opportunity to perform co-crystallization experiments that would lead to characterization of the interface at the atomic level.

CHAPTER III

Biochemical and biophysical characterization of CrArsM, an As(III) S-adenosylmethionine methyltransferase, from *Chlamydomonas reinhardtii*

(Parts of this chapter have been reproduced with permission of the [International Union of Crystallography](#) from Packianathan et al., 2014)

Introduction

While there are many toxins present in the environment, none is as pervasive as arsenic. In fact, the 2013 Environmental Protection Agency's Comprehensive Environmental Response, Compensation and Liability Act (CERCLA) Priority List of Hazardous Substances rank arsenic first based on a combination of their frequency, toxicity, and potential for human exposure (<http://www.atsdr.cdc.gov/spl/>). The widespread impact of arsenic toxicity can be attributed to the ubiquity of arsenic in the environment (Zhu et al., 2014). Natural sources of arsenic include soil and our water and food supplies. Arsenic consumption from foods, such as meats, vegetable and fish, have been linked with skin, bladder and lung cancer (Oberoi et al., 2014).

Genes for As(III) S-adenosylmethionine methyltransferases (As3MTs) are widespread in the genomes of bacteria, archaea, fungi, lower plants and animals, including humans. In microbes, the ArsM (synonymous with As3MT) orthologs detoxify arsenic (Qin et al., 2009; Qin et al., 2006). In contrast, the health effects of arsenic may be attributed to methylation of inorganic arsenic by the human ortholog, hAS3MT, which catalyzes the biotransformation of As(III), primarily in

liver, to methylated products that are more toxic and carcinogenic in humans (Thomas et al., 2007; Thomas et al., 2004).

To date the pathway of methylation remains controversial (Cullen, 2005). One hypothesis proposed by Challenger (Challenger, 1947) is that the enzyme catalyzes a series of alternating oxidative methylations and reductions, using S-adenosylmethionine as the methyl donor to generate the pentavalent products methylarsenate (MAs(V), dimethylarsenate (DMAs(V)) and a lesser amount of trimethylarsine oxide (TMAs(V)O). The trivalent species MAs(III), DMAs(III) and TMAs(III) are intermediates but not products. Most consistent with this hypothesis is that humans primarily excrete DMAs(V) and to a lesser extent MAs(V) (Engstrom et al., 2011; Vahter, 1999)}. However, with careful handling, trivalent methylated arsenicals can be detected in urine (Ding et al., 2012; Le et al., 2000). More recently, Hayakawa and coworkers (Hayakawa et al., 2005) proposed an alternate pathway in which the preferred substrates of the methyltransferase are the glutathione (GSH) conjugates As(GS)₃ and MAs(GS)₂, and the products are the trivalent conjugates MAs(GS)₂ and DMAs(GS). In this pathway there is no change in the oxidation state of arsenic, which remains trivalent throughout the catalytic cycle. The conjugates dissociate to unstable MAs(III) and DMAs(III), which rapidly oxidize non-enzymatically in air to MAs(V) and DMAs(V), the primary observed urinary species (Drobna et al., 2013; Le et al., 2000).

To differentiate between these two hypotheses, Marapakala et al analyzed the enzymatic properties of an orthologue of human As3MT, CmArsM, from an

environmental isolate of the thermoacidophilic eukaryotic red alga *Cyanidioschyzon merolae* (Marapakala et al., 2012; Qin et al., 2009). Purified CmArsM (411 residues, including a histidine tag) exhibits a temperature optimum of 60-70 °C. All As(III) SAM methyltransferases identified to date have four conserved cysteines, at positions 44, 72, 174, and 224 in CmArsM. Substitution of any of the four with alanine led to loss of As(III) methylation. However, the C44A and C72A enzymes retained the ability to methylate MAs(III). This indicates that Cys44 and Cys72 is not required MAs(III) methylation ((Marapakala et al., 2012) and unpublished observation). CmArsM has a single tryptophan residue that was changed to tyrosine to produce a tryptophan-free derivative. In this background, Tyr70 was changed to a tryptophan, producing the single-tryptophan derivative Y70W. Purified Y70W reported binding of As(III) and MAs(III) with quenching of protein fluorescence. As(GS)₃ and MAs(GS)₂ bound substantially faster than the free metalloids, supporting the hypothesis that glutathionylated arsenicals are preferred substrates for the enzyme (Hayakawa et al., 2005). In the Y70W background, each of the single cysteine mutants, exhibited fluorescence quenching with addition of As(III), suggesting that the mutants bind but do not methylate As(III). Moreover, the data indicated that all four cysteines are involved in As(III) methylation, but that only Cys174 and Cys224 are required for the second step, methylation of MAs(III) to DMAs(III). The rate-limiting step was identified as the conversion of DMAs(III) to TMs(III), and DMAs(III) accumulates as the principal product (Marapakala, 2012 #5680 and unpublished observation).

The crystal structure of CmArsM reveals the relationship between the arsenic and SAM binding sites to a final resolution of $\sim 1.6 \text{ \AA}$ (Ajees et al., 2012). In this structure, As(III) is bound by Cys174 and Cys224, while Cys72 moves towards Cys174 and Cys224 when SAM is bound. The first 49 residues including Cys44 are not visible in this structure. As(III) binding causes little change in conformation, but binding of SAM reorients helix $\alpha 4$ and a loop (residues 49–80) towards the As(III) binding domain, positioning the methyl group for transfer to the metalloid. There is no evidence of a reductase domain, suggesting that arsenic remains trivalent during the catalytic cycle. While this structure identifies the arsenic and SAM binding domains, as well as other residues potentially involved in arsenic biomethylation, a number of questions remain unanswered. For example, the structure and function of the N- and C-terminal domains that is not visible in this structure, and the participation of GSH in the catalytic mechanism.

A more complete understanding of the catalytic mechanism of this family of enzymes would be aided by additional crystal structures from other orthologs. Comparison of the structure of orthologs will illuminate which domains and residues may be functionally significant. A multiple amino acid sequence alignment of CmArsM with lower and higher eukaryotic ArsM homologues shows several conserved features (Figure 14). For example, Cys44, Cys72, Cys174, and Cys224 in CmArsM is conserved in the other species examined.

CrArsM from the eukaryotic green alga *Chlamydomonas reinhardtii* (AFS88933) catalyzes arsenic methylation and volatilization, leading to arsenic

resistance (Chen et al., 2013). The gene for CrArsM, a 379-residue enzyme (41.6 kDa), was synthesized and expressed in *Escherichia coli*. In this study, I describe the purification, preliminary biochemical characterization, crystallization, X-ray data collection and preliminary crystallographic analysis of CrArsM.

```

Cyanidioschyzon 1 -----MPCSCA-----
Ostreococcus 1 MAS-----ATVTAAPARATRRRRDSSRSATSPRATSARTRARA-R
Chlamydomonas 1 -----
Chlorella 1 MLCRVSTGRQFSVAAQPAARP-----PMSCCPPQNGAVKCLKPTPPA
Zebrafish 1 -----
Human 1 -----
Rat 1 -----

```

```

Cyanidioschyzon 7 -----S-----GCQKSKNGGSTPSIRDHVADYYGKTLQSSADLKTSACK
Ostreococcus 43 ASSSSSGALDALLGATI IAPGGDASVRASVQKYYGETLSTSDDLKTSACC
Chlamydomonas 1 --MVEPASIAELSRAEQL-GKDQDAVRATVKEYYGETLKTSNDLRTSACT
Chlorella 42 AVAGPASGIQELLEAKQL-GDNQQGVLDVKEYYGEVLTTSSEDLKTSACC
Zebrafish 1 -----MADAARDRTVTSVYNDVKEYYGKTLKQKSDLKSNACV
Human 1 -----MAA---LRDAEIQKDVQTYYGQVLKRSADLQTNQCV
Rat 1 -----MAA---PRDAEIQKDVQNYYGNVLKTSADLQTNACV

```

```

Cyanidioschyzon 46 LAA-AVPESHKILADTADDEVLEKFGYCGSTLPADGSLGATVLDLGCST
Ostreococcus 93 TPSEQIPKAVREALREVPEVKAKYYGCGSPTPI--GIDGLRVLDLGS
Chlamydomonas 48 ACK-APPPAVRAALADVPTVKEKFGYCGNPIPA--GIEGLRVLDLGC
Chlorella 91 TAG-SPPPLVRDALKKVPDEVKAKYYGCGSPFPM--GIQGLRVLDLGS
Zebrafish 38 PSAKPVSAYVRKVI AEIHPDVVAKYYGCVLVVPE--CLEGCRVLDLGC
Human 34 TTARPVPKHIREALQNVHEEVALRYGCVLVIPE--HLENCWILDLGS
Rat 34 TPAKGVPEYIRKSLQNVHEEVISRYGCVLVVPE--HLENCRILDLGS

```

```

Cyanidioschyzon 95 GRDVYLASKLVGEHGKVI GVDMLDNQLEVARKYVE--YHAEKFFGSPSR
Ostreococcus 141 GRDCYVAAKLVGENGSVLGVDMTDGQLEVARKYVDEYCTKTG--YAKAN
Chlamydomonas 95 GRDCYVAAKLVGEGKSVTGVDMPAQLEVAISHADAYCRDKL--YGKSN
Chlorella 138 GRDCYVCSALVGEKSVTGVDMPAQLEVAISHADAYCRDKL--YAQPN
Zebrafish 86 GRDCYVLSQLVGEKGHVTGIDMTAQLEVARNYID--YHMQRFG--YKNPN
Human 82 GRDCYVLSQLVGEKGHVTGIDMTKQVEVAEKYLD--YHMEKYG--FQASN
Rat 82 GRDCYVLSQLVGEKGHVTGIDMTKVQVEVAEKYLD--YHTEKFG--FQTPN

```

```

Cyanidioschyzon 144 VRFLKGF IENLATAEPEGVPDSSVDIVISNCVCNLSNKLALFKEIHRVL
Ostreococcus 189 MRFEKGTIEDLKA---AGVPDASVDMI I SNCVINLSPDKPAVLSEAYRVL
Chlamydomonas 143 MTFIQGEIEYLDR---AGLEDSSFDLVI SNCVINLSPDKARVLSECYRVL
Chlorella 186 MRFVEGEIEYLDK---AGIPDSSVDLII SNCVINLSPDKARVLREYRVL
Zebrafish 133 VNFVQGYIEALVE---AGLEDKSYDIII SNCVVNLSPDKSSVLRVAYCVL
Human 129 VTFIHGYIEKLGE---AGIKNESHDIVVSNVCINLVPDKQQVLQEAYRVL
Rat 129 VTFILHGQIEMLAE---AGIQKESYDIVI SNCVINLVPDKQKVLREYVQVL

```

Cyanidioschyzon	194	RDGGELYFSDVYADRRRLSEAAQQDPILYGECLGGALYLEDFRRLVAEAGF
Ostreococcus	236	ANGGEFYFSDVYCDRRLQEDLRSHEILLGECLGGAMYVEDFKRLCQAVGF
Chlamydomonas	190	APGGEMHFSVDVYVDRRLPQSVRSHPVLLGECLAGALYNNDFIRLSRKVGF
Chlorella	233	APGGEMYFSDVYCDRRLPAEVRTHPVLLGECLGGALYTQDFLRLCRQVGF
Zebrafish	180	KDGGELYFSDVYSDAIPEHLKANKTLWGECLSGALWWEDLIRLAAEEVGF
Human	176	KHGGELYFSDVYTSLELPEEIRTHKVLWGECLGGALYWKELAVLAQKIGF
Rat	176	KYGGELYFSDVYASLEVSEDIKSHKVLWGECLGGALYWKDLAVIAKKIGF
Cyanidioschyzon	244	RDVRLVSVGPDVSDPQLRKLVPDVQFYSCFRCFKVA--TLEATREDYG
Ostreococcus	286	TDPRVLAGEHEIEVRDPALAEELGEAKFYSSITYRFLFKLPPGCLETLCEDYG
Chlamydomonas	240	TDPRQLECEEIQIHDAELRDQVGEARFYSSITYRFLFKVP-GQIEDLCEDYG
Chlorella	283	LDPRTLSSAEIEVRDRELRELLGDARFFSSITYRFLFKLP-EAIEITLCEDYG
Zebrafish	230	CKPRLVSASIIITVGNTELESILGDYKFVSATYRFLFKLQKLEKKPCL---
Human	226	CPPRLVTANLITIQNKELERVIGDCRFVSATFRLFKHSKTGPTKRCQ---
Rat	226	CPPRLVTANIITVGNKELERVLGDCRFVSATFRLFKLPKTEPAGRCQ---
Cyanidioschyzon	292	QSATYLGIG---EEFKLDRFFTFPKEKPVVRDNTAEIIRHSRLHQWFS
Ostreococcus	336	QYAVYNGGLPGAPNAYQLDDHHRFEKNKPLVCGNTGSMVGETWLGKYFT
Chlamydomonas	289	QVAVYKGTIPGHSHAYDLDDHHRFVTNKPLVCGNTASMVGESWLAPHFT
Chlorella	332	QACKYKGTIPGAPHSYALDDHHTFQTGKWYEVCGNTAAMVGDSSWMGKHFE
Zebrafish	277	--VMYNGDITDSEESFEFDAQYAFKVDKVMVEVDGDVANILRNSRFSEEF
Human	273	--VIYNGGITGHEKELMFDANFTFKEGEIVEVDEETAAILKNSRFAQDFL
Rat	273	--VYNGGIMGHEKELIFDANFTFKEGEAVEVDEETAAILRNSRFAHDFL
Cyanidioschyzon	339	VSAEQ-QHMGLFKANDS--YALLHAPLSMQVEQLVCEVKKGSTDTDCSEQA
Ostreococcus	386	LVGDRSTHYGLFDCGSPVAA-----S-----SSA
Chlamydomonas	339	IIGDRAVHYGQFDCSGPKTTT-----GGAASPSNSAGA
Chlorella	382	VVGDRSTHYGLFACGPAPA-----AAP
Zebrafish	325	FQPQGVNTASSGGCWAKPN-AVSVNPFEL-----VQQ---LGSASV
Human	321	IRPIGEKLPTSGGCSALELKDIITDPFKL-----AEESDSMKSRCV
Rat	321	FTPVEASLL-----APQTKVIIRDPFKL-----AEESDKMKPRCA
Cyanidioschyzon	386	SANGASCCATGRRCC-
Ostreococcus	411	APAGGACC-----
Chlamydomonas	372	CGPGGACC-----
Chlorella	404	APAGGACC-----
Zebrafish	362	SPSTGGCCAGQESCCN
Human	362	PDAAGGCCGTTKSC--
Rat	356	PEGTGGCCGKRKSC--

Figure 14. Multiple alignment of ArsM orthologs. *Cyanidioschyzon merolae* ArsM (FJ476310) was aligned with orthologs from *Ostreococcus lucimarinus* (XP_001421969), *Chlamydomonas reinhardtii* (AFS88933), *Chlorella variabilis* (XP_005845903), Zebrafish (NP_001034928), Rat (NP_543166) and human (AAI19639). The black shading indicates identical amino acids; the grey shading indicates similar amino acids.

Materials and methods

Reagents

All chemicals were obtained from Sigma-Aldrich (St Louis, Missouri) unless otherwise mentioned.

Cloning, expression and purification of CrArsM

A *CrArsM* gene was designed based on the native gene with NcoI and XhoI restriction sites flanking 5' and 3' ends of the gene, respectively. The synthetic version of *CrArsM* retained the conserved cysteine residues at positions 46, 74, 170 and 220, while all other cysteine residues were changed to alanine. Trp332 and Tyr72 of native CrArsM protein were mutated to tyrosine and tryptophan residues, respectively. The gene was chemically synthesized by Genscript USA Inc. (NJ) and inserted into vector plasmid pUC57 (Thermo Fisher Scientific, Waltham, MA). The gene was subsequently cloned into vector plasmid pET29b(+) (EMD Biosciences, CA, USA) as a NcoI/XhoI digest, generating plasmid pET29-CrArsM in which the *CrArsM* gene is under control of T7 promoter and expressed with a six histidine tag at the C-terminus.

Cells of BL21(DE3) pET29-CrArsM were grown at 37 °C in Luria-Bertani medium (Green et al., 2012) containing 50 µg/ml of kanamycin with shaking at 240 rev min⁻¹. When the absorbance at 600 nm of the culture reached 0.6, 0.1 mM IPTG was added to induce expression of *CrArsM*. The cells were grown for another 4 h, harvested by centrifugation (3,500 x g) for 30 min, washed once with buffer A (50 mM MOPS, pH 7.5, 0.5 M NaCl, containing 20% (w/v) glycerol, 20

mM imidazole and 10 mM 2-mercaptoethanol), and suspended in 5 ml of buffer A per g of wet cells. The cells were lysed by two passes through a French pressure cell press at 20,000 psi and immediately treated with 2.5 μ l/g wet cells of the protease inhibitor diisopropyl fluorophosphate. Membranes and unbroken cells were removed by centrifugation at 150,000 x g for 1 h (Qin et al., 2006), and the supernatant solution at a flow rate of 0.5 ml/min was loaded on a 5 ml His-trap HP column (GE Healthcare) pre-equilibrated with buffer A using an AKTA-FPLC purification system (GE Healthcare). The column was washed with 5 column volumes of buffer A, followed by elution with 5 column volumes of buffer A containing 0.2 M imidazole. Purified synthetic CrArsM was identified by SDS PAGE. The migration of the band corresponded to the mass of CrArsM. Fractions containing CrArsM were concentrated by centrifugation using a 10-kDa cutoff Amicon Ultrafilter (EMD Millipore Corporation, Billerica, Massachusetts, USA) and was buffer exchanged with buffer C consisting of 50 mM MOPS, pH 7.5, containing 0.5 M NaCl, 5 mM dithiothreitol (DTT), 2.5 mM EDTA and 10% (w/v) glycerol, for storage at -80 °C until use. The yield from 1 L of cell culture was 23 mg of purified protein.

Arsenic methylation

Methylation of As(III) and MAs(III) was assayed both in cells of *E. coli* expressing *CrArsM* genes and by purified proteins. Individual colonies of *E. coli* strain BL21(DE3) bearing the appropriate plasmids were inoculated into 2 ml of LB medium supplemented with the appropriate antibiotics and incubated at 37 °C

overnight. Late exponential phase cells were diluted 200-fold into 2 ml of LB medium containing 50 µg/ml kanamycin, 0.3 mM IPTG and 20 µM sodium arsenite. After 12 h at 37 °C, the cells were removed by centrifugation, and the supernatant solution was immediately passed through a 3-kDa cut-off Amicon Ultrafilter (Millipore, Billerica, MA). The filtrate was speciated by high-pressure liquid chromatography (HPLC) (PerkinElmer Series 2000) using a C18 reversed-phase column eluted with a mobile phase consisting of 3 mM malonic acid, 5 mM tetrabutylammonium hydroxide, and 5% (v/v) methanol (pH 5.9) with a flow rate of 1 ml/min, and arsenic content was determined by inductively coupled plasma mass spectroscopy (ICP-MS) using an ELAN DRC-e spectrometer (PerkinElmer, Waltham, MA).

Methylation activity of purified CrArsMs was assayed at 30 °C in a buffer consisting of 50 mM MOPS, pH 7.5, containing 150 mM KCl. The assay mix contained 1 mM tris(2-carboxyethyl)phosphine (TCEP), 0.5 mM SAM, 10 µM As(III) and 1 µM CrArsM. The reaction was terminated by adding 15% (v/v) H₂O₂ to oxidize all arsenic species. Denatured protein was removed by centrifugation using a 3 kDa cut-off Amicon Ultrafilter. The filtrate was speciated by HPLC-ICP-MS.

Fluorescence assays

Fluorescence measurements were performed on a temperature-controlled QuantaMaster™ UV VIS QM-4 Steady State Spectrofluorometer (Photon Technology International, Birmingham, NJ) at 25 °C. For steady state

measurements, both emission and excitation monochromator slits were set at 1 nm. Samples were excited at 295 nm to excite tryptophan, and emission was set at 336 nm for time-based data acquisition. Spectra were corrected for background fluorescence and Raman scattering by subtracting buffer spectra. The buffer used was 50 mM MOPS, 150 mM KCl, pH 7.5. For determination of relative binding of free metalloids, As(III) and MAs(III), and preformed GSH conjugates, fluorescence spectra were acquired at the indicated concentrations of arsenicals in presence and absence of GSH. To obtain binding rates, time-based fluorescence quenching data were fitted to a single exponential decay isotherm using Prism 6 (GraphPad Software Inc).

Crystallization

The purified CrArsM was buffer exchanged into a buffer consisting of 50 mM MOPS, pH 7.0 containing 0.5 M NaCl and 5 mM DTT. Initial crystallization trials were performed using Hampton Research (Aliso Viejo, California, USA), Emerald Biosciences Inc. (Bainbridge Island, Washington, USA), and Jena Biosciences GmbH (Jena, Germany) crystal screen conditions using a hanging drop vapor diffusion method.

At 18 °C and 20 °C, crystallization trials produced crystalline aggregates upon mixing 2.0 µl each of protein and reservoir (20% PEG 3350, 0.2 M calcium acetate, 0.1 M Tris-HCl, pH 7.0) solutions. Reduction of the PEG concentration from 20% to 18% led to formation of needle-like crystals that were used for seeding experiments. The needles were transferred from the hanging drop to

Eppendorf tubes containing seed beads (Hampton Research) and 0.1 ml of well solution. Sample preparation for seeding was as described previously (Marapakala et al., 2010). Diffraction-quality crystals were obtained at room temperature using LINBRO 24 well plates (HR3-110) from Hampton Research. The wells, sealed with a cover slip, held 0.5 μ l of seed stock (1:100 ratio) in drops containing equal volumes of protein and reservoir solutions (10% PEG 8000, 2.0 M NaCl). The crystals from a single drop were washed several times in 50% glycerol and dissolved in water for analysis by SDS PAGE.

Data collection and processing

Crystals were transferred to a cryoprotectant solution (10% PEG 8000, 2.0 M NaCl, 20% 2-methyl-2,4-pentanediol) and flash-cooled in liquid nitrogen for data collection. Initial crystals were screened at the Advanced Light Source of the Berkeley Center for Structural Biology. Subsequent data sets were collected at the Southeast Regional Collaborative Access Team (SER-CAT) facility at the Advanced Photon Source (APS), Argonne, IL. Data were obtained from 360 image frames with 1° rotation angle about φ using a MAR-300 CCD detector under standard cryogenic conditions (100 °K) at a synchrotron beam line 22-BM with a crystal to detector distance of 240 mm. The data sets were indexed, integrated and scaled with the HKL-2000 suite (Otwinowski and Minor, 1997).

Results

Chemical synthesis of CrArsM

The native *CrArsM* gene (Accession number JX480492.2) was expressed and purified as described (Chen et al., 2013). However, the purified protein proved refractory to crystallization. Native CrArsM has 17 cysteine residues, of which four are conserved in orthologs (Figure 14). Multiple cysteine residues in proteins often interfere with crystallization. For that reason, the *CrArsM* gene was chemically synthesized. In the synthetic version, the four conserved cysteine residues at positions 46, 74, 170 and 220 were retained, while the other 13 cysteine residues were changed to alanine residues. Also, in order to measure ligand binding by monitoring the changes in intrinsic tryptophan fluorescence, Trp332 and Tyr72 of native CrArsM protein were mutated to tyrosine and tryptophan residues, respectively (Figure 15). The sequence of the gene was optimized using the OptimumGene™ algorithm (Genscript) which improves expression by analyzing and upgrading the codon adaptation index (Sharp and Li, 1987), modifying GC content and disrupting stem-loop structures that affect ribosome binding and stability of the mRNA (Figure 16). Otherwise the sequence of the synthetic protein was the same as native CrArsM (Figure 15).

Synthetic CrArsM 1 MVEPASIAELSRAEQLGKDQDAVRATVKEYYGETLKTSNDLRTSACTAAKAPPPAVRAAL
 Native CrArsM 1 MVEPASIAELSRAEQLGKDQDAVRATVKEYYGETLKTSNDLRTSACTACKAPPPAVRAAL

Synthetic CrArsM 61 ADVPTEVKEKF~~WG~~C~~GN~~P~~IP~~AGIEGLRVLDLGA~~GS~~GRDA~~YV~~AAKLVGEKGSVTGVDMPAQ
 Native CrArsM 61 ADVPTEVKEKF~~YG~~C~~GN~~P~~IP~~AGIEGLRVLDLGA~~GS~~GRDC~~YV~~AAKLVGEKGSVTGVDMPAQ

Synthetic CrArsM 121LEVAISHADAYARDKLGYGKSNMTFIQGEIEYLDRAGLEDSSFDLVISNCVINLSPDKAR
 Native CrArsM 121LEVAISHADAYCRDKLGYGKSNMTFIQGEIEYLDRAGLEDSSFDLVISNCVINLSPDKAR

Synthetic CrArsM 181VLSEAYRVLAPGGEMHFSVYVDRRLPQSVRSHPVLLGEC~~LAG~~ALYNNDFIRLARKVGF~~T~~
 Native CrArsM 181VLSECYRVLAPGGEMHFSVYVDRRLPQSVRSHPVLLGEC~~LAG~~ALYNNDFIRL~~CR~~KVGF~~T~~

Synthetic CrArsM 241DPRQLEAEEIQIHDAELRDQVGEARFYSITYRLFKVPGQIEDLAEDYQVAVYKGTIPGH
 Native CrArsM 241DPRQLECEEQIHDAELRDQVGEARFYSITYRLFKVPGQIEDLCE~~ED~~YQVAVYKGTIPGH

Synthetic CrArsM 301SHAYDLDDHHRFVTNKPMLVAGNTASMVGESYLAPHFTIIGDRAVHYGQFDASGPKTTTG
 Native CrArsM 301SHAYDLDDHHRFVTNKPMLVCGNTASMVGESW~~L~~APHFTIIGDRAVHYGQFD~~C~~SGPKTTTG

Synthetic CrArsM 361 GAASPSNSAGAA~~G~~PGGAAALEHHHHHH
 Native CrArsM 361 GAASPSNSAGAC~~G~~PGGAC~~C~~LEHHHHHH

Figure 15. Comparison of sequence of native and synthetic CrArsM

M V E P A S I A E L S R A E Q L G K D Q
1 ATGGTGGAACCGGCATCTATCGCTGAACTGTCCCCTGCTGAACAACCTGGGCAAAGACCAA 60
D A V R A T V K E Y Y G E T L K T S N D
61 GACGCTGTCCGTGCTACCGTGAAGGAATACTATGGTGAAACGCTGAAAACCGCAACGAT 120
L R T S A C T A A K A P P P A V R A A L
121 CTGCGCACGTCTGCTTGTACCGCCGCAAAGGCACCGCCCGCCGCGTGCCTGCAGCTCTG 180
A D V P T E V K E K F W G C G N P I P A
181 GCCGATGTGCCGACGGAAGTTAAAGAAAAGTTTTGGGGCTGTGGTAATCCGATTCCGGCG 240
G I E G L R V L D L G A G S G R D A Y V
241 GGTATCGAAGGCCTGCGCGTTCTGGATCTGGGCGCTGGTAGTGGCCGTGACGCGTATGTC 300
A A K L V G E K G S V T G V D M T P A Q
301 GCGGCCAAACTGGTGGGTGAAAAGGGCTCCGTTACGGGCGTGCATATGACCCCGGCTCAG 360
L E V A I S H A D A Y A R D K L G Y G K
361 CTGGAAGTGGCGATTTTACATGCAGATGCTTATGCGCGGACAAACTGGGTTACGGCAAG 420
S N M T F I Q G E I E Y L D R A G L E D
421 TCGAACATGACCTTTATTCAAGGTGAAATCGAATACCTGGATCGTGCAGGCCTGGAAGAT 480
S S F D L V I S N C V I N L S P D K A R
481 AGTCTTTTCGACCTGGTTATTAGTAACTGCGTCAATCAATCTGTCCCCGGATAAAGCGCGT 540
V L S E A Y R V L A P G G E M H F S D V
541 GTCCTGAGCGAAGCATATCGTGTGCTGGCACCGGGCGGTGAAATGCATTTTTTCTGATGTG 600
Y V D R R L P Q S V R S H P V L L G E C
601 TACGTTGACCGTCCGCTGCCGAGAGTGTGCGTTCCACCCGTTCTGCTGGGTGAATGT 660
L A G A L Y N N D F I R L A R K V G F T
661 CTGGCCGGCGCACTGTATAACAATGATTTTTATTTCGTCTGGCCCGCAAAGTGGGTTTTACC 720
D P R Q L E A E E I Q I H D A E L R D Q
721 GACCCGCGTCAGCTGGAAGCTGAAGAAATTCAAATCCACGATGCGGAACTGCGTGACCAA 780
V G E A R F Y S I T Y R L F K V P G Q I
781 GTGGGCGAAGCACGCTTTTATTCTATTACGTACCGTCTGTTCAAAGTTCGGGTCAGATC 840
E D L A E D Y G Q V A V Y K G T I P G H
841 GAAGATCTGGCCGAAGACTATGGCCAAGTCGCAGTGTACAAGGTACCATCCCGGGCCAT 900
S H A Y D L D D H H R F V T N K P M L V
901 AGCCACGCCTACGATCTGGATGACCATCACCGCTTCGTTACGAACAAACCGATGCTGGTC 960
A G N T A S M V G E S Y L A P H F T I I
961 GCCGGTAATACCGCATCAATGGTCCGGCAATCGTATCTGGCGCCGATTTTTACCATTATC 1020
G D R A V H Y G Q F D A S G P K T T T G
1021 GGTGATCGTGCCGTTCACTACGGCCAGTTTCGACGCAAGTGGCCCCGAAAACCACGACCGGT 1080
G A A S P S N S A G A A G P G G A A A L
1081 GGTGCGGCAAGTCCGTCAAACCTCAGCGGGTGCGGCGGGTCCGGGCGGTGCGGCGGGCTC 1140
E H H H H H H *
1141 GAGCACCACCACCACCACCACTGA 1164

Figure 16. Translation of optimized sequence of synthetic CrArSM

Catalytic properties of synthetic CrArsM

Wild-type CrArsM and the synthetic variant, both with a 6 x His tag were expressed in *E. coli* and purified in a single step by Ni(II)-nitrilotriacetic acid (NTA) chromatography. Both proteins were examined for their ability to methylate inorganic As(III). While it is possible that the mutations may create structural alterations that could affect activity, synthetic CrArsM was produced in amounts comparable to that of the wild type and was soluble in the cytosol, indicating relatively normal folding.

In the presence of TCEP and SAM, and after 1 h of incubation at 30 °C, 1 μ M of wild-type CrArsM was able to near completely methylate 10 μ M As(III) to DMAs(III), which was converted to DMAs(V) upon treatment with H₂O₂ (Figure 17). Under similar conditions, the synthetic variant could convert ~50% As(III) to MAs(III) and DMAs(III), which are detected as MAs(V) and DMAs(V) after oxidation with H₂O₂. The low activity of synthetic CrArsM may be on account of local conformational changes due to multiple alterations of cysteines to alanines.

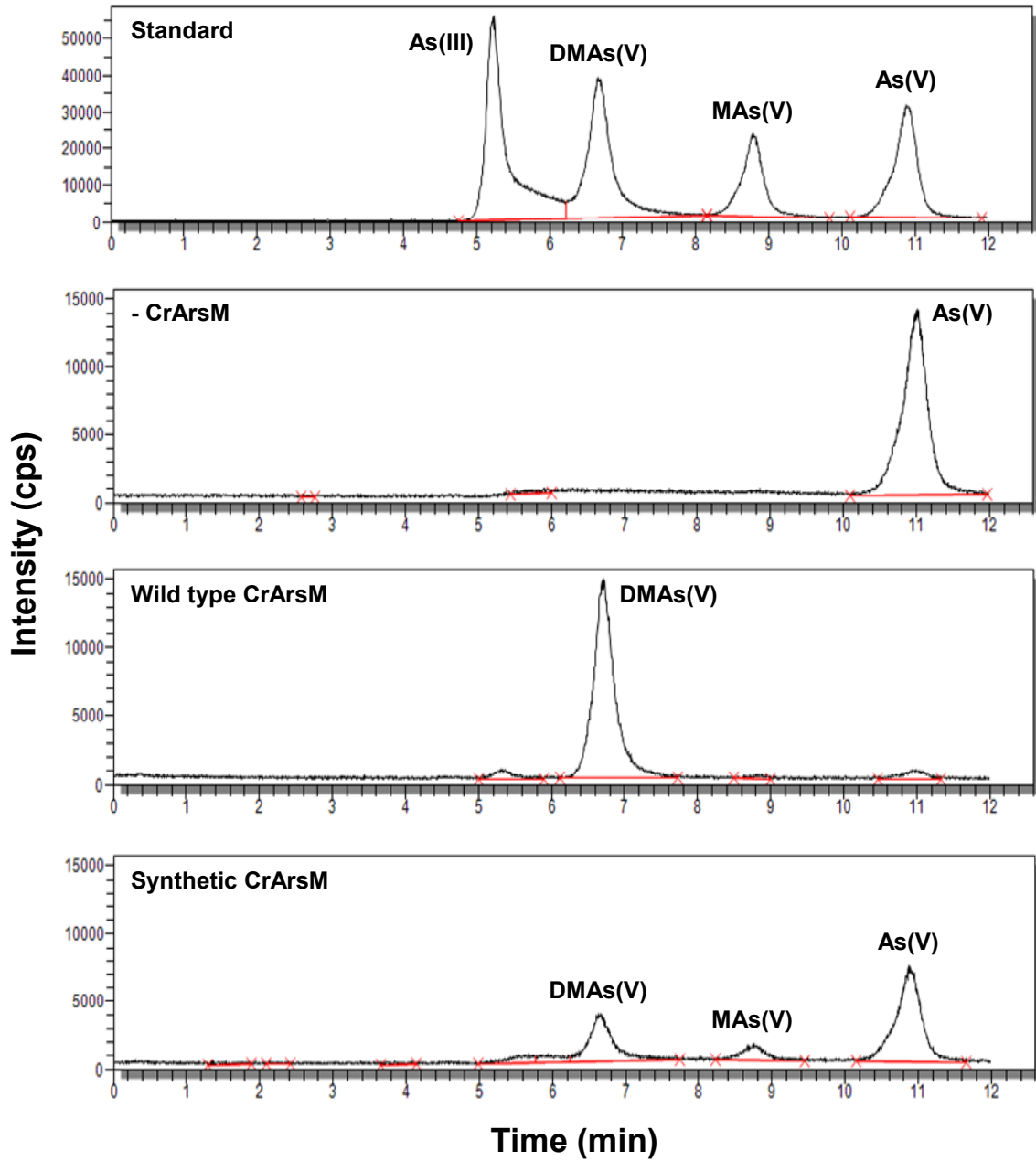


Figure 17. Methylation of As(III) by wild-type and synthetic CrArsM

Tryptophan fluorescence spectroscopy

Intrinsic tryptophan fluorescence has been extensively exploited in examining arsenic binding in arsenic detoxification proteins (Marapakala et al., 2012; Yang et al., 2010; Zhou and Rosen, 1997; Zhou et al., 2002). CrArsM has a single tryptophan at position 332, but the fluorescence of the wild-type protein does not

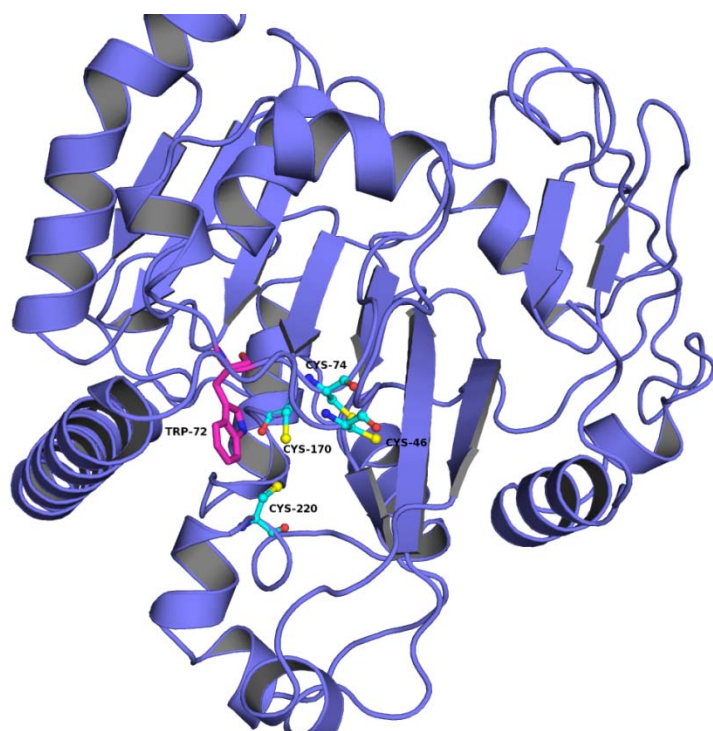


Figure 18. Homology modeling of CrArsM based on CmArsM native structure.

respond to ligand binding (data not shown). A homology model of CrArsM built on the CmArsM native structure (PDB Id: 4FS8) using the SWISS-MODEL fully automated protein structure homology modeling server (<http://swissmodel.expasy.org/>) (Kiefer et al.,

2009) (Figure 18) shows

that, Tyr72 is located on a loop near Cys74, and may respond to metalloid binding at the active site cysteines. Therefore, Trp332 was changed to a tyrosine residue and Tyr72 was replaced by a tryptophan in the synthetic CrArsM.

The polarity of microenvironment of tryptophan residues in a protein can be assessed from their fluorescence emission spectra (Lakowicz, 1983). In a less polar environment the maximum emission wavelength (λ_{\max}) of tryptophan shifts to a lower wavelength, with an increase in the fluorescence yield (Lakowicz, 1983). When excited at 295 nm, free tryptophan in an aqueous solution has a λ_{\max} at 356 nm (Figure 19), whereas the λ_{\max} of Trp72 (synthetic CrArsM) was 348 nm.

Addition of either $\text{As}(\text{OH})_3$ or $\text{As}(\text{GS})_3$ to CrArsM resulted in a blue shift with a λ_{\max} at 340 nm, which suggests that Trp72 is positioned in a more hydrophobic environment after the addition of metalloids. There is also significant quenching of tryptophan fluorescence. Our interpretation is that the Trp72 is forming a stable complex with metalloids, thereby reducing

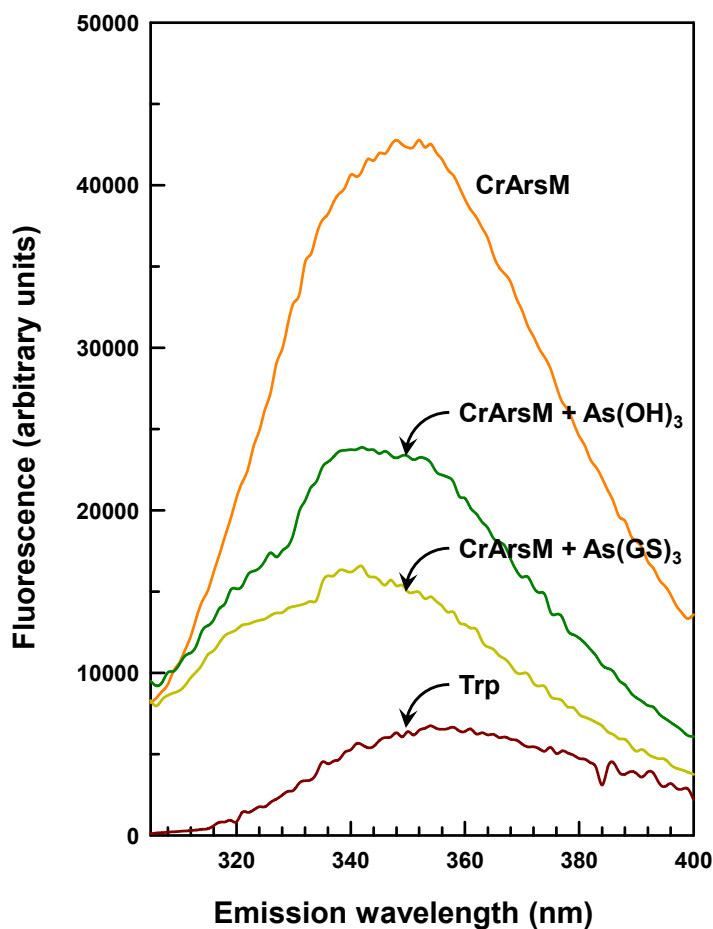


Figure 19. Emission spectra of synthetic CrArsM. Samples were excited at 295 nm and emission spectra were acquired at 23 °C as described in Materials and Methods. The emission spectra of 1 μM CrArsM and upon addition of either 100 μM $\text{As}(\text{OH})_3$ or $\text{As}(\text{GS})_3$ were compared with that of 1 μM tryptophan.

the number of fluorophores that can emit. Further experiments are needed to determine the quenching mechanism.

The effect of arsenicals on the time course of fluorescence quenching of synthetic CrArsM was examined (Figure 20). Addition of As(III) showed a gradual quenching of the fluorescence signal. In contrast, the rate of quenching upon addition of As(GS)₃ follows a biphasic curve with an extremely fast phase that is difficult to quantify by traditional methods. Overall, the experiment shows that binding of glutathione conjugates is extremely rapid, but detailed rate determinations will require stopped-flow analysis.

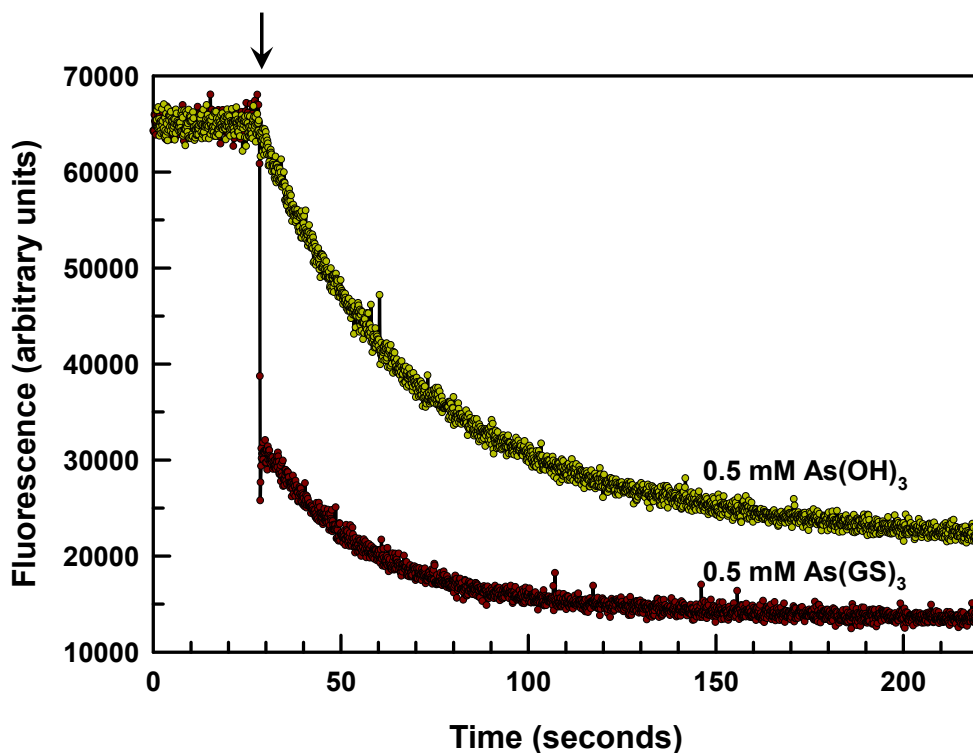


Figure 20. Effect of As(OH)₃ and As(GS)₃ on the fluorescence of synthetic CrArsM. Protein fluorescence was assayed at 23 °C with excitation and emission wavelengths of 295 and 355 nm, respectively, as described in Materials and Methods. Each assay contained 2 μM CrArsM. Arrow indicates the addition of either As(OH)₃ or As(GS)₃.

Crystallization studies

Needle crystals of CrArsM initially diffracted to a resolution range from 7.0 Å to 4.5 Å, but improved with seeding. Diffraction-quality crystals formed overnight with dimensions of 0.3 x 0.3 x 0.2 mm (Figure 21).

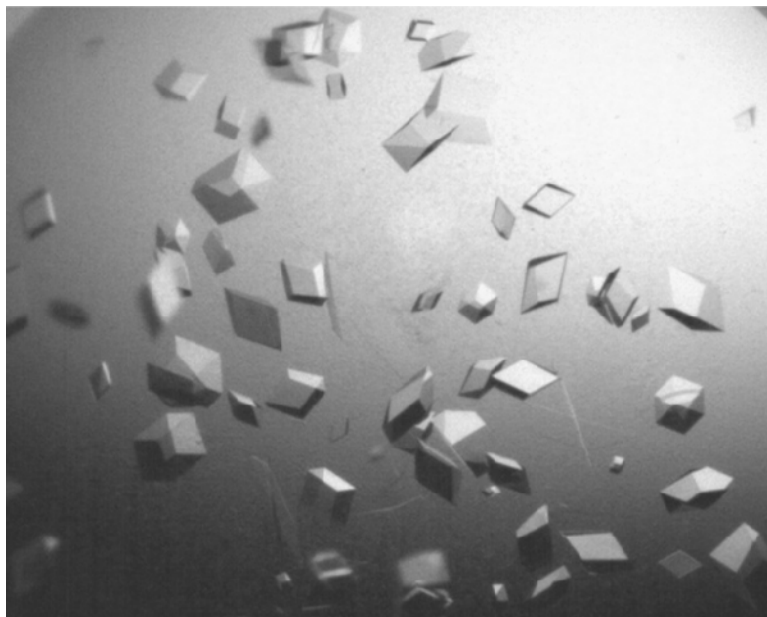


Figure 21. Crystals of CrArsM were grown by hanging drop vapor diffusion.

Complete data sets were collected up to 2.40 Å resolution using a single crystal of CrArsM (Figure 22). The data processing statistics are shown in Table 6. The crystals belonged to R3: H space group with unit cell parameters of $a = b = 157.8$ Å and $c = 95.4$ Å; $\gamma = 120^\circ$. Evaluation of crystal packing parameters indicated that the lattice can accommodate two molecules in the asymmetric unit with a Matthews's coefficient of 2.73 Å³Da⁻¹ and a solvent content of 54.9 %.

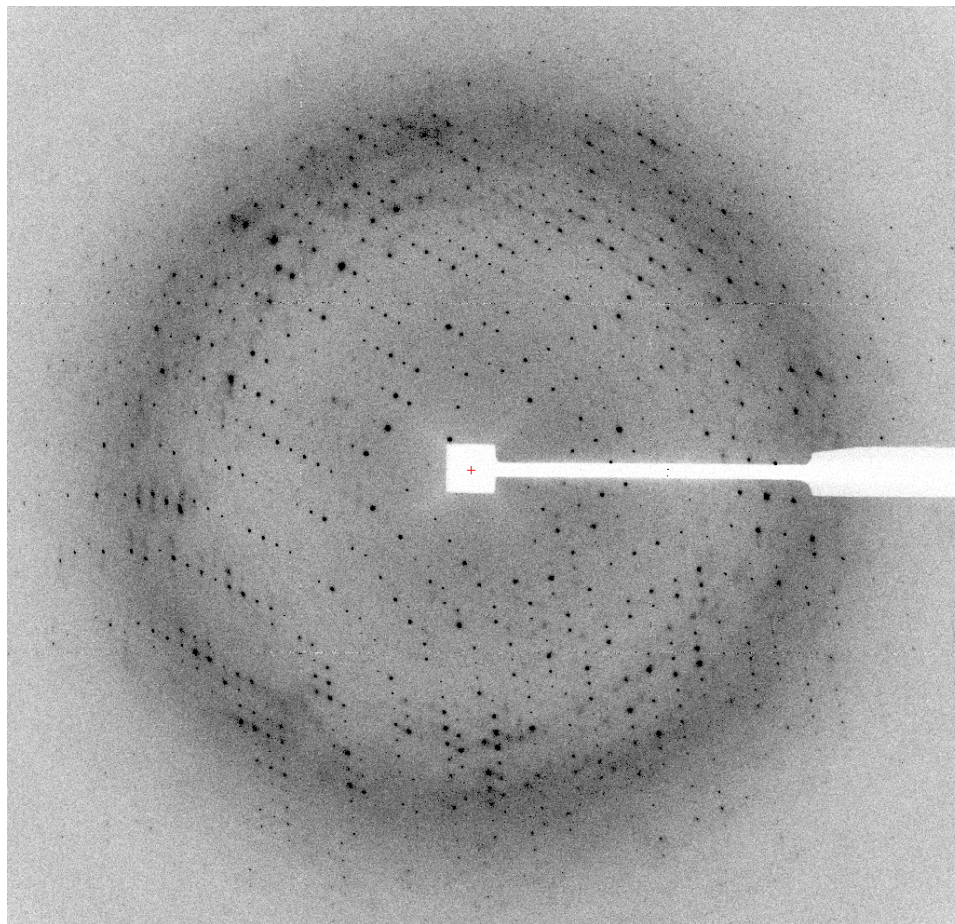


Figure 22. The diffraction images (1° oscillation) were collected from CmArsM crystals at APL, Argonne National Laboratory, using a MAR 300 detector at 100°K . The edge of the image corresponds to 2.40 \AA resolution.

Table 6. Data collection and processing

Diffraction source	Synchrotron (APS 22-BM)
Wavelength (Å)	1.00
Temperature (K)	100
Detector	MAR-300 CCD detector
Crystal-detector distance (mm)	240
Rotation range per image (°)	1
Total rotation range (°)	360
Exposure time per image (s)	3.9
Space group	R3:H
<i>a</i> , <i>b</i> , <i>c</i> (Å)	157.8, 157.8, 95.4
α , β , γ (°)	90.0, 90.0, 120.0
Mosaicity (°)	0.2
Resolution range (Å)	50-2.40 (2.40-2.49)
Total No. of reflections	404,464 (40,054)
No. of unique reflections	34,690 (3483)
Completeness (%)	100 (100)
Redundancy	11.7 (11.5)
$\langle I/\sigma(I) \rangle$	34.1 (6.8)
$R_{r.i.m.}$	8.3 (42.8)
R_{merge}	8.0 (40.9)
Mattews coefficient (Å ³ Da ⁻¹)	2.73
Overall <i>B</i> factor from Wilson plot (Å ²)	45.2

Note: Values for the outer shell are given in parentheses.

$R_{merge} = \frac{\sum_{hkl} \sum_i |I_i(hkl) - \langle I(hkl) \rangle|}{\sum_{hkl} \sum_i I_i(hkl)}$, where $I_i(hkl)$ is the observed intensity and $\langle I(hkl) \rangle$ is the average intensity over symmetry equivalent measurements.

Structure of CrArsM

The structure of CrArsM has been determined to a final resolution of 2.4 Å (Packianathan et al, *unpublished data*). Overall, the structure has three domains:

N-terminal domain, SAM

binding domain, and the

C-terminal domain. The

structure shows residues

50 through 372. The first

49 residues in the N-

terminal domain are not

visible. The three

conserved cysteines,

Cys74, Cys170 and

Cys220 form the As(III)

binding site. Cys46, one

of the four conserved

cysteines, cannot be seen

in this structure (Figure

23). The novelty of this

structure is the

observation of a disulfide

bond between the

conserved cysteines, Cys74 and Cys170.

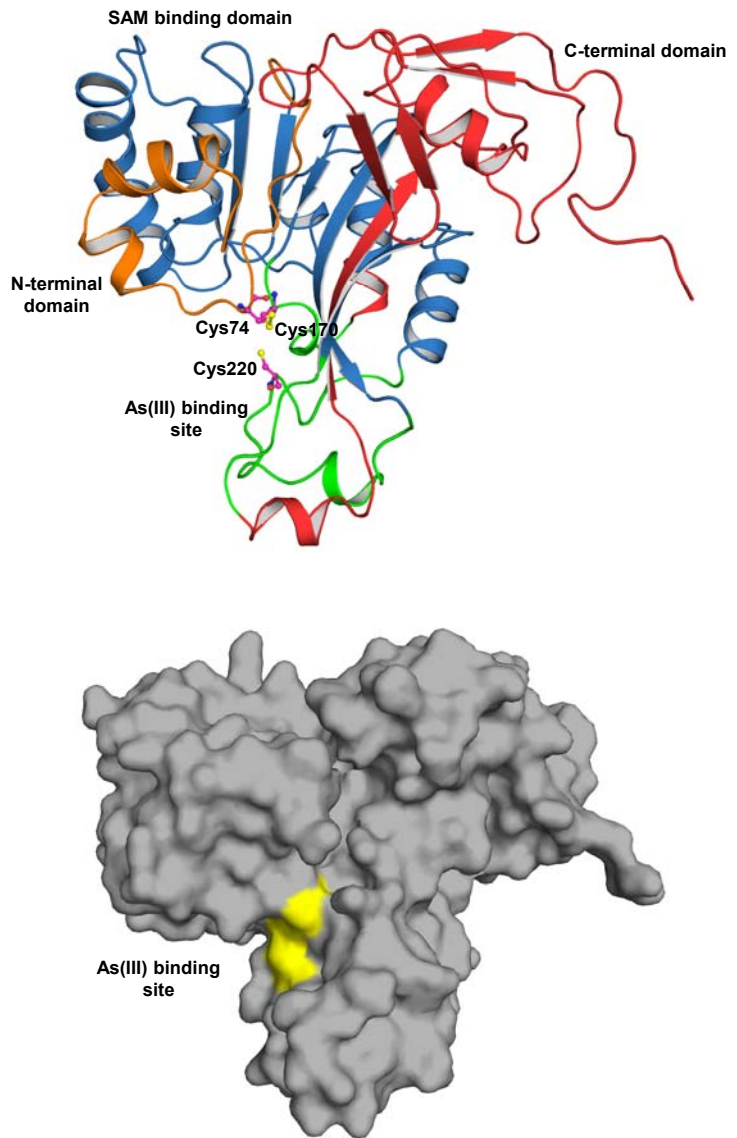


Figure 23. Overall structure of CrArsM. *Top*, The secondary structure elements are drawn as cartoon diagram. *Bottom*, Surface representation of CrArsM with the As(III) binding site shown in yellow

Discussion

Eukaryotic ArsMs have been refractory to crystallization. This may be because ArsM have a number of cysteine residues, which give rise to undefined aggregates, thereby hindering the crystallization process. A multiple sequence alignment of several eukaryotic ArsM homologs shows the presence of four conserved cysteines (Figure 14). A synthetic variant of CrArsM was constructed that retained the four conserved cysteines at position 46, 74, 170 and 220 of the primary sequence. The remaining 13 cysteines were altered to alanine. Synthetic CrArsM was able to convert As(III) to mono- and dimethyl derivatives, although at a reduced efficiency than the wild type enzyme. Furthermore, synthetic CrArsM bound the glutathione conjugate of As(III) extremely rapidly. These preliminary experiments indicated that the synthetic version behaved similarly as the wild type. Diffraction quality crystals of synthetic CrArsM formed overnight at room temperature. The structure was resolved at 2.4 Å resolution. Cys74, Cys170 and Cys220 form the As(III) binding site. This structure does not have any As(III) bound to its active site. Cys74 and Cys170 form a disulfide bond. This structure is different from that of CmArsM (PDB ID: 4FS8) where no disulfide bonds were found in the native structure.

Human As(III) S-adenosylmethionine (SAM) methyltransferase (hAS3MT) has four conserved cysteines, Cys32, Cys61, Cys156, Cys206 (Figure 14). A synthetic gene encoding *hAs3MT* was expressed, and the purified enzyme characterized (Dheeman et al 2014). The synthetic enzyme is considerably more active than a cDNA-expressed enzyme using endogenous reductants thioredoxin

(Trx), thioredoxin reductase (TR), NADPH and reduced glutathione (GSH). Each of the seven cysteines (the four conserved residues Cys32, Cys61, Cys156, Cys206, and non-conserved Cys72, Cys85, Cys250) was individually changed to serine. The non-conserved cysteine derivatives were still active. None of the individual C32S, C61S, C156S and C206S derivatives was able to methylate As(III). However, the C32S and C61S enzymes retained the ability to methylate MAs(III). These observations suggest that Cys156 and Cys206 play a different role in catalysis than Cys32 and Cys61. Two other observations shed light on the pathway of methylation. First, binding assays using the fluorescence of a single-tryptophan derivative indicate that As(GS)₃ binds to the enzyme much faster than inorganic As(III). Second, the major product of the first round of methylation is MAs(III), not MAs(V), and remains enzyme-bound until methylated a second time.

Marapakala et al (2014) have reported new crystal structures of CmArsM with the bound aromatic arsenical phenylarsenite (PhAs(III)) at 1.80 Å resolution (PDB ID: 4KW7) and reduced roxarsone (Rox(III)) at 2.38 Å resolution (PDB ID: 4KU9). These organoarsenicals are bound to two of four conserved cysteine residues, Cys174 and Cys224. The electron density extends the structure to include a newly identified conserved cysteine residue, Cys44, which is disulfide bonded to the fourth conserved cysteine residue, Cys72. A second disulfide bond between Cys72 and Cys174 is observed in crystals with bound SAM (PDB ID: 4FR0). In the SAM-bound structure, the helix containing Cys44 and Cys72 reorients by nearly 6.5 Å closer to the As(III) binding site, relative to the

unliganded structure, which suggests that this movement leads to formation of the Cys72-Cys174 disulfide bond.

Based on these observations, a novel disulfide cascade reaction scheme has been proposed for CmArsM, which may also be extended to CrArsM mediated catalysis (Figure 24). The proposed reaction mechanism consists of at least two sequential disulfide bonds, the first between Cys46-Cys74, and the second between Cys74-Cys170 (Figure 24). The catalytic cycle for the first two rounds of methylation can be summarized in eight steps. 1) In the first round of methylation, CrArsM binds As(III) in a series of three thiol transfer reactions from $\text{As}(\text{GS})_3$, which is the preferred substrate. 2) The methyl group of SAM is attacked by the arsenic lone pair, 3) which leads to formation of a positively charged pentavalent MAs(V) intermediate (Cullen, 2014). 4) The role of Cys46 is to provide electrons to reduce enzyme bound MAs(V) to MAs(III) and allow the next round of methylation. By donating electrons to the arsenic, Cys46 becomes oxidized, forming a disulfide bond with Cys74. 5) The role of Trx is to reduce the disulfide bond, consistent with the traditional role of thioredoxins in facilitating reduction of protein cysteine disulfides by thiol-disulfide exchange. Oxidized Trx is reduced by TR with electrons from NADPH. MAs(III) remains strongly bound by the thiol pair Cys74-Cys170. The disulfide bond is reduced with Trx, and 6) the enzyme undergoes the next round of methylation, forming a positively charged pentavalent DMAs(V) intermediate, 7) which is reduced to DMAs(III) by Cys74, forming a Cys74-Cys170 disulfide. 8) The disulfide is reduced by Trx,

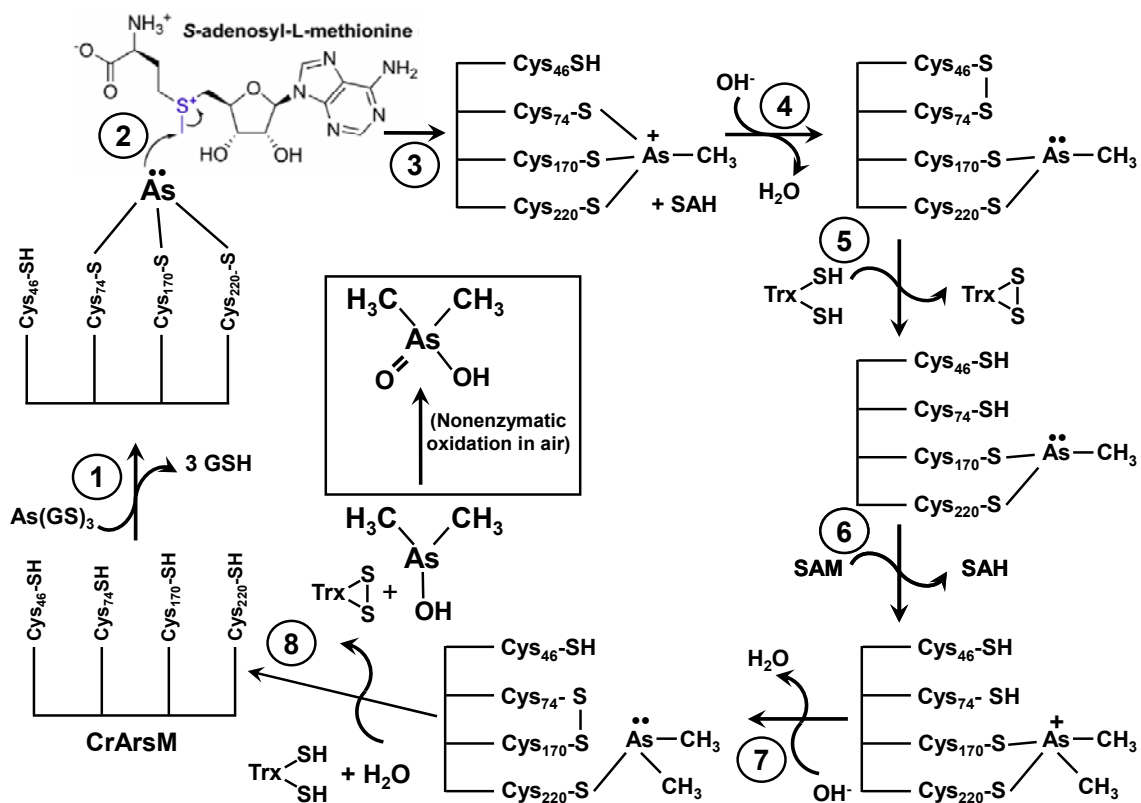


Figure 24. Proposed CrArsM reaction scheme

regenerating the enzyme and releasing the major soluble product, DMAs(III), which is oxidized nonenzymatically to DMAs(V). Thus, the substrates and products are all trivalent, as predicted by Hayakawa et al. (Hayakawa et al., 2005), but the arsenic undergoes a cycle of oxidation and reduction, as hypothesized by Challenger (Challenger, 1947), but only when enzyme-bound. GSH and Trx are involved, but not as reductants of pentavalent intermediates. Instead, $\text{As}(\text{GS})_3$ serves as the arsenic donor to the enzyme, as hypothesized by Hayakawa et al. (Hayakawa et al., 2005), and Trx is a protein disulfide reductase (Holmgren, 1988). The above hypothesis leads to many unanswered questions.

For example, how does ArsM use the glutathione conjugate, As(GS)₃? What is the role of the four conserved cysteine residues in arsenic binding and catalysis? How does the enzyme know whether the substrate is As(III), where Cys46 and Cys74 are required, and MAs(III), where they are not? These questions may be resolved by an array of biochemical and biophysical experiments, including fluorescence measurements, isothermal titration calorimetry, site-directed mutagenesis as well as crystallization of additional orthologs in the presence of substrates and effectors.

CHAPTER IV

Conclusion

Life on earth originated in primordial environments where there were excess metals and harsh conditions. The abundance of metals made it necessary for the first organisms to develop detoxification systems and modify the metals. Arsenic may have been present in very high concentrations as were other toxic metalloids (Sforna et al., 2014). This is one of the reasons why arsenic related extrusion mechanisms are found in almost all the organisms from simple bacteria to humans. Arsenate mimics phosphate and thus enters organisms through the various phosphate uptake systems (Rosenberg et al., 1977). The necessity for arsenic detoxification is common but organisms have evolved different mechanisms to realize this need. The overarching theme of my research has been to elucidate the mechanisms of arsenic resistance, in particular how proteins bind As(III). In my dissertation research, I investigated two prominent arsenite detoxification mechanisms – ATPase-based extrusion and methyltransferase based biomethylation. It is clear that ATPase-based extrusion is a mechanism to extrude arsenite from cells and hence produce resistance. However, there are contradicting views about the role of arsenic biomethylation in detoxification. Several of the key events of arsenite biomethylation are not clear, and understanding them will help elucidate the role of this enzyme.

The ubiquity of arsenic in environment around us, both from anthropogenic sources and from human activities makes it the most ubiquitous

environmental toxin and Group 1 human carcinogen according to the U.S. Environmental Protection Agency (EPA) and the Agency for Toxic Substances and Disease Registry (ATSDR) Priority List of Hazardous Substances (<http://www.atsdr.cdc.gov/SPL/index.html>). Humans with long-term chronic and occupational exposure to arsenic have been shown to have high prevalence to multi-organ cancers (Chappell *et al.*, 1997; Kozul *et al.*, 2009). Both pentavalent As(V) and trivalent As(III) are toxic, with the latter more toxic than the former. Arsenolysis of arsenate compounds and the ability of arsenite to form strong bonds with thiol (-SH) groups are the major mechanisms for the action of arsenic. Arsenic enters cells adventitiously through uptake systems for phosphate (Willisky and Malamy, 1980), sugars (Liu *et al.*, 2004) and other polyols (Sanders *et al.*, 1997; Meng *et al.*, 2004). All identified extrusion systems of arsenic to date have been for As(III). One of the most common As(III) extrusion system found in microorganisms is ArsAB pump, which was first discovered in the R773 *ars* operon of *E. coli* (Moblely *et al.*, 1983). The *arsA* and *arsD* genes of *ars* operons are always found together, and their linkage suggests that they co-evolved (Lin *et al.*, 2006). Later, ArsD was shown to a metallochaperone which transfers metalloid to ArsA ATPase (Lin *et al.*, 2007; Yang *et al.*, 2010). The presence of an *arsD* gene in addition to *arsAB* genes gives cells a competitive advantage over cells having only the *arsAB* genes while growing in sub-toxic concentrations of arsenic. Additionally, cells expressing *arsDAB* accumulate less As(III) than those expressing only *arsAB* (Lin *et al.*, 2006). Although extensive research have been carried out on both the structural details of ArsA

and ArsD and their biochemical roles, limited work has been performed to understand and identify the surface residues of ArsA that interact with ArsD (Yang *et al.*, 2011).

In the second chapter, I studied the interaction between ArsA and ArsD. ArsD mutant K2A/K37A/K62A/K104A (4KA ArsD) does not interact with wild type ArsA in a yeast two-hybrid assay (Yang *et al.*, 2011). I isolated three suppressor mutations in ArsA (Q56R, F120I, and D137V) through a e-PCR-based yeast two-hybrid approach, which screened for mutants exhibiting increased interaction with wild type ArsD compared with 4KA ArsD (Figure 9). Each of these three residues in ArsA (Gln56, Phe120, and Asp137) is located in NBD1. Gln56 is situated in between the H3-S3 loop and exposed to solvent. Phe120 is in the middle of H6 helix and surrounded by hydrophobic residues. Asp137 is in the H7-S5 loop and exposed to solvent (Lin *et al.*, 2006). When wild type ArsD was added to an *in vitro* ATPase assay, the apparent affinity of wild type ArsA for As(III) increased 8.5-fold (Figure 11 and Table 4). Addition of 4KA ArsD to the assay decreased the half maximal concentration for As(III) 1.6-fold. Q56R ArsA showed basal ATPase activity similar to the wild type, which was stimulated 2.8-fold in the presence of As(III). Addition of either wild type or 4KA ArsD to the assay increased the affinity for As(III) 9- and 2-fold, respectively. These results indicate that, although 4KA ArsD does not stimulate ArsA ATPase activity to the same degree as the wild type, it has a small but significant effect on the affinity of ArsA for As(III). F120I and D137V ArsA showed a basal ATPase rate of 80 and

60 nmol ATP hydrolyzed/min/mg protein, respectively. The ATPase activity of either proteins was not stimulated by As(III); nor were any changes observed upon addition of either wild type or 4KA ArsD. The difference in metalloid binding of wild type ArsA versus Q56R ArsA is not significant. F120I and D137V ArsA do not show metalloid-stimulated ATPase activity, but their affinity for metalloid is unaffected by the mutations in antimony binding assay. A new *in silico* model (Fig. 13A) is proposed that supports our experimental data indicating that Q56R ArsA strongly interacts with wild-type ArsD and weakly with 4KA ArsD. The new model also accommodates most of the ArsD residues that were shown to interact with ArsA by two-hybrid analysis (Yang et al., 2011).

In the third chapter, I investigated the As(III) binding properties of the ArsM As(III) S-adenosylmethionine (SAM) methyltransferase. Methylation is a common biotransformation found in nature carried out by methyltransferase (MT) class of enzymes (Liscombe *et al.*, 2012). Addition of a methyl group to an atom modulates its bioavailability, bioactivity and reactivity. SAM is the most common source of the transfer of methyl group in MTs. It is the most used substrate after ATP (Loenen, 2006). SAM is the methyl donor to a wide variety of biological molecules like DNA, RNA, histones and proteins. Low levels of serum folate, high levels of plasma homocysteine and polymorphisms in the MTHF receptor are implicated in SAM depletion and a wide range of diseases in humans (Coppen & Bolander-Gouaille, 2005, Ulrey *et al.*, 2005). Biomethylation of arsenite is widespread and occurs in all three domains of life, bacteria, archaea

and eukaryota (Ye *et al.*, 2012, Sumi & Himeno, 2012, Zhu *et al.* 2014). There are two major hypotheses about the pathway of arsenic methylation: Challenger's pathway (Challenger, 1944) and Hirano's pathway (Hayakawa *et al.*, 2005). Whether arsenic biomethylation is a pathway of arsenic detoxification is still being debated. Some of the intermediate products, MAs(III) and DMAs(III), are more toxic than As(III) (Styblo *et al.*, 2000, Sakurai *et al.*, 2006, Hirano & Kobayashi, 2006). However, the pentavalent intermediate products, MAs(V) and DMAs(V), are much less toxic than As(III) (Styblo *et al.*, 2000), and the end product, TMA(III), is almost nontoxic (Cullen, 2005). Understanding the molecular process of arsenic biomethylation is important in solving the paradox of As(III) biotransformation into potentially more toxic arsenic species.

In this third chapter, I studied the molecular mechanism of arsenic biomethylation using biochemistry and biophysical approaches. A synthetic variant of CrArsM was constructed that retained the four conserved cysteines at position 46, 74, 170 and 220 of the primary sequence. The remaining 13 cysteines were altered to alanine. Synthetic CrArsM was able to convert As(III) to mono- and dimethyl derivatives, although at a reduced efficiency of 25% than the wild type enzyme. Synthetic CrArsM bound the triglutathione conjugate of As(III), As(GS)₃, extremely rapidly compared to inorganic As(III), which is As(OH)₃ in solution (Figure 20). These experiments indicated that the synthetic version behaved similarly as the wild type. Diffraction quality crystals of synthetic CrArsM formed overnight at room temperature, allowed, the structure to be

resolved at 2.4 Å resolution. This was done in collaboration with Charles Packianathan. Cys74, Cys170 and Cys220 form the As(III) binding site. This structure does not have As(III) bound to its active site. Cys74 and Cys170 form a disulfide bond. This structure is different from that of CmArsM (PDB ID: 4FS8), where no disulfide bonds were found in the native structure. A novel disulfide cascade reaction scheme has been proposed for CmArsM, which may also be extended to CrArsM catalysis (Figure 24). The substrates and products are all trivalent, as predicted by Hayakawa et al. (Hayakawa et al., 2005), but the arsenic undergoes a cycle of oxidation and reduction, as hypothesized by Challenger (Challenger, 1947), but only when enzyme-bound.

This study has isolated three ArsA mutants showing increased interaction with wild type ArsD - the Q56R, F120I and D137V ArsA mutants. The new interaction model of the ArsA-ArsD interface suggests that the salt bridges along with the increased intermolecular hydrogen bonding contributes to the increased interaction between Q56R ArsA and wild-type ArsD. The probable interactions according to this new model should be further studied by protein-protein interaction assays or ATPase activity assays. . Attempts at crystallization of the increased interaction mutants have been unsuccessful in past. These increased interactions may contribute to a stable co-crystal that can solve the interaction interface. The increased hydrogen bonding may provide the required interaction to keep the ArsA and ArsD together during crystallization. The synthetic CrArsM shows the involvement and requirement of 4 cysteines for biomethylation of arsenite by ArsM. These four conserved cysteines should be

the target of future studies of arsenite binding and enzymatic methylation. The native crystal structure of CrArsM resembles the 4FS8 structure of CmArsM except for the disulfide bond between Cys74 and Cys170. Previously reported structures of CmArsM have shown disulfide bond between active site cysteines in the presence of organoarsenicals (4KW7 and 4KU9) or SAM (4FRD). The solved structure of native synthetic CrArsM is the first reported disulfide bond in native crystal structure. Future crystallization with ligands can shed light on the presence/absence of disulfide bonds when ligand is bound to synthetic CrArsM. A biochemical analysis of disulfide bond formation during enzyme catalysis can be performed to test the disulfide bond cascade hypothesis.

References:

- Abernathy, C.O., Liu, Y.P., Longfellow, D., Aposhian, H.V., Beck, B., Fowler, B., Goyer, R., Menzer, R., Rossman, T., Thompson, C., *et al.* (1999). Arsenic: health effects, mechanisms of actions, and research issues. *Environ Health Perspect* *107*, 593-597.
- Adams, A., Gottschling, D.E., Kaiser, C., and Stearns, T. (1998). *Methods in Yeast Genetics: A Cold Spring Harbor laboratory course manual* (Cold Spring Harbor, NY.: Cold Spring Harbor laboratory).
- Ajees, A.A., Marapakala, K., Packianathan, C., Sankaran, B., and Rosen, B.P. (2012). Structure of an As(III) S-adenosylmethionine methyltransferase: insights into the mechanism of arsenic biotransformation. *Biochemistry* *51*, 5476-5485.
- Auld, K.L., Hitchcock, A.L., Doherty, H.K., Fietze, S., Huang, L.S., and Silver, P.A. (2006). The conserved ATPase Get3/Arr4 modulates the activity of membrane-associated proteins in *Saccharomyces cerevisiae*. *Genetics* *174*, 215-227.
- Beane Freeman, L.E., Dennis, L.K., Lynch, C.F., Thorne, P.S., and Just, C.L. (2004). Toenail arsenic content and cutaneous melanoma in Iowa. *Am J Epidemiol* *160*, 679-687.
- Bennett, M.S., Guan, Z., Laurberg, M., and Su, X.D. (2001). *Bacillus subtilis* arsenate reductase is structurally and functionally similar to low molecular weight protein tyrosine phosphatases. *Proc Natl Acad Sci USA* *98*, 13577-13582.
- Bhattacharjee, H., Choudhury, R., and Rosen, B.P. (2008). Role of conserved aspartates in the ArsA ATPase. *Biochemistry* *47*, 7218-7227.
- Bhattacharjee, H., Li, J., Ksenzenko, M.Y., and Rosen, B.P. (1995). Role of cysteinyl residues in metalloactivation of the oxyanion-translocating ArsA ATPase. *J Biol Chem* *270*, 11245-11250.
- Bhattacharjee, H., and Rosen, B.P. (1996). Spatial proximity of Cys113, Cys172, and Cys422 in the metalloactivation domain of the ArsA ATPase. *J Biol Chem* *271*, 24465-24470.
- Bhattacharjee, H., and Rosen, B.P. (2000). Role of conserved histidine residues in metalloactivation of the ArsA ATPase. *Biometals* *13*, 281-288.

- Bhattacharjee, H., Sheng, J., Ajees, A.A., Mukhopadhyay, R., and Rosen, B.P. (2010). Adventitious arsenate reductase activity of the catalytic domain of the human Cdc25B and Cdc25C phosphatases. *Biochemistry* 49, 802-809.
- Bhattacharjee, H., Zhou, T., Li, J., Gatti, D.L., Walmsley, A.R., and Rosen, B.P. (2000). Structure-function relationships in an anion-translocating ATPase. *Biochem Soc Trans* 28, 520-526.
- Bobrowicz, P., Wysocki, R., Owsianik, G., Goffeau, A., and Ulaszewski, S. (1997). Isolation of three contiguous genes, *ACR1*, *ACR2* and *ACR3*, involved in resistance to arsenic compounds in the yeast *Saccharomyces cerevisiae*. *Yeast* 13, 819-828.
- Bozkurt, G., Stjepanovic, G., Vilardi, F., Amlacher, S., Wild, K., Bange, G., Favaloro, V., Rippe, K., Hurt, E., Dobberstein, B., *et al.* (2009). Structural insights into tail-anchored protein binding and membrane insertion by Get3. *Proc Natl Acad Sci USA* 106, 21131-21136.
- Bun-Ya, M., Nishimura, M., Harashima, S., and Oshima, Y. (1991). The *PHO84* gene of *Saccharomyces cerevisiae* encodes an inorganic phosphate transporter. *Mol Cell Biol* 11, 3229-3238.
- Bun-ya, M., Shikata, K., Nakade, S., Yompakdee, C., Harashima, S., and Oshima, Y. (1996). Two new genes, *PHO86* and *PHO87*, involved in inorganic phosphate uptake in *Saccharomyces cerevisiae*. *Curr Genet* 29, 344-351.
- Cadwell, R.C., and Joyce, G.F. (1992). Randomization of genes by PCR mutagenesis. *PCR Methods Appl* 2, 28-33.
- Calatayud, M., Barrios, J.A., Velez, D., and Devesa, V. (2012). *In vitro* study of transporters involved in intestinal absorption of inorganic arsenic. *Chem Res Toxicol* 25, 446-453.
- Challenger, F. (1947). Biological methylation. *Sci Prog* 35, 396-416.
- Challenger, F. (1951). Biological methylation. *Advances in enzymology and related subjects of biochemistry* 12, 429-491.
- Challenger, F., and Higginbottom, C. (1935). The production of trimethylarsine by *Penicillium brevicaulis* (*Scopulariopsis brevicaulis*). *Biochem J* 29, 1757-1778.
- Chappell, W.R., Beck, B.D., Brown, K.G., Chaney, R., Cothorn, R., Cothorn, C.R., Irgolic, K.J., North, D.W., Thornton, I., and Tsongas, T.A. (1997). Inorganic arsenic: a need and an opportunity to improve risk assessment. *Environ Health Perspect* 105, 1060-1067.

Chen, C.M., Misra, T.K., Silver, S., and Rosen, B.P. (1986). Nucleotide sequence of the structural genes for an anion pump. The plasmid-encoded arsenical resistance operon. *J Biol Chem* 261, 15030-15038.

Chen, J., Qin, J., Zhu, Y.G., de Lorenzo, V., and Rosen, B.P. (2013). Engineering the soil bacterium *Pseudomonas putida* for arsenic methylation. *Appl Environ Microbiol* 79, 4493-4495.

Chen, Y., and Rosen, B.P. (1997). Metalloregulatory properties of the ArsD repressor. *J Biol Chem* 272, 14257-14262.

Cole, S.P., Sparks, K.E., Fraser, K., Loe, D.W., Grant, C.E., Wilson, G.M., and Deeley, R.G. (1994). Pharmacological characterization of multidrug resistant MRP-transfected human tumor cells. *Cancer Res* 54, 5902-5910.

Coppen, A., and Bolander-Gouaille, C. (2005). Treatment of depression: time to consider folic acid and vitamin B₁₂. *Journal of psychopharmacology* 19, 59-65.

Cui, X., Kobayashi, Y., Hayakawa, T., and Hirano, S. (2004). Arsenic speciation in bile and urine following oral and intravenous exposure to inorganic and organic arsenics in rats. *Toxicol Sci* 82, 478-487.

Cullen, W.R. (2005). The toxicity of trimethylarsine: an urban myth. *Journal of environmental monitoring : JEM* 7, 11-15.

Cullen, W.R. (2014). Chemical mechanism of arsenic biomethylation. *Chem Res Toxicol* 27, 457-461.

DeLano, W.L. (2001). *The PyMOL user's manual* (San Carlos, CA: DeLano Scientific).

Delnomdedieu, M., Basti, M.M., Styblo, M., Otvos, J.D., and Thomas, D.J. (1994). Complexation of arsenic species in rabbit erythrocytes. *Chem Res Toxicol* 7, 621-627.

Denic, V., Dotsch, V., and Sinning, I. (2013). Endoplasmic reticulum targeting and insertion of tail-anchored membrane proteins by the GET pathway. *Cold Spring Harb Perspect Biol* 5, a013334.

Dey, S., Dou, D., Tisa, L.S., and Rosen, B.P. (1994). Interaction of the catalytic and the membrane subunits of an oxyanion-translocating ATPase. *Arch Biochem Biophys* 311, 418-424.

Dey, S., and Rosen, B.P. (1995). Dual mode of energy coupling by the oxyanion-translocating ArsB protein. *J Bacteriol* 177, 385-389.

Dheeman, D.S., Packianathan, C., Pillai, J.K. and Rosen, B.P. The pathway of human AS3MT arsenic methylation *Chem Res Toxicol*. (submitted September 2014)

Ding, L., Saunders, R.J., Drobna, Z., Walton, F.S., Xun, P., Thomas, D.J., and Styblo, M. (2012). Methylation of arsenic by recombinant human wild-type arsenic (+3 oxidation state) methyltransferase and its methionine 287 threonine (M287T) polymorph: Role of glutathione. *Toxicol Appl Pharmacol* 264, 121-130.

Doudoroff, M., Barker, H.A., and Hassid, W.Z. (1947). Studies with bacterial sucrose phosphorylase; the mechanism of action of sucrose phosphorylase as a glucose-transferring enzyme (transglucosidase). *J Biol Chem* 168, 725-732.

Drobna, Z., Del Razo, L.M., Garcia-Vargas, G.G., Sanchez-Pena, L.C., Barrera-Hernandez, A., Styblo, M., and Loomis, D. (2013). Environmental exposure to arsenic, AS3MT polymorphism and prevalence of diabetes in Mexico. *Journal of exposure science & environmental epidemiology* 23, 151-155.

Drobna, Z., Walton, F.S., Paul, D.S., Xing, W., Thomas, D.J., and Styblo, M. (2010). Metabolism of arsenic in human liver: the role of membrane transporters. *Arch Toxicol* 84, 3-16.

Engstrom, K., Vahter, M., Mlakar, S.J., Concha, G., Nermell, B., Raqib, R., Cardozo, A., and Broberg, K. (2011). Polymorphisms in arsenic(+III oxidation state) methyltransferase (AS3MT) predict gene expression of AS3MT as well as arsenic metabolism. *Environ Health Perspect* 119, 182-188.

Fauman, E.B., Cogswell, J.P., Lovejoy, B., Rocque, W.J., Holmes, W., Montana, V.G., Piwnica-Worms, H., Rink, M.J., and Saper, M.A. (1998). Crystal structure of the catalytic domain of the human cell cycle control phosphatase, Cdc25A. *Cell* 93, 617-625.

Fields, S., and Song, O. (1989). A novel genetic system to detect protein-protein interactions. *Nature* 340, 245-246.

Fontecave, M., Atta, M., and Mulliez, E. (2004). S-adenosylmethionine: nothing goes to waste. *Trends Biochem Sci* 29, 243-249.

Fu, H.L., Meng, Y., Ordonez, E., Villadangos, A.F., Bhattacharjee, H., Gil, J.A., Mateos, L.M., and Rosen, B.P. (2009). Properties of arsenite efflux permeases (Acr3) from *Alkaliphilus metalliredigens* and *Corynebacterium glutamicum*. *J Biol Chem* 284, 19887-19895.

Ge, R.G., Wang, D.X., Hao, M.C., and Sun, X.S. (2013). Nickel trafficking system responsible for urease maturation in *Helicobacter pylori*. World journal of gastroenterology : WJG 19, 8211-8218.

Ghosh, M., Shen, J., and Rosen, B.P. (1999). Pathways of As(III) detoxification in *Saccharomyces cerevisiae*. Proc Natl Acad Sci USA 96, 5001-5006.

Gill, S.C., and von Hippel, P.H. (1989). Calculation of protein extinction coefficients from amino acid sequence data. Anal Biochem 182, 319-326.

Gladysheva, T.B., Oden, K.L., and Rosen, B.P. (1994). Properties of the arsenate reductase of plasmid R773. Biochemistry 33, 7288-7293.

Green, M.R., Sambrook, J., and Sambrook, J. (2012). Molecular cloning : a laboratory manual, 4th edn (Cold Spring Harbor, NY: Cold Spring Harbor Laboratory Press).

Hagenbuch, B., and Meier, P.J. (2004). Organic anion transporting polypeptides of the OATP/ SLC21 family: phylogenetic classification as OATP/ SLCO superfamily, new nomenclature and molecular/functional properties. Pflugers Arch 447, 653-665.

Hayakawa, T., Kobayashi, Y., Cui, X., and Hirano, S. (2005). A new metabolic pathway of arsenite: arsenic-glutathione complexes are substrates for human arsenic methyltransferase Cyt19. Arch Toxicol 79, 183-191.

Hirano, S., and Kobayashi, Y. (2006). Cytotoxic effects of S-(dimethylarsino)-glutathione: a putative intermediate metabolite of inorganic arsenicals. Toxicology 227, 45-52.

Hirst, M., Ho, C., Sabourin, L., Rudnicki, M., Penn, L., and Sadowski, I. (2001). A two-hybrid system for transactivator bait proteins. Proc Natl Acad Sci USA 98, 8726-8731.

Holmgren, A. (1988). Thioredoxin and glutaredoxin: small multi-functional redox proteins with active-site disulphide bonds. Biochem Soc Trans 16, 95-96.

Hsu, C.M., and Rosen, B.P. (1989). Characterization of the catalytic subunit of an anion pump. J Biol Chem 264, 17349-17354.

Hua, S.B., Qiu, M., Chan, E., Zhu, L., and Luo, Y. (1997). Minimum length of sequence homology required for *in vivo* cloning by homologous recombination in yeast. Plasmid 38, 91-96.

Humphrey, W., Dalke, A., and Schulten, K. (1996). VMD: visual molecular dynamics. *J Mol Graph* 14, 27-38.

Ji, G., and Silver, S. (1992). Reduction of arsenate to arsenite by the ArsC protein of the arsenic resistance operon of *Staphylococcus aureus* plasmid pI258. *Proc Natl Acad Sci USA* 89, 9474-9478.

Jiang, Y., Bhattacharjee, H., Zhou, T., Rosen, B.P., Ambudkar, S.V., and Sauna, Z.E. (2005). Nonequivalence of the nucleotide binding domains of the ArsA ATPase. *J Biol Chem* 280, 9921-9926.

Joshi, P.B., Hirst, M., Malcolm, T., Parent, J., Mitchell, D., Lund, K., and Sadowski, I. (2007). Identification of protein interaction antagonists using the repressed transactivator two-hybrid system. *Biotechniques* 42, 635-644.

Kagan, R.M., and Clarke, S. (1994). Widespread occurrence of three sequence motifs in diverse S-adenosylmethionine-dependent methyltransferases suggests a common structure for these enzymes. *Arch Biochem Biophys* 310, 417-427.

Kala, S.V., Neely, M.W., Kala, G., Prater, C.I., Atwood, D.W., Rice, J.S., and Lieberman, M.W. (2000). The MRP2/cMOAT transporter and arsenic-glutathione complex formation are required for biliary excretion of arsenic. *J Biol Chem* 275, 33404-33408.

Karkaria, C.E., Chen, C.M., and Rosen, B.P. (1990). Mutagenesis of a nucleotide-binding site of an anion-translocating ATPase. *J Biol Chem* 265, 7832-7836.

Kaur, P., and Rosen, B.P. (1992). Mutagenesis of the C-terminal nucleotide-binding site of an anion-translocating ATPase. *J Biol Chem* 267, 19272-19277.

Kiefer, F., Arnold, K., Kunzli, M., Bordoli, L., and Schwede, T. (2009). The SWISS-MODEL Repository and associated resources. *Nucleic Acids Res* 37, D387-392.

Klopotowski, T., and Wiater, A. (1965). Synergism of aminotriazole and phosphate on the inhibition of yeast imidazole glycerol phosphate dehydratase. *Arch Biochem Biophys* 112, 562-566.

Kozbial, P.Z., and Mushegian, A.R. (2005). Natural history of S-adenosylmethionine-binding proteins. *BMC Struct Biol* 5, 19.

Kozul, C.D., Ely, K.H., Enelow, R.I., and Hamilton, J.W. (2009). Low-dose arsenic compromises the immune response to influenza A infection *in vivo*. *Environ Health Perspect* 117, 1441-1447.

Krissinel, E., and Henrick, K. (2007). Inference of macromolecular assemblies from crystalline state. *J Mol Biol* 372, 774-797.

Lakowicz, J.R. (1983). Principles of fluorescence spectroscopy (New York: Plenum Press).

Le, X.C., Lu, X., Ma, M., Cullen, W.R., Aposhian, H.V., and Zheng, B. (2000). Speciation of key arsenic metabolic intermediates in human urine. *Anal Chem* 72, 5172-5177.

Leslie, E.M., Haimeur, A., and Waalkes, M.P. (2004). Arsenic transport by the human multidrug resistance protein 1 (MRP1/ABCC1). Evidence that a tri-glutathione conjugate is required. *J Biol Chem* 279, 32700-32708.

Li, J., and Rosen, B.P. (2000). The linker peptide of the ArsA ATPase. *Mol Microbiol* 35, 361-367.

Li, S., Chen, Y., and Rosen, B.P. (2001). Role of vicinal cysteine pairs in metalloid sensing by the ArsD As(III)-responsive repressor. *Mol Microbiol* 41, 687-696.

Lin, S., Shi, Q., Nix, F.B., Styblo, M., Beck, M.A., Herbin-Davis, K.M., Hall, L.L., Simeonsson, J.B., and Thomas, D.J. (2002). A novel S-adenosyl-L-methionine:arsenic(III) methyltransferase from rat liver cytosol. *J Biol Chem* 277, 10795-10803.

Lin, Y.F., Walmsley, A.R., and Rosen, B.P. (2006). An arsenic metallochaperone for an arsenic detoxification pump. *Proc Natl Acad Sci USA* 103, 15617-15622.

Lin, Y.F., Yang, J., and Rosen, B.P. (2007a). ArsD residues Cys12, Cys13 and Cys18 form an As(III) binding site required for arsenic metallochaperone activity. *J Biol Chem* 282, 16783-16791.

Lin, Y.F., Yang, J., and Rosen, B.P. (2007b). ArsD: an As(III) metallochaperone for the ArsAB As(III)-translocating ATPase. *J Bioenerg Biomembr* 39, 453-458.

Liscombe, D.K., Louie, G.V., and Noel, J.P. (2012). Architectures, mechanisms and molecular evolution of natural product methyltransferases. *Natural product reports* 29, 1238-1250.

Liu, Z., Boles, E., and Rosen, B.P. (2004a). Arsenic trioxide uptake by hexose permeases in *Saccharomyces cerevisiae*. *J Biol Chem* 279, 17312-17318.

- Liu, Z., Carbrey, J.M., Agre, P., and Rosen, B.P. (2004b). Arsenic trioxide uptake by human and rat aquaglyceroporins. *Biochem Biophys Res Commun* 316, 1178-1185.
- Liu, Z., Sanchez, M.A., Jiang, X., Boles, E., Landfear, S.M., and Rosen, B.P. (2006). Mammalian glucose permease GLUT1 facilitates transport of arsenic trioxide and methylarsonous acid. *Biochem Biophys Res Commun* 351, 424-430.
- Loenen, W.A. (2006). S-adenosylmethionine: jack of all trades and master of everything? *Biochem Soc Trans* 34, 330-333.
- Lu, W.J., Tamai, I., Nezu, J., Lai, M.L., and Huang, J.D. (2006). Organic anion transporting polypeptide-C mediates arsenic uptake in HEK-293 cells. *Journal of biomedical science* 13, 525-533.
- Maciaszczyk-Dziubinska, E., Wawrzycka, D., Sloma, E., Migocka, M., and Wysocki, R. (2010). The yeast permease Acr3p is a dual arsenite and antimonite plasma membrane transporter. *Biochim Biophys Acta* 1798, 2170-2175.
- Macindoe, G., Mavridis, L., Venkatraman, V., Devignes, M.D., and Ritchie, D.W. (2010). HexServer: an FFT-based protein docking server powered by graphics processors. *Nucleic Acids Res* 38, W445-449.
- Marapakala, K., Ajees, A.A., Qin, J., Sankaran, B., and Rosen, B.P. (2010). Crystallization and preliminary X-ray crystallographic analysis of the ArSM arsenic(III) S-adenosylmethionine methyltransferase. *Acta crystallographica Section F, Structural biology and crystallization communications* 66, 1050-1052.
- Marapakala, K., Qin, J., and Rosen, B.P. (2012). Identification of catalytic residues in the As(III) S-adenosylmethionine methyltransferase. *Biochemistry* 51, 944-951.
- Marapakala, K., Packianathan, C., Ajees, A.A., Dheeman, D.S., Sankaran, B., Kandavelu, P. and Rosen, B.P. A disulfide bond cascade mechanism for As(III) S-adenosylmethionine methyltransferases *Acta Crystallogr D Biol Crystallogr.* (submitted September 2014)
- Martin, J.L., and McMillan, F.M. (2002). SAM (dependent) I AM: the S-adenosylmethionine-dependent methyltransferase fold. *Curr Opin Struct Biol* 12, 783-793.
- Mateja, A., Szlachcic, A., Downing, M.E., Dobosz, M., Mariappan, M., Hegde, R.S., and Keenan, R.J. (2009). The structural basis of tail-anchored membrane protein recognition by Get3. *Nature* 461, 361-366.

- Meng, Y.L., Liu, Z., and Rosen, B.P. (2004). As(III) and Sb(III) uptake by GlpF and efflux by ArsB in *Escherichia coli*. *J Biol Chem* **279**, 18334-18341.
- Messens, J., Hayburn, G., Desmyter, A., Laus, G., and Wyns, L. (1999). The essential catalytic redox couple in arsenate reductase from *Staphylococcus aureus*. *Biochemistry* **38**, 16857-16865.
- Mobley, H.L., Chen, C.M., Silver, S., and Rosen, B.P. (1983). Cloning and expression of R-factor mediated arsenate resistance in *Escherichia coli*. *Mol Gen Genet* **191**, 421-426.
- Moore, S.A., Moennich, D.M., and Gresser, M.J. (1983). Synthesis and hydrolysis of ADP-arsenate by beef heart submitochondrial particles. *J Biol Chem* **258**, 6266-6271.
- Mukhopadhyay, R., Bhattacharjee, H., and Rosen, B.P. (2014). Aquaglyceroporins: generalized metalloid channels. *Biochim Biophys Acta* **1840**, 1583-1591.
- Mukhopadhyay, R., and Rosen, B.P. (1998). *Saccharomyces cerevisiae* ACR2 gene encodes an arsenate reductase. *FEMS Microbiol Lett* **168**, 127-136.
- Mukhopadhyay, R., and Rosen, B.P. (2002). Arsenate reductases in prokaryotes and eukaryotes. *Environ Health Perspect* **110 Suppl 5**, 745-748.
- O'Halloran, T.V., and Culotta, V.C. (2000). Metallochaperones: an intracellular shuttle service for metal ions. *J Biol Chem* **275**, 25057-25060.
- Oberoi, S., Barchowsky, A., and Wu, F. (2014). The global burden of disease for skin, lung, and bladder cancer caused by arsenic in food. *Cancer Epidemiol Biomarkers Prev* **23**, 1187-1194.
- Otwinowski, Z., and Minor, W. (1997). Processing of X-ray diffraction data collected in oscillation mode. *Methods Enzymol* **276**, 307-326.
- Packianathan, C., Pillai, J.K., Riaz, A., Kandavelu, P., Sankaran, B., and Rosen, B.P. (2014). Crystallization and preliminary X-ray crystallographic studies of CrArsM, an arsenic(III) S-adenosylmethionine methyltransferase from *Chlamydomonas reinhardtii*. *Acta crystallographica Section F, Structural biology and crystallization communications* **70**, 1385-1388.
- Palumaa, P. (2013). Copper chaperones. The concept of conformational control in the metabolism of copper. *FEBS Lett* **587**, 1902-1910.

Pettersen, E.F., Goddard, T.D., Huang, C.C., Couch, G.S., Greenblatt, D.M., Meng, E.C., and Ferrin, T.E. (2004). UCSF Chimera-a visualization system for exploratory research and analysis. *J Comput Chem* 25, 1605-1612.

Phillips, J.C., Braun, R., Wang, W., Gumbart, J., Tajkhorshid, E., Villa, E., Chipot, C., Skeel, R.D., Kale, L., and Schulten, K. (2005). Scalable molecular dynamics with NAMD. *J Comput Chem* 26, 1781-1802.

Philpott, C.C. (2012). Coming into view: eukaryotic iron chaperones and intracellular iron delivery. *J Biol Chem* 287, 13518-13523.

Porquet, A., and Filella, M. (2007). Structural evidence of the similarity of Sb(OH)₃ and As(OH)₃ with glycerol: implications for their uptake. *Chem Res Toxicol* 20, 1269-1276.

Qin, J., Lehr, C.R., Yuan, C., Le, X.C., McDermott, T.R., and Rosen, B.P. (2009). Biotransformation of arsenic by a Yellowstone thermoacidophilic eukaryotic alga. *Proc Natl Acad Sci U S A* 106, 5213-5217.

Qin, J., Rosen, B.P., Zhang, Y., Wang, G., Franke, S., and Rensing, C. (2006). Arsenic detoxification and evolution of trimethylarsine gas by a microbial arsenite S-adenosylmethionine methyltransferase. *Proc Natl Acad Sci USA* 103, 2075-2080.

Ramirez-Solis, A., Mukopadhyay, R., Rosen, B.P., and Stemmler, T.L. (2004). Experimental and theoretical characterization of arsenite in water: insights into the coordination environment of As-O. *Inorg Chem* 43, 2954-2959.

Rosen, B.P., Weigel, U., Karkaria, C., and Gangola, P. (1988a). Molecular characterization of a unique anion pump: the ArsA protein is an arsenite(antimonate)-stimulated ATPase. *Prog Clin Biol Res* 273, 105-112.

Rosen, B.P., Weigel, U., Karkaria, C., and Gangola, P. (1988b). Molecular characterization of an anion pump. The *arsA* gene product is an arsenite (antimonate)-stimulated ATPase. *J Biol Chem* 263, 3067-3070.

Rosenberg, H., Gerdes, R.G., and Chegwidan, K. (1977). Two systems for the uptake of phosphate in *Escherichia coli*. *J Bacteriol* 131, 505-511.

Ruan, X., Bhattacharjee, H., and Rosen, B.P. (2006). Cys-113 and Cys-422 form a high affinity metalloloid binding site in the ArsA ATPase. *J Biol Chem* 281, 9925-9934.

Ruan, X., Bhattacharjee, H., and Rosen, B.P. (2008). Characterization of the metalloactivation domain of an arsenite/antimonite resistance pump. *Mol Microbiol* 67, 392-402.

Sakurai, T., Kojima, C., Kobayashi, Y., Hirano, S., Sakurai, M.H., Waalkes, M.P., and Himeno, S. (2006). Toxicity of a trivalent organic arsenic compound, dimethylarsinous glutathione in a rat liver cell line (TRL 1215). *British journal of pharmacology* 149, 888-897.

Sali, A., and Blundell, T.L. (1993). Comparative protein modelling by satisfaction of spatial restraints. *J Mol Biol* 234, 779-815.

San Francisco, M.J., Hope, C.L., Owolabi, J.B., Tisa, L.S., and Rosen, B.P. (1990). Identification of the metalloregulatory element of the plasmid-encoded arsenical resistance operon. *Nucleic Acids Res* 18, 619-624.

Sanders, O.I., Rensing, C., Kuroda, M., Mitra, B., and Rosen, B.P. (1997). Antimonite is accumulated by the glycerol facilitator GlpF in *Escherichia coli*. *J Bacteriol* 179, 3365-3367.

Sato, T., and Kobayashi, Y. (1998). The *ars* operon in the skin element of *Bacillus subtilis* confers resistance to arsenate and arsenite. *J Bacteriol* 180, 1655-1661.

Scavetta, R.D., Thomas, C.B., Walsh, M.A., Szegedi, S., Joachimiak, A., Gumport, R.I., and Churchill, M.E. (2000). Structure of *RsrI* methyltransferase, a member of the *N6*-adenine β class of DNA methyltransferases. *Nucleic Acids Res* 28, 3950-3961.

Sharp, P.M., and Li, W.H. (1987). The codon Adaptation Index--a measure of directional synonymous codon usage bias, and its potential applications. *Nucleic Acids Res* 15, 1281-1295.

Shen, J., Hsu, C.M., Kang, B.K., Rosen, B.P., and Bhattacharjee, H. (2003). The *Saccharomyces cerevisiae* Arr4p is involved in metal and heat tolerance. *Biometals* 16, 369-378.

Shen, Z., Luangtongkum, T., Qiang, Z., Jeon, B., Wang, L., and Zhang, Q. (2014). Identification of a novel membrane transporter mediating resistance to organic arsenic in *Campylobacter jejuni*. *Antimicrob Agents Chemother* 58, 2021-2029.

Slocum, D.H., and Varner, J.E. (1960). Transfer of O^{18} in arsenolysis reactions. *J Biol Chem* 235, 492-495.

Smith, A.H., Lopipero, P.A., Bates, M.N., and Steinmaus, C.M. (2002). Public health. Arsenic epidemiology and drinking water standards. *Science* 296, 2145-2146.

Stybło, M., Del Razo, L.M., Vega, L., Germolec, D.R., LeCluyse, E.L., Hamilton, G.A., Reed, W., Wang, C., Cullen, W.R., and Thomas, D.J. (2000). Comparative toxicity of trivalent and pentavalent inorganic and methylated arsenicals in rat and human cells. *Arch Toxicol* 74, 289-299.

Sumi, D., and Himeno, S. (2012). Role of arsenic (+3 oxidation state) methyltransferase in arsenic metabolism and toxicity. *Biological & pharmaceutical bulletin* 35, 1870-1875.

Thomas, D.J., Li, J., Waters, S.B., Xing, W., Adair, B.M., Drobna, Z., Devesa, V., and Stybło, M. (2007). Arsenic (+3 oxidation state) methyltransferase and the methylation of arsenicals. *Experimental biology and medicine* (Maywood, NJ 232, 3-13.

Thomas, D.J., Waters, S.B., and Stybło, M. (2004). Elucidating the pathway for arsenic methylation. *Toxicol Appl Pharmacol* 198, 319-326.

Tisa, L.S., and Rosen, B.P. (1990). Molecular characterization of an anion pump. The ArsB protein is the membrane anchor for the ArsA protein. *J Biol Chem* 265, 190-194.

Ulrey, C.L., Liu, L., Andrews, L.G., and Tollefsbol, T.O. (2005). The impact of metabolism on DNA methylation. *Hum Mol Genet* 14 Spec No 1, R139-147.

Vahter, M. (1999). Methylation of inorganic arsenic in different mammalian species and population groups. *Sci Prog* 82 (Pt 1), 69-88.

Villa-Bellosta, R., and Sorribas, V. (2010). Arsenate transport by sodium/phosphate cotransporter type IIb. *Toxicol Appl Pharmacol* 247, 36-40.

Villadangos, A.F., Fu, H.L., Gil, J.A., Messens, J., Rosen, B.P., and Mateos, L.M. (2012). Efflux permease CgAcr3-1 of *Corynebacterium glutamicum* is an arsenite-specific antiporter. *J Biol Chem* 287, 723-735.

Vogel, G., and Steinhart, R. (1976). ATPase of *Escherichia coli*: purification, dissociation, and reconstitution of the active complex from the isolated subunits. *Biochemistry* 15, 208-216.

Waddell, T.G., Eilders, L.L., Patel, B.P., and Sims, M. (2000). Prebiotic methylation and the evolution of methyl transfer reactions in living cells. *Origins of life and evolution of the biosphere : the journal of the International Society for the Study of the Origin of Life* 30, 539-548.

- Walmsley, A.R., Zhou, T., Borges-Walmsley, M.I., and Rosen, B.P. (1999). The ATPase mechanism of ArsA, the catalytic subunit of the arsenite pump. *J Biol Chem* 274, 16153-16161.
- Walmsley, A.R., Zhou, T., Borges-Walmsley, M.I., and Rosen, B.P. (2001a). Antimonite regulation of the ATPase activity of ArsA, the catalytic subunit of the arsenical pump. *Biochem J* 360, 589-597.
- Walmsley, A.R., Zhou, T., Borges-Walmsley, M.I., and Rosen, B.P. (2001b). A kinetic model for the action of a resistance efflux pump. *J Biol Chem* 276, 6378-6391.
- Willsky, G.R., and Malamy, M.H. (1980a). Characterization of two genetically separable inorganic phosphate transport systems in *Escherichia coli*. *J Bacteriol* 144, 356-365.
- Willsky, G.R., and Malamy, M.H. (1980b). Effect of arsenate on inorganic phosphate transport in *Escherichia coli*. *J Bacteriol* 144, 366-374.
- Winski, S.L., and Carter, D.E. (1998). Arsenate toxicity in human erythrocytes: characterization of morphologic changes and determination of the mechanism of damage. *Journal of toxicology and environmental health Part A* 53, 345-355.
- Wu, J., Tisa, L.S., and Rosen, B.P. (1992). Membrane topology of the ArsB protein, the membrane subunit of an anion-translocating ATPase. *J Biol Chem* 267, 12570-12576.
- Wysocki, R., Chery, C.C., Wawrzycka, D., Van Hulle, M., Cornelis, R., Thevelein, J.M., and Tamás, M.J. (2001). The glycerol channel Fps1p mediates the uptake of arsenite and antimonite in *Saccharomyces cerevisiae*. *Mol Microbiol* 40, 1391-1401.
- Yang, J., Abdul Salam, A.A., and Rosen, B.P. (2011). Genetic mapping of the interface between the ArsD metallochaperone and the ArsA ATPase. *Mol Microbiol* 79, 872-881.
- Yang, J., Rawat, S., Stemmler, T.L., and Rosen, B.P. (2010). Arsenic binding and transfer by the ArsD As(III) metallochaperone. *Biochemistry* 49, 3658-3666.
- Ye, J., Ajees, A.A., Yang, J., and Rosen, B.P. (2010). The 1.4 Å crystal structure of the ArsD arsenic metallochaperone provides insights into its interaction with the ArsA ATPase. *Biochemistry* 49, 5206-5212.

- Ye, J., He, Y., Skalicky, J., Rosen, B.P., and Stemmler, T.L. (2011). Resonance assignments and secondary structure prediction of the As(III) metallochaperone ArsD in solution. *Biomolecular NMR assignments* 5, 109-112.
- Ye, J., Rensing, C., Rosen, B.P., and Zhu, Y.G. (2012). Arsenic biomethylation by photosynthetic organisms. *Trends in plant science* 17, 155-162.
- Zhou, T., Liu, S., and Rosen, B.P. (1995). Interaction of substrate and effector binding sites in the ArsA ATPase. *Biochemistry* 34, 13622-13626.
- Zhou, T., Radaev, S., Rosen, B.P., and Gatti, D.L. (2000). Structure of the ArsA ATPase: the catalytic subunit of a heavy metal resistance pump. *Embo J* 19, 4838-4845.
- Zhou, T., Radaev, S., Rosen, B.P., and Gatti, D.L. (2001). Conformational changes in four regions of the *Escherichia coli* ArsA ATPase link ATP hydrolysis to ion translocation. *J Biol Chem* 276, 30414-30422.
- Zhou, T., and Rosen, B.P. (1997). Tryptophan fluorescence reports nucleotide-induced conformational changes in a domain of the ArsA ATPase. *J Biol Chem* 272, 19731-19737.
- Zhou, T., Shen, J., Liu, Y., and Rosen, B.P. (2002). Unisite and multisite catalysis in the ArsA ATPase. *J Biol Chem* 277, 23815-23820.
- Zhou, Y., Messier, N., Ouellette, M., Rosen, B.P., and Mukhopadhyay, R. (2004). *Leishmania major* LmACR2 is a pentavalent antimony reductase that confers sensitivity to the drug pentostam. *J Biol Chem* 279, 37445-37451.
- Zhu, Y.-G., Yoshinaga, M., Zhao, F.-J., and Rosen, B.P. (2014). Earth abides arsenic biotransformations. *Annu Rev Earth Planet Sci* 42, 443-467.

VITA

JITESH KANNAN PILLAI

EDUCATION

2009-2014	Doctoral Candidate in Biology Florida International University Miami, FL
2006-2008	M.S. Biotechnology Bangalore University Bangalore, India
2003-2006	B.S. Biotechnology University of Mumbai Mumbai, India

PUBLICATIONS AND PRESENTATIONS

Pillai, J.K., Venkadesh, S., Ajees, a. A., Rosen, B.P., and Bhattacharjee, H. (2014) Mutations in the ArsA ATPase that restore interaction with the ArsD metallochaperone. *Biometals*. PMID:25183649.

Packianathan, C., Pillai, J.K., Riaz, A., Kandavelu, P., Sankaran, B., and Rosen, B.P. A disulfide bond cascade mechanism for As(III) S-adenosylmethionine methyltransferases *Acta Crystallogr F Biol Crystallogr*. (accepted August 2014)

Dheeman, D.S., Packianathan, C., Pillai, J.K. and Rosen, B.P. The pathway of human AS3MT arsenic methylation *Chem Res Toxicol*. (submitted September 2014)

Attended the NIEHS workshop on Health Effects and Mitigation of Arsenic: Current Research Efforts and Future Directions at North Carolina in March 2014 and presented poster on 'AsGS₃ is the substrate of AS3MT'.

Attended the 9th ISPTS Conference in October 2012 at Miami and presented poster on "Mapping the interface of the ArsA ATPase with the ArsD metallochaperone and As(III) binding studies of ArsD".

Attended the FASEB Conference in June 2012 at Snowmass, Colorado and presented poster on "Mapping the interface of the ArsA ATPase with the ArsD metallochaperone and As(III) binding studies of ArsD".